AGU PUBLICATIONS

Reviews of Geophysics

REVIEW ARTICLE
10.1002/2014RG000468

Dedicated to the Memory of Klaus Beheng

Key Points:
- Review of concepts of microphysical methods
- Analysis of errors in representation of microphysical processes
- Comparison of results obtained by different methods

Correspondence to:
A. P. Khain,
alexander.khain@mail.huji.ac.il

Citation:
Khain, A. P., et al. (2015), Representation of microphysical processes in cloud-resolving models: Spectral (bin) microphysics versus bulk parameterization, *Rev. Geophys.*, *53*, 247–322, doi:10.1002/2014RG000468.

Received 18 JUL 2014
Accepted 26 JAN 2015
Accepted article online 30 JAN 2015
Published online 23 MAY 2015

Representation of microphysical processes in cloud-resolving models: Spectral (bin) microphysics versus bulk parameterization

A. P. Khain[1], K. D. Beheng[2], A. Heymsfield[3], A. Korolev[4], S. O. Krichak[5], Z. Levin[5,6], M. Pinsky[1], V. Phillips[7], T. Prabhakaran[8], A. Teller[9], S. C. van den Heever[10], and J.-I. Yano[11]

[1]Department of Atmospheric Sciences, Hebrew University of Jerusalem, Jerusalem, Israel, [2]Institut für Meteorologie und Klimaforschung, Universität/Forschungszentrum Karlsruhe, Karlsruhe, Germany, [3]National Center for Atmospheric Research, Boulder, Colorado, USA, [4]Environment Canada, Toronto, Ontario, Canada, [5]Department of Geophysical, Atmospheric and Planetary Sciences, Tel Aviv University, Tel Aviv, Israel, [6]Energy, Environment and Water Research Center, Cyprus Institute, Nicosia, Cyprus, [7]Department of Physical Geography and Ecosystem Science, Lund University, Lund, Sweden, [8]Indian Institute of Tropical Meteorology, Pune, India, [9]Department of Earth and Planetary Sciences, Weizmann Institute of Science, Rehovot, Israel, [10]Department of Atmospheric Science, Colorado State University, Fort Collins, Colorado, USA, [11]GAME/CNRS, URA1357, CNRS-INSU-Météo France, Toulouse, France

Abstract Most atmospheric motions of different spatial scales and precipitation are closely related to phase transitions in clouds. The continuously increasing resolution of large-scale and mesoscale atmospheric models makes it feasible to treat the evolution of individual clouds. The explicit treatment of clouds requires the simulation of cloud microphysics. Two main approaches describing cloud microphysical properties and processes have been developed in the past four and a half decades: bulk microphysics parameterization and spectral (bin) microphysics (SBM). The development and utilization of both represent an important step forward in cloud modeling. This study presents a detailed survey of the physical basis and the applications of both bulk microphysics parameterization and SBM. The results obtained from simulations of a wide range of atmospheric phenomena, from tropical cyclones through Arctic clouds using these two approaches are compared. Advantages and disadvantages, as well as lines of future development for these methods are discussed.

1. Introduction: Two Methods for Representing Cloud Microphysics

Latent heat release in clouds leading to convective or stratiform heating/cooling constitutes one of the main energy sources for atmospheric motions on spatial scales ranging from local turbulence and single clouds to global circulation. Latent heating associated with the condensation of water vapor and subsequent precipitation within clouds are realized through microphysical processes that take place at scales of cloud particle sizes from several micrometers to a few centimeters. Paradoxically, then, the global dynamics of the atmosphere and climate are dependent upon microscale-level processes. In addition to convective heating, clouds control, to a large extent, the shortwave (solar) and the longwave (thermal) radiation budgets of the atmosphere. The effects of clouds on radiation vary by cloud coverage, cloud top altitude, cloud particle size, habits, size distributions, and phase. The types of cloud particles, as well as their size distributions, are affected by atmospheric aerosols that give rise to the formation of droplets and ice crystals. Clouds also determine precipitation and are the major component in the hydrological cycle.

Limited area models (LAMs) and global circulation models (GCMs) (see Table 1 for the list of acronyms) have grid spacings typically exceeding approximately 10–20 km and do not resolve most cloud scales. To describe convective heating/cooling, traditional methods of convective parameterization are usually used. The goal of these parameterizations is to describe the overall effect of subgrid cumulus convection on the large spatial scales explicitly represented in the models. These parameterizations are based largely on empirical or semiempirical mass and energy balance considerations. Convective parameterizations use a simple representation of clouds in the form of plumes with an intensity defined by a atmospheric instability (CAPE) closure and entrainment-detrainment rate. These parameterizations take into account microphysics only in a very crude manner.

Table 1. List of Acronyms and Some Definitions

Acronyms	Definitions
CAIPEEX	Cloud Aerosol Interaction and Precipitation Enhancement Experiment
CAPE	Convective Available Potential Energy
CCN	Cloud condensational nuclei
Condensation coefficient	Condensation coefficient is a ratio of the number of molecules absorbed by the liquid phase and the number of molecules impinging on the liquid phase
CWC	Cloud water mixing ratio or cloud water content
COSMO NWP	Consortium for Small-Scale Modeling, Numerical Weather Prediction
COST	Cooperation in Science and Technology
DHARMA	Distributed Hydrodynamic Aerosol and Radiative Modeling Application
DSD	Drop size distribution or droplet size distribution
GATE	Global Atlantic Tropical Experiment
GCCN	Giant cloud condensational nuclei
GCE	Goddard Cloud Ensemble Model
GCM	Global circulation model
CFADs	Contoured Frequency Altitude Diagrams
HUCM	Hebrew University Cloud Model
IN	Ice nucleus
INSPECT	Ice Nuclei Spectroscopy campaigns
ISDAC	Indirect and Semi-Direct Aerosol Campaign
IWP	Ice water path
JMA-NHM	Japan Meteorological Agency Nonhydrostatic Model
K theory	Description of turbulent (subgrid) fluxes under the assumption that the fluxes are proportional to gradients of averaged (model-resolved) values
Köhler theory	Theory of nucleation of haze particles into droplets
LAM	Limited area model
LBA-SMOCC	Large-Scale Biosphere-Atmosphere Experiment in Amazonia-Smoke, Aerosols, Clouds, Rainfall, and Climate
LEM	Lagrangian Eulerian Cloud Model
LES	Large-eddy simulations
LWC, RWC	Liquid water content, rain water content
LWP	Liquid water path
the Marshall-Palmer distribution	Exponential size distribution
MMM	Microphysical method of moments
NAM-SCA	Nonhydrostatic Anelastic Model with Segmental Approximation
NCAR, NOAA	National Center for Atmospheric Research
PSD	Particle size distribution
RAMS	Regional Atmospheric Mesoscale System (Colorado State University)
REG2M and 3MHAIL	RG2M denotes the regular two-moment scheme applied in RAMS; 3MHAIL is a bin-emulating bulk scheme in RAMS, which is a two moment for all hydrometeors, while it is a three-moment scheme with respect to hail
RSD	Raindrop size distribution
RWC	Rain water mining ratio or rain water content
SCA	Segmentally Constant Approximations
SAM	System of Atmospheric Modeling
SBM	Spectral bin microphysics
Sc	Stratocumulus cloud
SCE	Stochastic collection equation
SDM	Super Droplet Method
SPRINTARS	Spectral Radiation Transport Model for Aerosol Species
TAU	Cloud model of Tel Aviv University
TC	Tropical cyclone
Twomey formula	Formula relating concentration of nucleated CCN as function of supersaturation
TRMM	Tropical Rainfall Measuring Mission - NASA
WRF	Weather Research Forecasting model
UWNMS	University of Wisconsin Nonhydrostatic Modeling System
Z and Zdr	Radar reflectivity and differential radar reflectivity
Z-R relationships	Relationships between radar reflectivity and the rate of surface precipitation

Within LAMs and GCMs, convectively induced heating/cooling and cloud-induced radiative effects are treated by two independent parameterization schemes, despite the fact that these effects are caused by the same clouds. The convective parameterizations do not allow for the determination of cloud coverage. Instead, cloud coverage is empirically related to horizontally averaged relative humidity. These simplifications cause the wide diversity of results seen in different models.

Methods for convective parameterization development in LAMs and GCMs have been discussed in several studies [e.g., *Arakawa*, 2004; *Yano et al.*, 2005, 2013; *Plant*, 2010; *De Rooy et al.*, 2013]. The need to improve the representation of convection in large-scale models has led to the idea of the "superparameterization" of small-scale and mesoscale processes in large-scale models and GCMs [*Grabowski and Smolarkiewicz*, 1999; *Grabowski*, 2001; *Khairoutdinov and Randall*, 2001; *Khairoutdinov et al.*, 2005; *Grabowski*, 2003, 2006; *Tao et al.*, 2009a; *Tao and Moncrieff*, 2009]. According to this idea, clouds are explicitly simulated on high-resolution, 2-D cloud-resolving meshes implemented within grid columns of GCM models. The convective heating rate, precipitation rate, and other parameters characterizing the combined effect of clouds on large-scale processes are obtained by horizontal averaging over these 2-D grids and then transferring them to the GCM. In this way, traditional parameterization of convection is replaced by explicitly calculated heating/cooling profiles. The NAM-SCA (nonhydrostatic anelastic model with segmentally approximation) approach [*Yano et al.*, 2010, 2012a; *Yano and Bouniol*, 2010; *Yano and Baizig*, 2012], in turn, fills a gap between superparameterization and more traditional parameterizations.

The rapid and continuous increase in computing capabilities has made it feasible to utilize cloud-resolving grid spacing in continental-scale numerical weather predictions or within nested meshes of GCM. Explicit simulations of clouds allow one to handle more consistently and without parameterization all the elements of the processes associated with clouds, including thermodynamics and radiation, as well as the microphysical processes leading to precipitation formation. The explicit simulation of clouds (with appropriate microphysics) in large-scale models would likely lead to dramatic improvements in large-scale and mesoscale atmospheric modeling.

In cloud-resolving models, parameterization of convection is replaced by schemes describing cloud evolution, i.e., by microphysical schemes. From the very outset, microphysical scheme development has gone in two distinct directions: *bulk microphysics parameterization* (hereinafter bulk parameterizations or bulk schemes) and *spectral* (*bin*) *microphysics* (hereinafter SBM). Despite the fact that in both approaches the same microphysical processes are described and have similar outputs (cloud and rain water mixing ratios or contents, CWC and RWC, cloud ice content, precipitation rates, etc.), the two approaches diverge quite markedly.

Bulk parameterizations aim to replace traditional schemes of convective parameterization in cloud-resolving mesoscale and large-scale models. Bulk parameterization schemes represent the most general microphysical cloud properties using a semiempirical description of particle size distributions $f(m)$ (hereinafter PSD) (here m is particle mass). Accordingly, this approach is assumed to be computationally efficient. *Kessler* [1969] developed the first bulk parameterization scheme allowing for the reproduction of cloud microphysics and cloud evolution in numerical models.

The computational efficiency of bulk parameterization schemes lies in their consideration of microphysical equations not for PSDs of different hydrometeor types (e.g., cloud droplets, raindrops, ice crystals, aggregates, graupel, and hail) themselves, but for a number of PSD moments. The kth moment of the PSD is defined as $M^{(k)} = \int_0^\infty m^k f(m)\mathrm{d}m$ with k primarily an integer value. Schemes that use only one moment (typically, the mass contents of variables hydrometeors, $k = 1$) are known as one-moment or single-moment schemes, while schemes using two moments (typically, number concentrations, $k = 0$, and mass contents, $k = 1$) are known as two-moment schemes. Less frequently, three-moment bulk schemes are used. In these, the variables are number densities (concentrations), mass densities, and radar reflectivity ($k = 2$). The system of equations for the moments of PSD is not closed, since the equations for kth moment $M^{(k)}$ include terms with a higher-order moment $M^{(k+1)}$ [*Seifert and Beheng*, 2001]. The closure problem is circumvented by representing PSD in the form of specific mathematical functions which are completely determined by a few parameters only. A four-parameter gamma distribution is typically used as the master function.

The bulk parameterization scheme proposed by *Kessler* [1969] describes only warm microphysical processes. Since the work of *Lin et al.* [1983] and *Rutledge and Hobbs* [1984], all bulk parameterizations have described both warm and ice processes. A great number of bulk parameterization schemes developed since then have been used in different mesoscale models with spatial resolutions of several kilometers. Current mesoscale models allow their users to choose the most appropriate scheme among more than 20 different bulk parameterization schemes. The increasing complexity of bulk parameterization schemes is illustrated in Table 2.

Bulk parameterization schemes have also been implemented in a simplified form in climate models [*Boucher and Lohmann*, 1995; *Lohmann and Feichter*, 1997; *Ghan et al.*, 2001].

AGU Reviews of Geophysics

10.1002/2014RG000468

Table 2. The Main Characteristics of Widely Used Bulk Parameterization Schemes[a]

Authors	Name, Comments	Type of Hydrometeors: Cloud *N q Z*	Drizzle *N q Z*	Rain *N q Z*	Ice *N q Z*	AGGR *N q Z*	Snow *N q Z*	GRAUP *N q Z*	Hail *N q Z*
Kessler [1969]	First warm rain bulk parameterization (used in WRF).	- X -		- X -					
Lin et al. [1983]	One moment, hail is treated as a high-density hydrometeor.	- X -		- X -	- X -		- X -		- X -
Rutledge and Hobbs [1984]	1M scheme.	- X -		- X -	- X -		- X -	- X -	
Tao et al. [1989]	1M scheme of mixed-phase cloud. A new saturation technique is developed.	- X -		- X -	- X -		- X -	- X -	
Chen and Sun [2002]	Known as Purdue Lin Scheme (used in WRF). Based on *Lin et al.* [1983] and *Rutledge and Hobbs* [1984] studies.	- X -		- X -	- X -		- X -	- X -	
Cotton et al. [1986]	First bin parameterization used in RAMS. Ice multiplication, melting, and shedding are included.	- X -		- X -	- X -	- X -		- X -	- X -
Tao et al. [1989]	1M. Used in WRF. NASA Goddard scheme, based on *Lin et al.* [1983] and *Rutledge and Hobbs* [1984] schemes. A new procedure of ice-water saturation adjustment is included.	- X -		- X -	- X -		- X -		- X -
Murakami [1990]	1M, snow includes singly snow crystals and aggregates, many algorithms are similar to those in *Lin et al.* [1983] and *Cotton et al.* [1986]. Improved approach for calculation of relative fall velocity between different hydrometeors.	- X -		- X -	- X -		- X -	- X -	
Verlinde et al. [1990]	1M, used in RAMS, similar to *Cotton et al.* [1986] but with analytical expressions for integrals of collisions. Application of lookup tables.	- X -		- X -	- X -	- X -		- X -	- X -
Ferrier [1994]	2M. Ice and precipitation particle concentrations are predicted.	- X -		- X -	X X -		X X -	X X -	X X -
Walko et al. [1995]	1M, used in RAMS. Ice crystals are separated into small pristine crystals and large pristine crystals attributed to snow. Hail and graupel are of different density.	- X -		- X -	- X -	- X -	- X -	- X -	- X -
Meyers et al. [1997]	RAMS, 2M. Ice and precipitation particle concentrations are predicted.	- X -		X X -	X X -	X X -	X X -	X X -	X X -
Reisner et al. [1998]	NCAR/Penn State Mesoscale Model Version 5 (MM5), 2M.	- X -		X X -	X X -		X X -	X X -	
Cohard and Pinty [2000]	2M, warm microphysics. Implementation of some analytical expressions for rates.	X X -		X X -					
Seifert and Beheng [2001]	2M, warm processes, analytical formulas for autoconversion, accretion, and self-collection.	X X -		X X -					
Cotton et al. [2003]	2M, used in RAMS. Based on schemes by *Verlinde et al.* [1990] and *Walko et al.* [1995]. Bin-emulating bulk scheme. Ice is categorized into pristine ice, large pristine ice (snow) that can be rimed, aggregates, graupel, and hail.	- X -		X X -	X X -	X X -	X X -	X X -	X X -
Hong et al. [2004] and *Hong and Lim* [2006]	1M, used in WRF, three-class (WSM3) scheme. This scheme is efficient at grid spacing between the mesoscale and cloud resolving.	- X -		- X -	- X -				
Chen and Liu [2004]	2M, warm microphysics. This scheme does not use saturation adjustment. The masses of aerosols inside clouds and precipitation are two new prognostic variables to account for the aerosols recycled from the evaporation of cloud drops.	XX-		X X -					
Hong and Lim [2006]	1M, used in WRF, five-class scheme (WSM5), a gradual melting of snow is allowed. This scheme is efficient at grid spacing between the mesoscale and cloud-resolving grid.	- X -		- X -	- X -		- X -		
Hong and Lim [2006]	1M, used in WRF, six-class scheme (WSM6), includes graupel. The scheme is the most suitable for cloud-resolving grids.	- X -		- X -	- X -		- X -	- X -	
Skamarock et al. [2008]	Eta Grid-scale Cloud and precipitation scheme (2001), EGCP01 or the Eta Ferrier scheme, used in WRF; the mean size of precipitating ice is temperature dependent.	- X -		- X -	- X -		- X - Precipitation ice		

10.1002/2014RG000468

Table 2. (continued)

Authors	Name, Comments	Type of Hydrometeors							
		Cloud *N q Z*	Drizzle *N q Z*	Rain *N q Z*	Ice *N q Z*	AGGR *N q Z*	Snow *N q Z*	GRAUP *N q Z*	Hail *N q Z*
Milbrandt and Yau [2005b, 2006]	3M, implementation of dependencies between parameters of gamma distributions, simulation of hail.	X X X		X X X	X X X		X X X	X X X	X X X
Thompson et al. [2004]	1M, used in WRF, empirical relation between parameters of gamma distributions, and between the parameters and environmental conditions. Calculation of concentration of ice crystals.	- X -		- X -	- XX -		- X -	- X -	
Thompson et al. [2008]	Between 1M and 2M, used in WRF. As *Thompson et al*. [2004], but the calculation of rain drop concentration is included	- X -		- XX-	- XX -		- X -	- X -	
Thompson and Eidhammer [2014]	2M, used in WRF. Variable density snow is used. Prediction of the concentration of available aerosols. "Graupel" category also captures hail since graupel particles can be of hail size.	- XX -		- XX -	- XX -		- X -	- X -	
Morrison et al. [2005a, 2009a]	2M, used in WRF. Improved calculation of supersaturation is included. Concentration of CCN is prescribed.	X X -		X X -	X X -		X X -	X X -	
Lim and Hong [2010]	2M for droplets and rain, used in WRF6. A prognostic treatment of cloud condensation nuclei (CCN) is introduced.	X X -		X X -	- X -		- X -	- X -	
Mansell et al. [2010]	2M, NSSL seven-class, used in WRF. Graupel density is calculated. An additional hail category is available. Conversion of graupel to hail takes place when wet growth begins. Used for calculation of cloud electrification.	X X -		X X -	X X -		X X -	X X -	
Tsai et al. [2012]	2M, CLR2, used in WRF, based on *Chen and Liu* [2004], *Reisner et al*. [1998], and *Cheng et al*. [2010]. Three groups of CN (dry or interstitial CN, rain CN, and cloud CN), 16 variables.	X X -		X X -	X X -		X X -	X X -	
Lin and Colle [2011]	1M, five-class hydrometeor Stony Brook University Y. Lin scheme; the projected area, mass, and fall velocity of precipitating ice depends on riming intensity and temperature.	- X -		- X -	- X -	- X - Precipitating ice			
Saleeby and Cotton [2004]	2M, used in RAMS, bin-emulating scheme. Drizzle is included as a separate hydrometeor. Fully interactive with prognostic CCN and IN aerosol schemes.	X X -	X X -	X X -	X X -	X X -	X X -	X X -	X X -
Seifert and Beheng [2006a, 2006b]	2M, the rates of collisions are calibrated versus a bin scheme. The collision rate is time dependent.	X X -		X X -	X X -	X X -	X X -	X X -	
Saleeby and van den Heever [2013]	Same as *Saleey and Cotton* [2004] except modified prognostic aerosol schemes. IN are parameterized using *DeMott et al*. [2010] scheme. Many aerosol types and a variety of aerosol processes included.	X X -	X X -	X X -	X X -	X X -	X X -	X X -	X X -
Loftus et al. [2014]	3M for hail, RAMS. Same as *Saleeby and van den Heever* [2013] except that a triple-moment scheme has been included for hail.	X X -	X X -	X X -	X X -	X X -	X X -	X X -	X X X
Phillips et al. [2007a, 2008, 2009, 2013] and *Formenton et al*. [2013a, 2013b]	Bin-emulating for coagulation for snow, rain, and graupel/hail, in-cloud supersaturation is predicted, bulk treatment of six aerosol species is applied.	X X -		- X -	X X -		- X -	- X -	
Lang et al. [2007]	1M scheme, WRF. 3ICE scheme: Ice crystals, snow, and graupel.	-X-		-X-	-X-		-X-	-X-	
Lang et al. [2014]	1M scheme, GCE. 4ICE scheme: hail/frozen drops hydrometeor class has been added. A snow density mapping is applied.	-X-		-X-	-X-		-X-	-X-	-X-

[a]Notations: *N* is concentration, *q* is mixing ratio, and *Z* is radar reflectivity. These variables indicate moments of PSD used in the schemes. X: uses, -: not used.

Despite the significant variety of different components of bulk parameterization schemes, they all share a basic assumption about the shape of the PSD: in any bulk parameterization scheme, even in those containing more than 10 hydrometeor types, the PSDs of particles belonging to each hydrometeor type are approximated by exponential or gamma distributions and much more rarely by lognormal functions.

The SBM is the second main approach to microphysical process description. SBM is also referred to as explicit microphysics, bin microphysics, and bin-resolving or size-resolving microphysics. The SBM approach aims to simulate as accurately as possible cloud microphysical and precipitation processes in clouds of different types. Fundamental to bin microphysics is the calculation of PSDs by solving explicit microphysical equations. Hence, no a priori information about the form of PSDs is required or assumed. Instead, PSDs are calculated, for instance, on a finite difference mass grid containing from several tens to several hundred mass bins in different models. It should be stressed that contemporary SBM models substantially differ from the first generations of the schemes [*Clark*, 1973; *Takahashi*, 1976; *Kogan et al*., 1984; *Young*, 1975]. The earlier and later schemes differ notably with respect to degree of detail in their respective descriptions of microphysical processes. A massive increase in computing power has made it possible to explicitly describe cloud microstructure using the knowledge accumulated in cloud physics processes. In parallel to the improvement of the representation of separate microphysical processes, a number of SBM schemes have been implemented and successfully used in cloud models and cloud-resolving mesoscale models for the simulation of a wide range of meteorological phenomena (see section 6).

Equations used in bin microphysics are not contingent upon particular meteorological situations. Thus, the advantage of the SBM is its universality; that is, the same scheme can be used without any modification for simulations of different atmospheric phenomena ranging from stratiform Arctic clouds to tropical cyclones. As against that, in bulk schemes, microphysical parameters may need to be chosen on the basis of the cloud system being simulated.

The number of equations to be solved in SBM schemes is proportional to the number of bins and the number of hydrometeor types (including aerosol). Typically, SBM has about 200–300 prognostic variables, while bulk schemes have 6–18 variables. Therefore, the computational requirements in these schemes are substantially higher than in bulk parameterization schemes. Accordingly, the bin microphysics approach requires ~ 5 to 20 times more computer time than current bulk parameterization schemes, depending on the complexity of the particular bulk schemes.

There exists a third, "intermediate" approach for representing cloud microphysical processes: hybrid schemes that combine SBM and bulk parameterization. In light of the need for a very accurate description of drop formation and growth and comparatively large uncertainties in processes related to ice formation, *Onishi and Takahashi* [2011] developed a scheme in which warm microphysical processes are described using the SBM approach, while processes related to ice formation and evolution are described using bulk parameterization.

In addition to the SBM, another approach that aims at the detailed investigation of the formation of droplet size distributions in turbulent flows has recently been developed. In this approach, the motion of a great number of individual droplets within a flow field generated in large-eddy simulations (LES) is calculated. Such models, sometimes referred to as Lagrangian Cloud Models (LCM), have been described in studies by *Andrejczuk et al*. [2009, 2010], *Shima et al*. [2009], and *Riechelmann et al*. [2012]. To avoid the problem of handling an extremely large number of individual droplets, the concept of superdroplets was introduced [*Shima et al*., 2009]. This concept is known as the Super Droplet Method (SDM). Each superdroplet represents a large number of real droplets, equal in size and identical in location. In this sense, a superdrop corresponds to the droplets belonging to the same mass bin in SBM. Turbulent mixing in such models is treated explicitly, without any parameterization. The accuracy of the representation of this process depends on the ability of the corresponding LES model to adequately reproduce the turbulent structure of the atmosphere and on the LES grid spacing. This potentially powerful approach is currently still in the development stage, and further efforts are required to properly take into account processes related to collisions, droplet nucleation, and the formation of raindrops. Furthermore, the representation of ice processes using such a scheme has not as yet been addressed.

Bin-emulating schemes represent another example of a hybrid approach. This approach is used in Colorado State University's *Regional Atmospheric Modeling System* (RAMS) [*Meyers et al*., 1997; *Cotton et al*., 2003; *Saleeby*

and Cotton, 2004, 2008; *van den Heever and Cotton*, 2004, 2007; *Carrió et al*., 2007; *van den Heever et al*., 2006, 2011; *Seigel and van den Heever*, 2012; *Storer and van den Heever*, 2013; *Igel et al*., 2013; *Saleeby and van den Heever*, 2013]. In this approach, the rates of various microphysical processes for a wide range of atmospheric conditions are calculated offline using a Lagrangian parcel model with SBM. Examples of such models are presented in studies by *Heymsfield and Sabin* [1989] and *Feingold and Heymsfield* [1992]. The results of the SBM parcel model calculations for each of the microphysical processes (e.g., collision and sedimentation) are then included in lookup tables incorporated within the bulk microphysical module of the 3-D RAMS model in which gamma distributions are used as the master functions. The bin results are thus fully accessible to the model within cloud-resolving simulations. In this way, the sophistication of bin schemes is exploited, while a relatively high computational efficiency is maintained. The details of this approach are discussed below.

Bulk parameterizations, SBM, and mixed, combined bin bulk approaches are all critical contributions to atmospheric modeling. Researchers place high hopes on cloud-resolving models with advanced descriptions of microphysical processes to solve problems of climate change, as well as local and global precipitation regime change. One of the main problems of interest is the effect of the anthropogenic emission of large masses of aerosols into the atmosphere. In the past two decades, a great number of observational and numerical studies have been dedicated to quantifying the effects of aerosols on radiation, precipitation, and other atmospheric features at a wide range of scales, from that of single cloud to global scales [*Khain et al*., 2005; *van den Heever et al*., 2006; *Levin and Cotton* 2007; *Rosenfeld et al*., 2008; *Khain*, 2009; *van den Heever et al*., 2011; *Tao et al*., 2007, 2012; *Fan et al*., 2013]. Aerosols affect cloud microphysics through their influence on cloud particle number concentration and size. Two-moment bulk parameterization schemes are able to take into account the effect of a decrease in droplet size with an increase in aerosol concentration. Many studies highlight the advantages of two-moment bulk parameterization schemes as compared to one-moment schemes, as well as the advantages of three-moment schemes as compared to two-moment schemes.

One of the first applications of the SBM model was the investigation of possible precipitation enhancement and hail suppression by the seeding of clouds with hygroscopic or ice-forming aerosols [*Khvorostyanov et al*., 1989; *Reisin et al*., 1996c; *Yin et al*., 2000]. Thus, taking into account of aerosol effects on cloud microphysics has been a characteristic feature of bin microphysics from the inception of bin schemes.

At times, it is difficult to choose between microphysical approaches. The relative advantages and disadvantages of each must be carefully evaluated for both short- and long-term simulations [*Tao et al*., 2009a, 2009b]. It is critical to identify in advance the shortcomings of the representation of each microphysical process and to attempt to improve a given algorithm. However, some defects of the microphysical schemes are an integral part of the design and are thus highly resistant to improvement. Examples of such defects are presented below.

A number of studies have compared these core microphysical approaches (see section 6). The relative merits of bin and bulk schemes were extensively discussed during a meeting held at the Institute of Earth Sciences of the Hebrew University in Jerusalem from 12 to 16 November 2012 under a COST (Cooperation in Science and Technology) Activity ES0905 "Basic concepts for convection parameterization in weather forecast and climate models." The present overview is derived from this meeting. The structure of the survey is as follows. Sections 2 and 3 give the main concepts and basic equations of SBM and bulk parameterization schemes. Section 4 describes the representation of basic microphysical processes in SBM and bulk parameterization schemes. Uncertainties in numerical cloud microphysics are discussed in section 5. In section 6, the results obtained using SBM and bulk parameterizations are compared. Discussions and conclusions are presented in section 7, where perspectives on the development of microphysical schemes are also discussed.

2. SBM: Two Approaches to Representing Size Distributions

The kinetic equations for PSD of the kth hydrometeor type of $f_k(m)$ used in the SBM models can be written in the form

$$\frac{\partial \rho f_k}{\partial t}+\frac{\partial \rho u f_k}{\partial x}+\frac{\partial \rho v f_k}{\partial y}+\frac{\partial \rho (w-V_t(m)) f_k}{\partial z}=\left(\frac{\delta f_k}{\delta t}\right)_{\mathrm{nucl}}+\left(\frac{\delta f_k}{\delta t}\right)_{c/e}+\left(\frac{\delta f_k}{\delta t}\right)_{d/s}+\left(\frac{\delta f_k}{\delta t}\right)_{f/m}+\left(\frac{\delta f_k}{\delta t}\right)_{\mathrm{col}}....+\frac{\partial}{\partial x_j}\left(K\frac{\partial}{\partial x_j}\rho f_k\right) \quad (1)$$

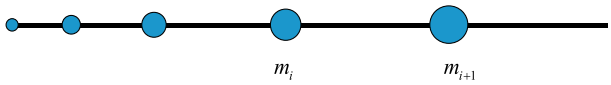

Figure 1. A mass grid used for representation of PSD in the bin microphysical approach.

where u, v, and w are components of wind speed, V_t is the fall velocity that depends on the particle mass, type of the hydrometeor, and the air density ρ. Terms on the right hand of equation (1) determine the rates of different microphysical processes such as nucleation $(\bullet)_{nucl}$, condensation/evaporation $(\bullet)_{c/e}$ (or deposition/sublimation) $(\bullet)_{d/s}$, freezing/melting $(\bullet)_{f/m}$, collisions $(\bullet)_{col}$, etc. The last term determined the changes of PSD due to turbulent mixing with the turbulent coefficient K. The methods of calculation of the rates of microphysical processes are described below.

Due to low concentrations of large hydrometeors, such as raindrops, ice particles, and, especially, hail, a determination of PSDs requires the counting of particles within comparatively large volumes of several tens of cubic meters and more. Accordingly, equation (1) is a result of spatial averaging over corresponding volumes that allows for a description of mixing using the K theory which assumes turbulent (subgrid) fluxes to be proportional to gradients of model-resolved values.

Two main schemes are used to compute the evolution of PSD by equation (1). They will be referred to as *bin microphysics* (hereinafter BM) and the *microphysical method of moments* (hereinafter MMM), respectively. Oftentimes, BM is referred to as SBM.

2.1. BM

This method dates back to the classic studies of *Berry and Reinhardt* [1974a, 1974b, 1974c]. In this method PSD $f(m)$ is defined on the logarithmic equidistance mass grid containing several tens of bins (Figure 1).

An important parameter of the grid is the ratio $m_{i+1}/m_i = \alpha = \text{const}$. In most cloud and cloud-resolving models $\alpha = 2$, but other values are also used, depending on the problem to be tackled and the number of bins being utilized. The advantage of such a grid is that the grid resolution is the highest for small particles, and gradually decreases with an increase in particle mass within a wide range of particle masses. This representation of continuous functions on a mass grid is similar to the representation of continuous functions on spatial finite difference grids in atmospheric models. The concentration of particles N and particle mass content M can be calculated by an appropriate integration of the PSD:

$$N = \int_{m_{\min}}^{m_{\max}} f(m)\mathrm{d}m\,;\; M = \int_{m_{\min}}^{m_{\max}} mf(m)\mathrm{d}m \tag{2}$$

From definition (2) the units of PSD are $\mathrm{g}^{-1}\ \mathrm{cm}^{-3}$. Following *Berry and Reinhardt* [1974a], it is convenient to define another PSD $g(\ln r)$, obeying the normalization condition:

$$M = \int_{\ln r_{\min}}^{\ln r_{\max}} g(\ln r)\mathrm{d}\ln r \tag{3}$$

Here r is the radius of "equivalent" sphere with mass m. The functions $f(m)$ and $g(\ln r)$ are related as $g(\ln r) = 3m^2 f(m)$. The finite difference equivalent of PSD is expressed as [*Berry and Reinhardt*, 1974a]

$$G_i \equiv g(\ln r_i) = 3m_i^2 f(m_i) \tag{4}$$

where i is number of bins and is an integer value. The finite difference representation of (3) on the logarithmically equidistant mass grid means that $\mathrm{d}\ln r = \ln r_{i+1} - \ln r_i = \ln\frac{r_{i+1}}{r_i} = \ln\alpha^{1/3} = \frac{1}{3}\ln\alpha = \text{const}$. So, particle concentrations and mass contents in ith bin can be written in a simple way as $N_i = \frac{1}{3}\ln\alpha\cdot\frac{G_i}{m_i}$ and $M_i = \frac{1}{3}\ln\alpha\cdot G_i$. The total concentration and total mass content are determined as a sum of corresponding values over all bins:

$$N = \frac{1}{3}\ln\alpha\cdot\sum_i \frac{G_i}{m_i};\; M = \frac{1}{3}\ln\alpha\sum_i G_i; \tag{5}$$

Such a representation of the PSD on the discrete mass grid is amenable to numerical simulations. Equation (5) uniquely relates the number concentration and the mass in the bins. The representation of the PSD in the SBM on a mass grid is similar to the representation of different variables on finite difference spatial grids in

any numerical model. The total concentration and total mass are calculated in the SBM using a summation of the corresponding values in the bins based on a rectangular formula (equation (5)).

In the Hebrew University Cloud Model (HUCM), size distribution of condensational nuclei f_{cn} is defined as $N_{cn} = \int_{r_{min}}^{r_{max}} f_{cn}(r)\mathrm{dln}r$, where r is the radius of aerosol particle. The units of f_{cn} are $\#\,\mathrm{cm}^{-3}$. Note also that size distributions for aerosol particles are represented mostly on a logarithmically equidistant mass (radius) grid covering a wide range of aerosol sizes (or masses).

Using equation (1), the kinetic equation for the PSD determined on the mass grid can be represented by a set of equations for the values of the PSD in ith bin:

$$\frac{\partial \rho f_{i,k}}{\partial t} + \frac{\partial \rho u f_{i,k}}{\partial x} + \frac{\partial \rho v f_{i,k}}{\partial y} + \frac{\partial \rho (w - V_t(m_i)) f_{i,k}}{\partial z} = \left(\frac{\delta f_{i,k}}{\delta t}\right)_{\mathrm{nucl}} + \left(\frac{\delta f_{i,k}}{\delta t}\right)_{c/e} + \left(\frac{\delta f_{i,k}}{\delta t}\right)_{d/s} + \left(\frac{\delta f_{i,k}}{\delta t}\right)_{f/m} + \left(\frac{\delta f_{i,k}}{\delta t}\right)_{\mathrm{col}} .... + \frac{\partial}{\partial x_j}\left(K \frac{\partial}{\partial x_j} \rho f_{i,k}\right) \quad (6)$$

Note that $f(m_i)$ is not a conservative variable. In an updraft, the volume of ascending air increases, so the particle concentration decreases. This leads to a change of PSD in updrafts and downdrafts. To advect and sediment PSD, it is necessary to write it in the conservative form of mixing ratios $q_{i,k} = \frac{M_{i,k}}{\rho} = \frac{1}{3}\mathrm{ln}\alpha \cdot \frac{G_i}{\rho}\,[g/g]$, which does not change during vertical displacements. Accordingly, in studies using this PSD representation, advection, sedimentation, and mixing should be performed for $q_{i,k}$, using equations similar to equation (6).

The main particle characteristic in BM schemes is particle mass. In reality, particles of the same mass have different characteristics such as density, capacitance, shape, salinity, fall velocity, and charge. For different purposes these parameters should also be determined. In advanced schemes, ice particles are also characterized by rimed or liquid water fraction [*Benmoshe et al*., 2012; *Phillips et al*., 2014, 2015]. In principle, the growth rates of particles of the same mass (and even of the same hydrometeor class) but of different shape or salinity are different. Strictly speaking, particles of the same mass should be further categorized by other parameters, and multidimensional PSDs should be used. There are several studies that use two-dimensional size distributions. For instance, to investigate the effects of aerosols on drop growth in a boundary layer stratocumulus cloud, *Bott* [2000] used two-dimensional distributions by introducing the categorization of droplets with respect to their solute concentration. To investigate the effects of drop charge on their collisions, *Khain et al*. [2004b] introduced categorization with respect to drop charge. However, the utilization of such multidimensional PSDs is too complicated from both a mathematical and computational point of view. The typical approach used in cloud models is to average the values of other parameters over the particles belonging to a certain mass bin. With this simplification, all particle parameters such as bulk density, equivalent radius (or diameter), shape parameters, and fall velocity are expressed via their mass using empirical relationships [see, for example, *Pruppacher and Klett*, 1997]. As a result, the PSD of a particular hydrometeor type turns out to be one-dimensional, being dependent only on particle mass. In this case, the number of equations for PSDs is equal to the number of bins multiplied by the number of hydrometeor types.

For these and other reasons, SBM may be considered a type of parameterization, and thus, an approximation of reality. However, unlike bulk parameterizations, these microphysical formulations do not involve the explicit averaging over particle spectra (SBM has been referred to as a size-resolved scheme) and use a reduced number of simplifying assumptions.

The advantage of this method is its simplicity. It is amenable to modifications and new implementations. For example, the method allows for the easy implementation of new types of hydrometeors, as well as for the implementation of new parameters of cloud particles. Further, the method permits the utilization of any type of collision kernel, including kernels in a turbulent flow which vary randomly in space and time [*Pinsky et al*., 2008b; *Benmoshe et al*., 2012]. These advantages explain its widespread utilization in different versions of BM in the HUCM, as well as in mesoscale cloud- resolving models such as WRF (Weather Research Forecasting) [*Khain and Lynn*, 2009; *Khain et al*., 2009, 2010], Goddard Cumulus Ensemble (GCE) [*Tao et al*., 2007; *Li et al*., 2009a, 2009b], WRF and SAM (System of Atmospheric Modeling) [*Fan et al*., 2009, 2012a, 2012b, 2013], WRF and JMA-NHM (Japan Meteorological Agency Nonhydrostatic Model) [*Iguchi et al*., 2008, 2012a, 2012b, 2014], SAM

AGU Reviews of Geophysics

10.1002/2014RG000468

Table 3. Characteristics of Different Models Using the SBM Schemes

Authors	Type of SBM, Name of Model	Classes of Hydrometeors	Number of Bins or Categories	Specific Features of Models
Young [1975]	MMM	Five classes: liquid water, freezing water, ice crystals, snowflakes, and graupel.	45	Parcel framework, dynamics is prescribed; number density of drops is linearly proportional to drop radius; number density of ice crystals is linear over axis lengths; simplified description of all microphysical processes.
Khvorostyanov et al. [1989]	BM	Drops, ice particles	33	2-D, the size distributions are defined on the grids linear with the respect to square of particle radii.
Hall [1980]	BM	Drops and ice		Axisymmetric, two size distributions are used: for drops and ice. Density of ice particles increases with their size.
Tzivion et al. [1987] and *Reisin et al.* [1996a, 1996b]	MMM TAU	Drops, ice crystals, snow, and graupel	34	Axisymmetric geometry, Immediate melting at $T>0$.
Kogan [1991]	BM	warm	30 for drops, 19 for CCN	3-D, logarithmically equidistant mass grid.
Ackerman et al. [1995]	BM, DHARMA	warm	50	Logarithmically equidistant grid. Keeping track of the volume of dissolved CCN allows the model to conserve solute mass. Maximum drop radius is 500 μm. The radiative term *is included* in the droplet condensation equation.
Khain and Sednev [1996]	BM HUCM	drops, three types of crystals, snow, graupel, hail, CCN	33	2-D, logarithmically equidistant mass grid as *Berry and Reinhard* [1974a]. CCN budget included. Immediate melting at $T>0$. Solution of SCE using *Berry and Reinhard* [1974a] scheme.
Yin et al. [2000]	MMM TAU	As in *Tzivion et al.* [1987]	36	2-D slab symmetric geometry. Microphysics as in *Tzivion et al.* [1987]. Time-dependent melting of graupel is included. Liquid water shed immediately forming two equal drops.
Khain et al. [2004a] and *Phillips et al.* [2007b]	BM HUCM	As in *Khain and Sednev* [1996]; liquid water in snow, graupel, and hail are included.	33	As in *Khain and Sednev* [1996]; Improved description of collisions [*Bott*, 1998]. Collisional breakup and height-dependent collision kernels between drops as well as between drops and graupel are introduced. Size distributions for water mass within snow, graupel, and hail are implemented.
Muhlbauer et al. [2010] and *Hashino and Tripoli* [2007, 2008, 2011]	MMM UWNMS University of Wisconsin	Drops, pristine crystals (plates), rimed crystals, rimed aggregates, graupel	30 for drops, 20 for ice phase	Only one mass grid is used for all ice phases. Properties of particles belonging to the same category represent a mixture of properties of different hydrometeor types. Contribution of pristine ice crystals dominates in the low mass category; graupel contribute largely to category of large particle mass.
Khain et al. [2008a]	BM HUCM	*Khain et al.* [2004a]; Rimed mass in snow is included	33	As in *Khain et al.* [2004a]. Improved scheme of diffusion growth and size distribution of rimed mass in snow are implemented; snow density is calculated.
Lynn et al. [2005a, 2005b] and *Lynn and Khain* [2007]	BM MM5/SBM	As in *Khain et al.* [2004a]	33	3-D nested grid.
Tao et al. [2007] and *Li et al.* [2009a, 2009b]	BM GCE-SBM	As in *Khain et al.* [2004a]	33	Detailed analysis of formation of squall lines, comparison of bin and bulk schemes; testing sensitivity to fall velocities.
Fan et al. [2009]	BM SAM/SBM	As in *Khain et al.* [2004a] ; IN as a separate hydrometeor	33	As in *Khain et al.* [2004a]; an aerosol-dependent and a temperature- and supersaturation-dependent ice nucleation schemes are implemented; IN size distributions are treated prognostically.
Khain et al. [2010]	BM WRF/SBM-fast	Drops, snow, and graupel/hail	33	3-D nested grid.

Reviews of Geophysics

10.1002/2014RG000468

Table 3. (continued)

Authors	Type of SBM, Name of Model	Classes of Hydrometeors	Number of Bins or Categories	Specific Features of Models
Lebo and Seinfeld [2011]	MMM WRF/MMM	As in *Reisin et al*. [1996a 1996b]	36	3-D, *Long* [1974] collection kernel is used for collisions between drops. For ice-ice, ice-snow, ice-graupel, snow-graupel, snow-snow, liquid-ice, liquid-snow, liquid-graupel, graupel-graupel collisions, the gravitational collection kernel is used.
Khain et al. [2011]	SM	As in *Khain et al*. [2008a]	43	As in *Khain et al*. [2008a]; Improved description of graupel-hail conversion; calculation of polarimetric parameters is included.
Benmoshe et al. [2012] and *Benmoshe and Khain* [2014]	BM HUCM	As in *Khain et al*. [2011]	43	As in *Khain et al*. [2011]; calculation of turbulence intensity and turbulent collision kernels are implemented.
Iguchi et al. [2012a, 2012b]	BM the Japan Meteorological Agency Nonhydrostatic Model (JMA-NHM)	As in *Khain et al*. [2004a]	33	3-D model. The ice nucleation rate was updated following *Cotton et al*. [1986].
Fan et al. [2014]	BM WRF/SBM	As in *Fan et al*. [2009]	33	As in *Fan et al*. [2009]. Improvement of homogeneous freezing. Implementation of simplified procedure of time-dependent melting; melted water is shed immediately.
Phillips et al. [2014] and Ilotoviz et al. (in revision, 2015)	BM HUCM	As in *Khain et al*. [2011]; Freezing drops are included as a new hydrometeor type	43	Detailed time-dependent freezing procedure is included. A size distribution for freezing drops is implemented. Dry and wet growths of hail are considered.
Iguchi et al. [2014]	BM WRF/SBM	As in *Khain et al*. [2011]	33	3-D model.

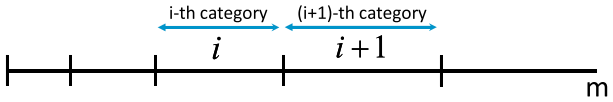

Figure 2. Separation of the mass axis into categories in the moment methods.

[*Ovchinnikov et al*., 2011, 2013, 2014], and RAMS (Regional Atmospheric Mesoscale System) [*Igel and van den Heever*, 2014]. The model acronyms are presented in Table 1. Some properties of models using the BM approach are presented in Table 3.

2.2. The MMM

The MMM is rooted in the work of *Young* [1975] and of *Enukashvily* [1980]. *Tzivion et al*. [1987, 1989], *Feingold et al*. [1988], and *Reisin et al*. [1996a, 1996b] further developed the method, and both axisymmetric and slab symmetric models using the MMM were created. In the MMM, the axis of mass is separated into categories (Figure 2). The boundaries of the categories form a logarithmic equidistance grid. In each category, the PSD is characterized by several moments. *Tzivion et al*. [1987, 1989], for instance, used two moments: mass content and number concentration.

Thus, the equations for each category are formulated not for the PSD, as in case of BM, but for its moments, which are defined for each category as

$$R_i^{(\nu)} = \int_{m_i}^{m_{i+1}} m^\nu f(m) dm \tag{7}$$

One sees that the zero-order moment $R_i^{(0)}$ is particle concentration in *i*th category, the first-order moment $R_i^{(1)}$ is related to mass content in *i*th category and the second-order moment $R_i^{(2)}$ is proportional to the radar reflectivity formed by particles belonging to *i*th category. To calculate these integrals, it is necessary to make some assumptions about the behavior of the size distribution within each category. In the MMM, the PSDs are assumed to be continuous within each category and are assumed to have a linear mass dependence. *Tzivion et al*. [1987, 2001] and many subsequent studies that used the MMM [*Yin et al*., 2000; *Saleeby and Cotton*, 2004; *Xue et al*., 2010, 2012; *Teller and Levin*, 2008; *Teller et al*., 2012] solve a system of equations for the zero and the first moments in each category. The form of the equations is similar to that of equation (6). To calculate the total concentration and mass of a particular hydrometeor, the MMM uses a numerical scheme analogous to a trapezium method for performing integrals (2).

The number of equations in MMM is equal to the product of the number of hydrometeor types, number of categories, and the number of moments used for each category. The MMM requires solving two equations for the moments of each category, and so it operates with twice as many variables as does the BM method. To simplify calculations, *Low and List*'s [1982a, 1982b] kernel with analytical expression is used to describe collisions between cloud particles. *Tzivion et al*. [1987] showed that using 36 categories yields an accuracy of results comparable to those obtained when 72 or even 144 categories are used.

The MMM scheme, originally developed at Tel Aviv University, is used in one form or another at National Center for Atmospheric Research (NCAR) (WRF), Colorado State University (RAMS), National Oceanic and Atmospheric Administration (NOAA), universities in the United States, China, Vietnam, Brazil, and more. The scheme has already been used for studying squall lines [*Ikeda et al*., 2008], orographic clouds [*Muhlbauer et al*., 2010; *Xue et al*., 2010, 2012], deep tropical convection [*Yin et al*., 2012], Mediterranean convective clouds [*Levin et al*., 2003; *Teller and Levin*, 2008; *Teller et al*., 2012], marine stratocumulus clouds [*Stevens et al*., 1996; *Feingold et al*., 1996, 1999; *Hill et al*., 2008; *Chen et al*., 2011], and warm cumulus clouds using LES [*Jiang et al*., 2006]. In its current state, the scheme is highly versatile and can be used for almost any WRF application, from simple 2-D ideal cases [*Rasmussen et al*., 2002] to complicated 3-D real cases [*Teller et al*., 2012]. The MMM and other schemes have been compared in several studies [*Muhlbauer et al*., 2010; *Lebo and Seinfeld*, 2011].

Some properties of models using the MMM approach are presented in Table 3. Both BM and MMM can calculate moments of the entire PSD of any order, according to the definition of the moments. For the sake of convenience, hereinafter, the BM method will be referred to as the SBM and so the two bin approaches will be referred to as SBM and MMM, respectively.

3. Modern Bulk Microphysics Parameterization

3.1. Equation System for PSD Moments in Bulk Parameterization Schemes

Multiplying equation (1) by m^k and integrating over all particle mass spectra, after some simplifications, one gets the equations for the kth PSD moment of the hydrometeor of kth type $M_k^{(k)} = \int_0^\infty m^k f(m)\mathrm{d}m$:

$$\frac{\partial \rho M_k^{(k)}}{\partial t} + \frac{\partial \rho u M_k^{(k)}}{\partial x} + \frac{\partial \rho v M_k^{(k)}}{\partial y} + \frac{\partial \rho \left(w - \overline{V}_{t,k}^{(k)}\right) M_k^{(k)}}{\partial z} = \left(\frac{\delta M_k^{(k)}}{\delta t}\right)_{\mathrm{nucl}} + \left(\frac{\delta M_k^{(k)}}{\delta t}\right)_{c/e} + \left(\frac{\delta M_k^{(k)}}{\delta t}\right)_{d/s} + \left(\frac{\delta M_k^{(k)}}{\delta t}\right)_{f/m} + \left(\frac{\delta M_k^{(k)}}{\delta t}\right)_{\mathrm{col}} \ldots\ldots + \frac{\partial}{\partial x_j}\left(K \frac{\partial}{\partial x_j} M_k^{(k)}\right), \quad (8)$$

where $\overline{V_{t,i}}^{(k)} = \frac{1}{M^{(k)}} \int m^k f(m) V_{t,k}(m)\mathrm{d}m$ is the averaged fall velocity of the kth moment of the PSD. The physical meaning of the terms in equation (8) is similar to that in equation (1), but all rates of microphysical processes are written for the moments of the PSD. The number of equations (8) is equal to the number of moments used in particular bulk parameterization schemes multiplied by the number of hydrometeor types. Thus, the number of equations in bulk parameterization schemes is typically an order of magnitude lower than that in the SBM method.

The current bulk parameterization schemes are much more sophisticated than those developed a decade ago. The new schemes contain more types of hydrometeors and more moments used to describe the PSDs of the hydrometeors (see Table 2). One can see that the number of microphysical variables predicted by bulk parameterization schemes increases over time from 2 in the *Kessler* [1969] scheme to 17 in the *Loftus et al.* [2014] and 18 in the *Milbrandt and Yau* [2005b, 2006].

3.2. Particle Size Distributions and Their Approximation Using the Master Functions

Most bulk parameterization schemes use the gamma distribution as a master function for the approximation of PSDs of different hydrometeors. This distribution has the form [*Seifert and Beheng*, 2001]

$$f(m) = N_0 m^\nu \exp(-\lambda m^\mu) \quad (9)$$

where N_0 is the intercept, ν is the shape parameter, λ is the slope or scale parameter, and μ is the dispersion parameter. The parameters ν and μ determine the shape of $f(m)$ at very small m (initial shape parameter) and for very large m (final shape parameter), respectively.

Note that sometimes radius r or "effective" diameter D is used as the independent variable instead of mass m. In this case, the PSD can be written as [*Ferrier*, 1994; *Milbrandt and McTaggart-Cowan*, 2010]

$$\varphi(D) = N_0' D^{\nu'} \exp\left(-\lambda' D^{\mu'}\right) \quad (10)$$

In the event of a one-to-one relation between radius and mass as for spherical particles, one can easily convert the respective PSDs. Using the relation $m = \frac{1}{6}\pi\rho D^3$ (ρ is bulk density of hydrometeor), one can get the following relations between parameters in equations (9) and (10): $N_0' = 3N_0\left(\frac{1}{6}\pi\rho\right)^{\nu+1}$, $\nu' = 3\nu + 2$, $\lambda' = \lambda\left(\frac{1}{6}\pi\rho\right)^{\mu}$, and $\mu' = 3\mu$. There are only a few theoretical studies attempting to derive expressions for master functions to approximate DSDs. *Yangang et al.* [1995] developed a theory on atmospheric particle systems by introducing Shannon's entropy, extending the classical statistical mechanics into atmospheric particle systems, and connecting the size distributions with the physical and/or chemical laws which control the systems. They obtained that the maximum likelihood distribution of cloud droplets is of the form equation (9) with $\nu' = 2$ and $\mu' = 3$. This is a special case of the Weibull distribution, under the assumptions of dynamically conservative total cloud droplet number and mass. Other expressions for PSD $\varphi(D)$ are also used, for instance [*Saleeby and Cotton*, 2004],

$$\varphi(D) = \frac{N_0''}{\Gamma(\nu'' + 1)\beta^{\nu+1}} D^{\nu''} e^{-D/\beta} \quad (11)$$

In the case of spherical particles, one can easily convert the respective PSDs. However, in the case of nonspherical particles such as pristine ice crystals, the utilization of PSD as a function of mass is more convenient.

The gamma distribution (equation (9)) is equal to zero at $m = 0$, has one maximum, and tends to zero when $m \to \infty$. Since observed drop size distributions have as a rule two modes, the first one corresponding to cloud

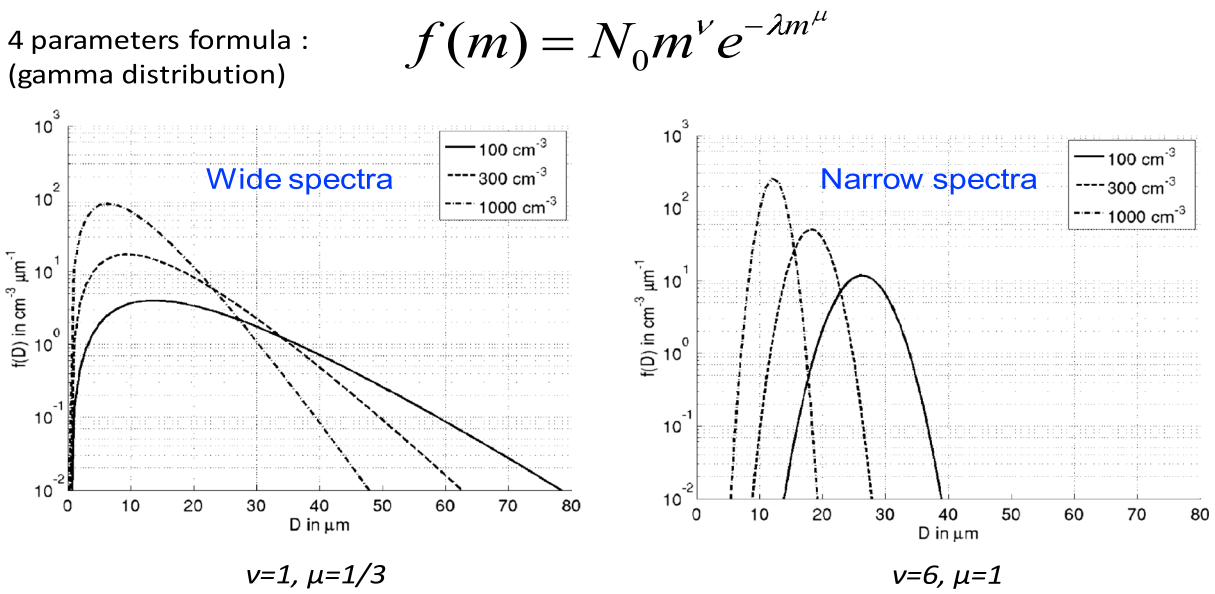

Figure 3. Examples of the gamma distributions chosen for approximation of (left) broad and (right) narrow DSDs. Parameters ν and μ are shown. The values of intercept parameter were chosen in such a way to get desirable concentrations of droplets indicated in the boxes. Solid, dash-dotted, and dotted lines show DSD for maritime, intermediate, and continental conditions, respectively. (From *Noppel et al*. [2010a]; courtesy of the American Geophysical Union.)

droplets with radii below 20–25 μm and centered at $r \sim 10$–15μm and the second one corresponding to raindrops with radii sometimes as large as 3–4 mm [*Pruppacher and Klett*, 1997], size distributions containing both small cloud droplets and raindrops obviously do not obey a single gamma distribution. To avoid this problem, all bulk parameterization schemes, without exception, distinguish between small cloud droplets with a distribution described by equation (9) and raindrops with a distribution typically, although not exclusively, approximated by exponential functions. Thus, liquid drops are represented by two types of hydrometeors: cloud droplets and raindrops. Such a distinction has physical grounds, as the collision process leads to a cloud droplet mode that is separated from the raindrop mode with a well-pronounced minimum located between the modes within the radii range from 25 μm to 60 μm. The drop radius separating cloud droplets and raindrops is typically accepted as equal to 30 μm. The PSD for drops is referred to as the drop size distribution (DSD). Quite often, DSD denotes only the distribution of small cloud droplets, while the distribution of raindrops is referred to as rain size distribution (RSD). Figure 3 shows examples of general gamma distributions used for approximations of wide and narrow DSDs in bulk parameterization schemes. As noted by *Morrison and Gettelman* [2008], a major advantage of using gamma functions is that microphysical process rates can be derived in a straightforward manner. Thus, it must be asked whether gamma functions sufficiently approximate observed PSDs. *Mazin et al*. [1989] demonstrated that DSDs averaged over large distances and over many clouds can be approximated reasonably by a gamma distribution with the droplet diameter serving as the independent variable written in the form (11), with $\nu'' = 2$, known as the Khrigian-Mazin distribution. It is a general practice to describe PSDs of precipitating particles assuming $\nu' = 0$ in equation (10). The obtained PSD is known as the Marshall-Palmer distribution. Such distributions are also obtained by the averaging of measurements over large distances of hundreds of kilometers. Figure 4 shows examples of DSDs measured in situ in deep convective clouds. One can see that local DSDs vary significantly along the flight traverses; many DSDs are bimodal. The existence of bimodal DSDs is regularly reported in observations [*Warner*, 1969; *Korolev*, 1994; *Prabha et al*., 2011]. The DSDs averaged over a flight traverse are often substantially broader than local DSDs and unimodal, as it is illustrated in Figure 4a. In some cases, the averaged DSDs are also bimodal (Figure 4b). Thus, the shape of observed DSDs depends on spatial and time averaging.

Note that the rates of microphysical processes are determined by local DSDs. One can see that the DSDs averaged over long traverses resemble gamma distributions in Figure 3. At the same time, there are obvious differences between the shapes of the observed local DSDs and of the gamma functions.

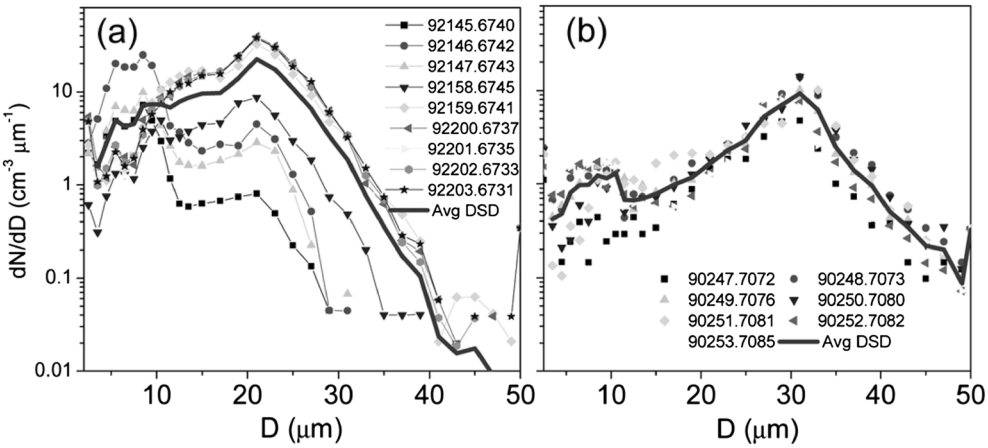

Figure 4. Plots of 1 Hz droplet size distributions measured along a flight pass length during the Cloud Aerosol Interaction and Precipitation Enhancement Experiment (CAIPEEX). (a) DSDs measured 21 June 2009 at the altitude of 6.7 km and (b) DSDs measured 22 June 2009 at altitude of 7 km. Averaged DSDs are denoted by solid lines. First five numbers denote time in seconds, last four numbers denote altitude in meters. (From *Prabha et al.* [2011]; courtesy of the American Meteorological Society.)

Ice particle size distributions above about 50–100 μm as measured by 2-D imaging probes have been represented by exponentials [*Sekhon and Srivastava*, 1970], bimodals [*Mitchell et al.*, 1996; *Yuter et al.*, 2006; *Lawson et al.*, 2006], normalized ice size distributions [*Delanoë et al.*, 2005], the sum of an exponential and gamma [*Field et al.*, 2005], lognormal [*Tian et al.*, 2010], and gamma [*Heymsfield et al.*, 2013] size distributions. In most studies, the PSDs were obtained by the averaging of measurements along traverses of several hundred kilometers and over different clouds. There are many observational uncertainties pertaining to the measurements of the PSDs of ice particles. First, the concentration of ice particles is low, so statistically significant PSDs can only be obtained along lengthy airplane traverses. In these cases, it is difficult to speak about local PSDs. Besides, airborne observations in deep convective clouds are dangerous, so in situ measurements within deep convective precipitating clouds are quite limited. These uncertainties are further discussed in section 5.1.

Because of the observational uncertainties of ice particles within clouds, the results obtained using SBM models are of interest. Justifications for the use of the SBM results include the correct prediction by the models of average concentrations, reasonable agreement of radar reflectivity [e.g., *Iguchi et al.*, 2014], and reasonable agreement of PSDs with the observations in cases when such observations are available [e.g., *Fan et al.*, 2009]. As follows from numerical simulations using SBM models, the *local* PSDs (at spatial scales of a few hundred meters) of aggregates, graupel, and hail can be close to gamma (exponential)- type, bimodal, or of a more complicated shape [*Khain et al.*, 2011; *Phillips et al.*, 2015]. *Ovchinnikov et al.* [2014] showed the importance of the accurate representation of ice PSDs in determining the partitioning of liquid and ice and the longevity of mixed-phase clouds.

In several studies, attempts were made to approximate measured DSDs by gamma, lognormal, and exponential master functions [*Costa et al.*, 2000]. Significant differences regarding droplet concentration and spectrum shape were observed among four different cloud types: maritime, coastal, continental, and "urban" types. The exponential distribution was shown to be unsuitable for most of the observed DSDs. The gamma distributions better approximate the observed DSDs. However, large differences in the width and shape of parameters were found between maritime, coastal, continental, and urban clouds; besides, significant variability in the values of the parameters was observed from cloud to cloud, as well as between different regions within clouds. Figure 5 shows histograms characterizing the occurrence of the shape parameter and scale diameter in all gamma fits. It was also found that for a relatively large number of cases (>10%), no fit was possible. *Costa et al.* [2000] conclude that such variability imposes important limitations on bulk microphysical modeling.

Analyses of observational data done by *Tampieri and Tomasi* [1978] and later by *Dooley* [2008] showed that the shape of DSDs in clouds evolves with time and height in such a way that all parameters of gamma

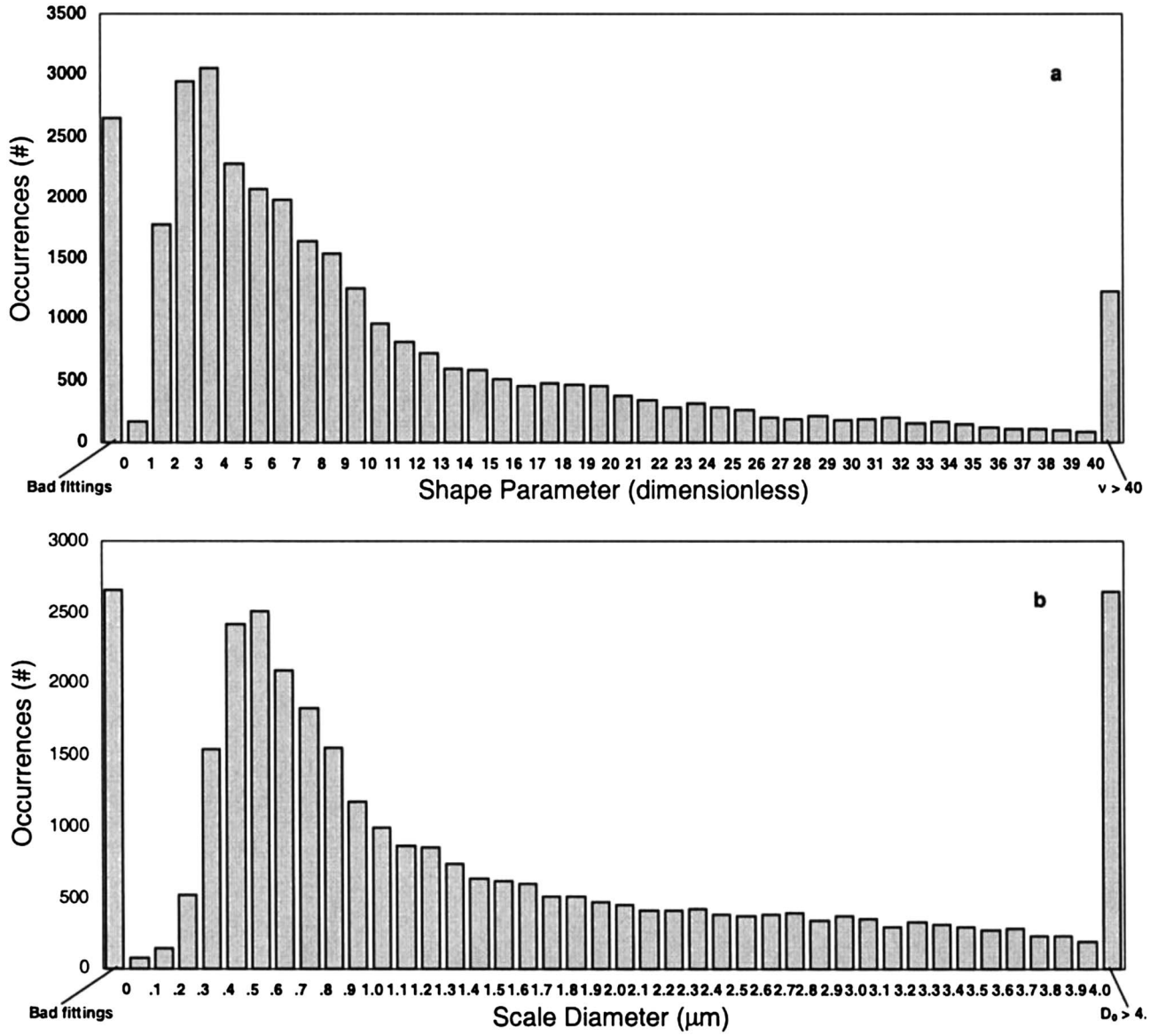

Figure 5. Occurrences of the (top) shape parameter and (bottom) scale diameter in all gamma fits. DSDs were measured in shallow cumuli, Northeast Brazil. (Adapted from *Costa et al*. [2000]; courtesy of Elsevier.)

distributions should be changed to preserve the approximation of DSDs. In this sense, the changes in parameters turn out to be related. This conclusion is illustrated in Figure 6 showing an intercept parameter N_0-slope parameter λ scattering diagram acquired by 10 s gamma fits to observed DSDs. Using the results of in situ measurements in the Cloud Aerosol Interaction and Precipitation Enhancement Experiment (CAIPEEX), India, Prabha (personal communication, 2013) found that the intercept parameter increases with increasing rain rate by 2–3 orders of magnitude.

Geoffroy et al. [2010] tried to relate the values of parameters of lognormal and gamma distributions with the values of DSD moments using DSDs measured in stratocumulus and small cumulus clouds. The dispersion in the values of parameters turned out to be very large, as each microphysical process affects the values of the parameters differently. These researchers tried to decrease the scatter by considering different microphysical processes. However, it was impossible to isolate from observations one process that could be considered most dominant. The researchers concluded that bulk schemes have serious limitations because of the

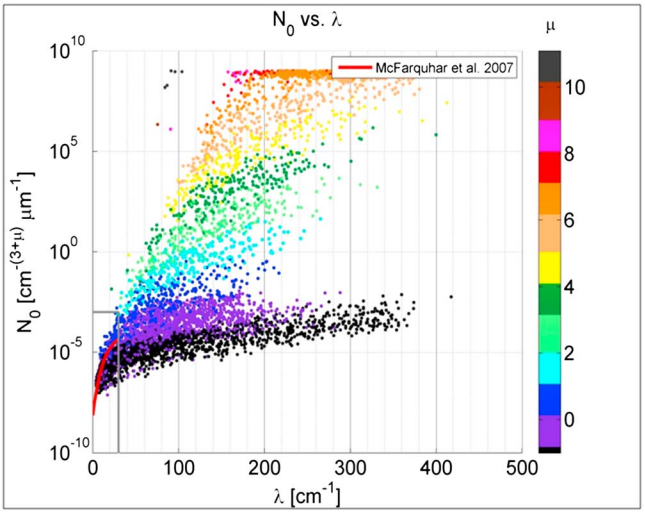

Figure 6. Scatterplots of parameters of gamma distributions used to fit observed DSDs. N_0 and λ acquired by 10 s gamma fits to observed DSDs. The solid red line represents the best fit line for the variation of N_0 versus λ obtained by *McFarquhar et al.* [2007]. (From *Dooley* [2008]; courtesy of Dr. McFarquhar.)

extremely high variability of observed DSD shapes and the corresponding problem in choice of master functions and their parameters. Also, several studies determined the parameters of gamma distributions for constructing Z-R relationships, allowing an estimation of rain rates using radar reflectivity or radar polarimetric parameters [*Illingworth and Blackman*, 2002; *Handwerker and Straub*, 2011]. In these studies too, a strong variability of parameters was noted.

Strictly speaking, to determine four parameters in the expression of a gamma distribution (8), four equations are to be solved. So, four-moment bulk-parameterization schemes should be used. However, state-of-the-art bulk schemes use no more than three PSD moments (see Table 2). So in one-, two-, and three-moment bulk parameterization schemes 3, 2, and 1 parameters, respectively, are either fixed a priori or are determined using additional semiempirical relationships.

3.3. Approaches Used in Bulk Schemes to Improve the Approximation of PSD

The analysis of observed PSDs reviewed thus far suggests that the fixing of parameters does not allow for a good approximation of PSDs by gamma (or exponential) distributions. *Three main approaches* have been suggested to improve PSD approximation by gamma functions in bulk parameterization schemes. The first approach, widely applied in two-moment bulk schemes, involves the implementation of dependencies between parameters of gamma functions similar to those shown in Figure 6. Such relations between the parameters were used in a bulk microphysics scheme by *Thompson et al.* [2004], who derived them from bin microphysics simulations. *Thompson et al.* [2004] used a relationship between N_0 and a rain mass mixing ratio to describe raindrop size distribution. For graupel with a gamma size distribution, the scheme by *Thompson et al.* [2004] presents a relation between the intercept parameter N_0 and slope parameter λ. The shape parameter is fixed. In the most recent version of the Thompson (personal communication, 2014) bulk parameterization, the graupel intercept parameter is a function of supercooled liquid water content and graupel content as shown in Figure 7.

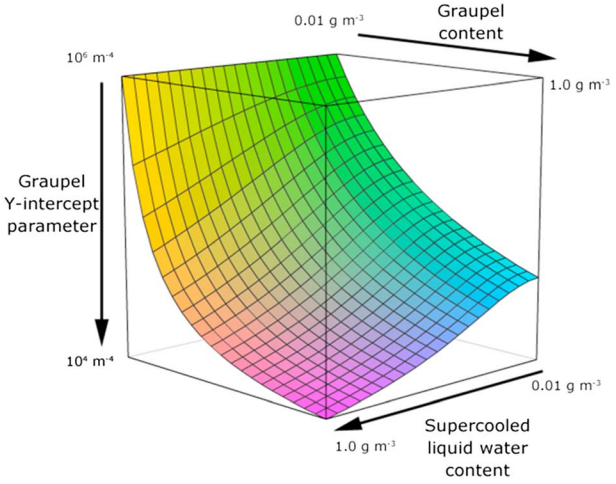

Figure 7. Dependence of graupel intercept parameter on supercooled liquid water content and graupel content in the Thompson bulk parameterization scheme (G. Thompson, personal communication 2014; courtesy of Dr. Thompson).

For snow, *Thompson et al.* [2004] used a relation between N_0 and temperature. *Formenton et al.* [2013a, 2013b] applied a similar idea by deriving an iterative numerical solution for shape, slope, and intercept parameters of a gamma size distribution in a one-moment treatment of snow. These parameters diagnosed from a given snow mass mixing ratio at every grid

point for each time step. *Formenton et al*. [2013a, 2013b] used an observed relation between the parameters of the gamma distributions, obtained by *Heymsfield et al*. [2002] in an analysis of aircraft data from various field campaigns.

The utilization of relationships between parameters of gamma distribution still keeps the PSDs unimodal. Note that shapes of DSDs contain very important information concerning microphysical processes. For instance, the bimodality and multimodality of DSDs may reflect the existence of in-cloud nucleation, when new small droplets arise within a wide range of heights above the cloud base of convective clouds [*Khain et al*., 2000; *Pinsky and Khain*, 2002; *Segal et al*., 2003]. Some observations [*Prabha et al*., 2011, 2012; *Khain et al*., 2012] indicate that such in-cloud nucleation may take place continuously over a significant range of altitudes. These small droplets can be a source of a large number of ice crystals in thunderstorm anvils around the level of homogeneous freezing, can intensify hail and graupel riming and foster lightning formation in clouds [*Rosenfeld and Woodley*, 2000; *Heymsfield et al*., 2009; *Khain et al*., 2012], etc. *Brenguier and Grabowski* [1993] reported the bimodality of DSD caused by droplet activation at cloud edges of shallow clouds through entrainment. *Khain et al*. [2013] found CCN nucleation at the edges of deep convective clouds. Bimodal DSDs in warm stratocumulus clouds were also observed by *Korolev* [1994, 1995] and have been simulated [*Magaritz et al*., 2009, 2010]. So representations of DSD in the form of single-mode gamma distribution may substantially misrepresent cloud microphysical structure and associated microphysical processes.

The second approach to improve the representation of PSDs consists in the implementation of additional modes into the master functions. This approach to improve the representation of the PSD while still using gamma functions is applied in RAMS, where a third liquid water drizzle mode has been implemented [*Saleeby and Cotton*, 2004]. The drizzle mode, which includes droplets with diameters from 50 to 100 μm, is located between the cloud droplets (diameters from 2 to 50 μm) and raindrop (diameters greater than 100 μm) modes. Implementation of the drizzle mode has been found to delay the process of rain formation and has led to significant improvements in simulated precipitation rates when compared with observations. The third (drizzle) mode was also introduced by *Sant et al*. [2013] for the simulation of drizzle formation in a warm stratocumulus cloud. *Thompson et al*. [2008] applied bimodal gamma function for the representation of snow. This approach provides greater flexibility in the construction of the PSD.

The third approach consists of the utilization of three-moment bulk parameterization schemes, thereby allowing for the calculation of three parameters in equations (9)–(11). This approach allowed *Milbrandt and Yau* [2006] and *Loftus and Cotton* [2014b] to simulate large hail, which had been unachievable using two-moment schemes.

Last, but not least, the problem concerning the choice of the master functions is the lack of the necessary volume of in situ observations in deep convective clouds, especially in the mixed phase region, to decide which master functions describe the natural PSDs more adequately. It is possible that parameters of the master functions, as well as the suitable functions themselves, are different for different cloud types and may differ for different aerosol conditions. This may create an additional problem in numerical simulations of cloud systems consisting of multiple types of clouds with different phase composition.

Summarizing this section, we conclude that the use of gamma distributions to represent PSDs appears too simple to adequately describe the variability and some specific features of local PSDs in clouds. At the same time, the answer to the question to what extent errors in the simulation of PSD shape affect model results such as precipitation, temperature, and radiation is not straightforward, because the predicted variables are typically affected by many factors, microphysics being only one of them. Moreover, some of the "integral" quantities (e.g., accumulated precipitation) may be sensitive largely to hydrometeor mass content and concentration, while the exact shape of the PSD may be of secondary importance. We shall discuss this topic briefly in section 6.

4. Representation of Microphysical Processes in SBM and Bulk Parameterization Schemes

In sections 2 and 3 we showed that while in SBM schemes the PSDs are represented by values in a set of points at the mass grid, the bulk parameterizations use a set of PSD moments. Both approaches are legitimate, because according to theoretical considerations the PSD can be fully represented either by an infinite number of discrete points in which the PSD is defined (The Nyquist-Shannon-Kotelnikov sampling theorem [R.J. *Marks II*, 1991]) or by the Gram-Charlier series in which the coefficients are calculated using an infinite number of PSD moments

Table 4. The Main Features of Different Microphysical Processes in SBM and Bulk Schemes

Microphysical Process	SBM	Bulk Parameterization Schemes
Droplet nucleation	Calculation of size distribution of nucleated droplets using size distribution of CCN and supersaturation; droplet nucleation depends on supersaturation history and is allowed both at cloud base and within clouds. Droplet nucleation affects size distribution of aerosols via nucleation scavenging.	Utilization of CCN activity spectrum to calculate droplet concentration at cloud base. Droplet nucleation does not affect the CCN activity spectrum.
Diffusional droplet growth	DSD is calculated by solving the equation for diffusional growth.	Saturation adjustment is used to calculate growth of the liquid water mixing ratio. In advanced schemes, the increase in the liquid water mixing ratio and in the droplet concentration allows for the evaluation of the mean drop radius.
Drop collisions and raindrop production	DSD of drops of all sizes is calculated by solving the stochastic collection equation. Size distribution of raindrops is calculated automatically as part of the entire drop size distribution.	The mixing ratio of raindrops is calculated using expressions for the rates of autoconversion. The expressions are either empirical or derived from solutions of the stochastic collection equation. The shape of the rain water mixing ratio is prescribed.
Collision in mixed-phase and ice clouds	PSDs are calculated by solving stochastic collection equations, where all collisions between cloud particles are calculated.	Mixing ratios (and concentrations) of hydrometeors of different classes are calculated using different parameterization expressions for the conversion of hydrometeors of one class to another.
Sedimentation	Sedimentation is calculated for particles belonging to different bins having different fall velocities. Fall velocities depend on particle mass and hydrometeor class. They also depend on the rate of riming, liquid water fraction, and other factors.	Typically, sedimentation is calculated with fall velocity averaged over all particle sizes. Mass-averaged fall velocity is larger than concentration- averaged fall velocity, so are mass and concentration sediment with different velocities. Bin-emulating schemes use a method resembling that used in SBM.
Freezing and melting	The rates of freezing and melting depend on particle size. Thus, freezing and melting lead to change in PSDs.	The average rates of freezing and melting are calculated by averaging over particles belonging to the same hydrometeor class.

[*Cramér*, 1999]. The accuracy of the PSD approximation is thought to increase in proportion to the number of bins or the number of moments. It is reasonable to expect that to get the same accuracy in the representation of any PSD, the number of moments should be smaller than the number of bins, since moments describe the most important characteristics of the PSD, namely, the zero moment is the particle concentration, the first moment is the mean mass, the second central moment characterizes the PSD width, the third central moment describes the asymmetry of PSD, the fourth central moment characterizes the length of the tail of the distribution and sharpness of the PSD maximum, and so on. Here the central moments are the moments calculated with respect to the mean value of distribution. The question then arises as to how many bins and how many moments should be used to obtain similar accuracy in the description of PSDs and microphysical processes.

This section briefly describes the representation of the main microphysical processes in SBM and bulk parameterization schemes as summarized in Table 4. Significantly, the rates of all microphysical processes are strongly dependent on particle size. The utilization of PSD moments, that is, quantities integrated over the entire size range, leads to some loss of sensitivity of the rates to particle size. We shall see that substantial simplifications related to the replacement of equations for size-dependent PSDs by the equations for one or two moments of the PSD leads to serious problems in the representation of the rates of major microphysical processes.

4.1. Droplet Nucleation

It is known that cloud condensational nuclei (hereinafter CCN) are activated and turn into cloud droplets if their sizes exceed a critical value which is a function of CCN size and supersaturation with respect to water. With higher supersaturation, smaller CCN can be activated. The process of drop nucleation typically occurs in the vicinity of the cloud base, where supersaturation reaches its local maximum. The concentration of nucleated droplets depends on vertical velocity, the size distribution of CCN particles, and, to a lesser extent, on the chemical composition of CCN [*Khain et al.*, 2000; *Dusek et al.*, 2006]. Since the supersaturation maximum near cloud base is not resolved in most cloud and cloud-resolving models, it must be parameterized. Various formulae and lookup tables for the supersaturation maximum value and for the concentration of nucleated droplets have

been proposed [*Ghan et al*., 2011; *Segal and Khain*, 2006; *Pinsky et al*., 2012, 2013]. In order to apply these parameterizations, CCN size distributions (e.g., maritime, continental, background, and urban) must be first specified [*Ghan et al*., 2011].

All observations indicate the existence of the smallest droplets with diameters smaller than 10 μm within clouds at any height above the cloud base. Due to in-cloud nucleation, these droplets form a new, second mode of DSDs. The second mode is sometimes very pronounced, and sometimes, is smoothed (see Figure 4). According to numerical studies by *Pinsky and Khain* [2002] and *Khain et al*. [2012] and an observational study by *Prabha et al*. [2011], the in-cloud nucleation and formation of the second mode is caused by a significant increase in supersaturation in the zones in which vertical velocity rapidly increases with height. Supersaturation value also increases in the areas of effective collection of cloud droplets by raindrops with sequential fallout of raindrops. Unloading in maritime clouds is one of the reasons for an increase in vertical velocity in these clouds. Far above cloud base, in the interior of deep clouds, as the supersaturation in updrafts exceeds the supersaturation maximum near cloud base, nucleation of small CCN takes place. The existence of such small CCN in the atmosphere and their role is discussed in detail by *Khain et al*. [2012].

4.1.1. Spectral Bin Microphysics

Cloud droplet nucleation parameterizations are formulated to be consistent with the particular bin microphysical scheme. In the case of a large number of mass bins (i.e., between several hundreds and 2000) [*Pinsky et al*., 2008a], the exact equation for diffusion growth is solved for each bin, and wet aerosol particles that exceed critical values begin growing as cloud droplets automatically, without applying any specific procedure of droplet nucleation. Smaller wet aerosols remain as haze particles, the size of which is determined by environmental humidity. In order to simulate the growth of wet aerosol particles, diffusion growth is calculated using time steps as small as 0.01 s.

In schemes in which the DSD and size distribution of aerosol particles are determined on a grid containing several tens of bins or categories, and the time step is several seconds, the growth of haze particles cannot be explicitly calculated. Instead, special procedures for droplet nucleation are applied. These procedures are broadly similar in both BM [*Kogan*, 1991; *Khain et al*., 2004a] and MMM schemes [*Yin et al*., 2000]. The procedures require knowledge of the size distribution of dry CCN, which is treated as a separate hydrometeor type, and supersaturation. Using the Köhler theory, the critical CCN radius is calculated for a given chemical composition of CCN. CCN with radii exceeding the critical value are activated and converted to small cloud droplets. Corresponding bins in the CCN size distribution become empty or partly filled. The size of nucleated droplets is determined by either the Köhler theory (for the smallest CCN) or using the results of simulations from a parcel model which are typically considered to be the benchmark of accuracy. The modern version of HUCM uses an analytical approach to calculate the supersaturation maximum near cloud base [*Pinsky et al*., 2012, 2013].

Since SBM schemes calculate CCN size distributions and supersaturation at each grid point, they describe processes of in-cloud nucleation leading to the formation of small droplets at significant heights above cloud base [*Pinsky and Khain*, 2002; *Khain et al*., 2012]. These smallest droplets have a relatively small effect on the formation of the first raindrops (which form aloft from droplets nucleated at cloud base), but they may affect ice microphysics, cloud dynamics, the number concentration of ice crystals in cloud anvils, lightning, and so forth.

4.1.2. Bulk Parameterization Schemes

In most two- and three-moment bulk parameterization schemes, the concentration of nucleated droplets is calculated using different expressions for CCN activity spectra which represent different modifications of the Twomey formula [*Ghan et al*., 2011]. These formulae describe a dependence of the number concentration of activated CCN on supersaturation. The supersaturation near cloud base is calculated either directly in the model grid points or by using expressions for the supersaturation maxima [*Ghan et al*., 2011]. In the numerical weather prediction (NWP) model Consortium for Small-Scale Modeling (COSMO), cloud droplet concentration at cloud base is calculated using lookup tables obtained using a detailed SBM Lagrangian parcel model [*Segal and Khain*, 2006]. These lookup tables relate the droplet concentration with parameters of CCN spectrum and vertical velocity.

Most bulk parameterization schemes do not include the CCN budget, that is, the concentration of CCN does not change in the presence of CCN nucleation. The lack of a CCN budget may lead to significant errors in the representation of cloud microphysics and precipitation (see section 6). In a few new numerical modeling systems, the calculation of microphysical quantities in bulk parameterization schemes is coupled with the

calculation of production and transport of aerosols [e.g., *Lim and Hong*, 2010; *Thompson and Eidhammer*, 2014; *Lang et al*., 2014].

In bulk parameterization schemes, the process of in-cloud particle nucleation is typically not considered in detail. In those bulk parameterization schemes that do take cloud nucleation explicitly into account, the new droplets nucleated at a certain altitude above cloud base must obey the same gamma distribution as other cloud droplets. This means that the new droplets are assumed to be immediately distributed over a wide range of sizes. Such a procedure may lead to the erroneous appearance of large cloud droplets in the DSD and distort the values of effective radius. In real clouds, the effective radius typically increases with height, which allows one to link raindrop formation to the critical value of the effective radius [*Freud et al*., 2008; *Freud and Rosenfeld*, 2012].

In the bin-emulating double-moment bulk scheme utilized in RAMS, the treatment and activation of CCN are very similar to those described in the previous section on bin droplet nucleation. As described above, a Lagrangian parcel model is initially used to perform offline bin calculations, and the critical CCN radius and the size of the nucleated drops are determined using the Köhler theory [*Saleeby and Cotton*, 2004]. Activation of CCN with the 3-D RAMS model then occurs as a function of the model-predicted vertical velocity, temperature, aerosol number concentration, aerosol median radius, and aerosol solubility fraction via the use of lookup tables [*Saleeby and van den Heever*, 2013]. Aerosol sources (such as aerosol regeneration following hydrometeor evaporation) and sinks (such as that following nucleation) are represented, and CCN budgets are carefully maintained. Representation of droplet nucleation in this manner allows for a better representation of secondary nucleation throughout the vertical depth of the cloud and tends to offset some of the above mentioned problems relating to bulk schemes.

4.2. Droplet Growth by Diffusion

After nucleation, the newly formed droplets continue growing through vapor diffusion. This constitutes a key microphysical process. The diffusion growth of droplets is a comparatively slow process as compared with the process of collisions and determines the lifetime of clouds. Diffusional droplet growth is accompanied by latent heat release of condensation, which is the main source of air buoyancy in clouds. A typical free tropospheric sounding is stably stratified with respect to the dry adiabat; thus, convective instability would not be realized without this release of latent heat. The heat budget calculated using SBM cloud models shows that heating due to diffusional droplet growth is the main mechanism responsible for buoyancy and updrafts in convective clouds [*Khain*, 2009; *Tao et al*., 2012]. The rate of droplet growth by diffusion is controlled by supersaturation, which in turn depends on vertical velocity and rate of water vapor absorption on cloud particles.

The rate of the diffusion droplet growth determines the altitude and time of raindrop formation and the comparative contribution of warm rain and ice processes during the cloud lifetime.

4.2.1. Spectral Bin Microphysics

Droplet growth by diffusion as well as deposition growth of ice particles is calculated by solving the classical equations of diffusional growth [*Pruppacher and Klett*, 1997]. In modern SBM models, the equation for the diffusional growth is solved together with the equations for supersaturation, so the value of supersaturation changes during diffusional growth. More specifically, *Lebo and Seinfeld* [2011], *Xue et al*. [2010, 2012], and *Teller et al*. [2012] as well as the bin-emulating bulk scheme of RAMS [*Saleeby and van den Heever*, 2013] treat aerosols in noncloudy air as dry CCN, whereas *Magaritz et al*. [2009, 2010] solve full equations for haze particles, and the evaporation of water leads to the formation of haze particles of high salinity. The methods describing aerosol recycling, i.e., the release of aerosols after drop evaporation, are different. *Magaritz et al*. [2009, 2010] solve full equations for salty particles, and the evaporation of water leads to the formation of haze particles of high salinity. In other models, aerosols in noncloudy air are returned to the atmosphere and once again treated as dry CCN. Accounting for aerosol becoming available through the evaporation of droplets is extremely complicated, especially because of the modification of aerosol chemistry within the droplets resulting from chemical reactions [*Wurzler et al*., 1995]. Simplified formulations were therefore proposed to link the available aerosol mass to the size of evaporated droplets.

The most serious numerical problem arising in SBM models with comparatively few bins is the artificial numerical DSD broadening that occurs while solving the equation of diffusional drop growth on the regular unmovable mass grid. This problem resembles the problem of spatial dispersion of a solution by diffusive finite difference schemes. At each diffusional growth substep, it is necessary to interpolate the DSD to the regular, fixed mass grid. During this interpolation (remapping), some portion of drops are transferred to bins corresponding to masses larger than those that should result from an explicit application of the diffusion growth equation. Eventually, this

may artificially accelerate raindrop formation. Schemes with high DSD broadening [e.g., *Kovetz and Olund*, 1969] lead to rapid rain formation at low levels, even in clouds developing under high aerosol concentration conditions. There were several attempts to decrease such broadening in SBM schemes. For instance, *Khain et al*. [2008a] proposed a method of remapping in which three DSD moments are conserved. This method substantially decreases artificial broadening and allows for the simulation of height dependence of the DSD width.

Another good way to avoid the problem of artificial DSD broadening is the utilization of a movable mass grid at which the DSD is defined. In this method, the masses corresponding to the centers of the bins increase (in case of condensation) or decrease (in case of evaporation) according to the equation of diffusion growth. As such a method does not require remapping, the consequent description of the condensation process is very accurate. The movable mass grids are used largely in Lagrangian parcel models or trajectory ensemble models [e.g., *Pinsky and Khain*, 2002; *Pinsky et al*., 2008a; *Magaritz et al*., 2010].

4.2.2. Bulk Parameterization

Most bulk parameterization schemes do not use an explicit equation for diffusional growth to calculate droplet growth by condensation. Instead, the hypothesis of saturation adjustment is typically applied according to which supersaturation over water is forced to zero at the end of each time step [*Tao et al*., 1989; *Straka*, 2009]. The typical procedure of the saturation adjustment is the following. After advection substep new temperature T and mixing ratio q are calculated. The mixing ratio is compared to the saturation value $q_s(T)$. If $q > q_s(T)$, (i.e., supersaturation takes place) a simple iteration procedure is performed during which q decreases and T increases, so to the end of the procedure $q_{new} = q_s(T_{\text{new}})$. Then the difference $q - q_{\text{new}}$ is added to cloud water content. This procedure does not depend on aerosols, so CWC will be the same at any CCN concentration. New parameters of the gamma distributions are then calculated using the droplet concentration obtained as a result of nucleation and the new drop mass content. Note that in convective updrafts, supersaturation never falls to zero and in contrast, may reach several percents as a result of an increase in vertical velocity and a decrease in drop concentration by collisions [*Khain et al*., 2012; *Prabha et al*., 2011]. The application of saturation adjustment under these conditions leads to an overestimation of the condensate mass and latent heat release at each time step, and hence may lead to an overestimation of vertical velocity and rate of convective precipitation. It is known that supersaturations in convective clouds arising in clean air are larger than in polluted clouds. Saturation adjustment that eliminates supersaturation decreases sensitivity of the bulk schemes to aerosols (see section 6.8).

One of the ways to improve bulk parameterization schemes is to avoid the procedure of saturation adjustment. Some steps in this direction were described by *Chen and Liu* [2004] and *Straka* [2009]. There are some exceptions to this treatment of supersaturation in bulk parameterization schemes. In the RAMS model, for example, the diffusional growth equation is solved, and hence, supersaturation is not forced to zero at the end of each time step, thereby leading to better representations of condensate production and latent heating, particularly within deep convection. *Phillips et al*. [2007a] predicted the in-cloud supersaturation and diffusional growth of all hydrometeors in a two-moment bulk scheme, treating in-cloud droplet activation. The procedure involves a linearized scheme for calculation of supersaturation and some subcycling of the time integration for diffusional growth.

4.3. Collisions Between Cloud Particles

4.3.1. Drop Collisions

Drop collision is one of the most important processes in raindrop formation.

4.3.1.1. Spectral Bin Microphysics

The evolution of DSD, $f(m)$, by collisions of liquid drops while neglecting drop breakup is described by the stochastic collection equation (SCE) [*Pruppacher and Klett*, 1997; *Ramkrishna*, 2000].

$$\frac{df(m,t)}{dt} = \underbrace{\int_0^{m/2} f(m')f(m-m')K(m-m',m')\,dm'}_{\text{GAIN}} - \underbrace{\int_0^{\infty} f(m)f(m')K(m,m')\,dm'}_{\text{LOSS}} \tag{12}$$

The first integral on the right-hand side of equation (12) is known as the gain integral (GAIN) that describes the rate of generation of drops with mass m by coalescence of drops with masses m' and $m - m'$. The second

integral is the loss integral (LOSS) which describes the decrease in the concentration of drops with mass m. The gravitational collection kernel $K_g(m, m')$ is

$$K_g(m_1, m_2) = \frac{\pi}{4}(D_1 + D_2)^2 E(m_1, m_2)|V_{t1} - V_{t2}| \tag{13}$$

where $E(m_1, m_2)$ is the collection efficiency between drops with masses m_1 and m_2. In all BM schemes, collisions are calculated by solving equation (12). The collection kernel $K_g(m, m')$ depends on the mass of the collecting drops (which automatically takes into account the effects of drop shape). The collision kernel in the case of gravitational collisions increases with height. This increase in the kernel is caused by an increase in the difference in the terminal fall velocities that occur with a decrease in air density. *Pinsky et al.* [2001] showed that an increase in the difference in the fall velocities also leads to an increase in collision efficiency. As a result, for some droplet pairs, the collision kernel at the altitude of 5–6 km is twice as large as that at the surface.

Clouds are zones of enhanced turbulence. In turbulent flows, the collision kernel increases in relationship to the intensity of turbulence and drop (or ice particles) inertia (i.e., the mass). In deep convective clouds, the collision kernel for some droplet pairs can increase 5–10 times [*Ayala et al.*, 2008; *Pinsky et al.*, 2008b; *Devenish et al.*, 2012]. *Benmoshe et al.* [2012] simulated the evolution of convective clouds where collisions were calculated using the collision kernel $K_{\text{turb}}(m_1, m_2, \varepsilon, Re_\lambda)$ parameterized as a function of four parameters: $K_{\text{turb}}(m_1, m_2, \varepsilon, Re_\lambda) = K_g(m_1, m_2) \cdot P_{\text{kern}}(m_1, m_2, \varepsilon, Re_\lambda) \cdot P_{\text{clust}}(m_1, m_2, \varepsilon, Re_\lambda)$, where ε and Re_λ are the dissipation rate and the Taylor microscale Reynolds number, respectively; P_{kern} and P_{clust} are collision enhancement factors related to the effects of turbulence on the hydrodynamic interaction between droplets and on the droplet clustering, respectively. The values of ε and Re_λ are calculated at each time step and at each point of the spatial grid. Then the values of P_{kern} and P_{clust} are calculated using lookup tables presented by *Pinsky et al.* [2008b].

There are several methods of solving the SCE [*Khain et al.*, 2000; *Straka*, 2009]. In the current version of HUCM, *Bott*'s [1998] scheme is used. In the MMM, equation (12) is integrated within each category to get equations similar to equation (12) but for the PSD moments within the categories.

Bott's [1998] method, as well as those applied in the MMM [*Tzivion et al.*, 1987; *Wang et al.*, 2007] are accurate and in accordance with known analytical solutions [*Golovin*, 1963; *Feingold et al.*, 1988]. Since equation (12) is solved explicitly for the entire drop spectra without separating it into cloud droplets and raindrops, the problems of treatment autoconversion, accretion, and other processes related to droplet-raindrop conversion do not arise. Some properties of equation (12) are discussed below in section 5.

4.3.1.2. Bulk Parameterization

It is accepted practice to distinguish the following types of collisions in the mixture of cloud droplets and raindrops (Figure 8): self collection (sc) denotes the collisions of drops belonging to the same type of hydrometeors, autoconversion (au) is the process of collisions of two cloud droplets resulting in raindrop formation, and accretion (ac) is the process of collisions between raindrops and cloud droplets leading to the growth of the raindrops.

Using equation (12), one can derive expressions for the PSD moments describing the rates of the corresponding microphysical processes [*Beheng*, 2010]:

$$\left(\frac{\partial M^{(k)}}{\partial t}\right)_{\text{au}} = -\int_{m'=0}^{m^*} \int_{m''=m^*-m'}^{m^*} f(m')f(m'')K(m', m'')(m')^k \mathrm{d}m''\mathrm{d}m' \tag{14}$$

$$\left(\frac{\partial M^{(k)}}{\partial t}\right)_{\text{ac}} = -\int_{m'=0}^{m^*} \int_{m''=m^*}^{\infty} f(m')f(m'')K(m', m'')(m')^k \mathrm{d}m''\mathrm{d}m' \tag{15}$$

$$\left(\frac{\partial M^{(k)}}{\partial t}\right)_{\text{sc}} = \frac{1}{2}\int_{m'=0}^{m^*} \int_{m''=0}^{m^*-m'} f(m')f(m'')K(m', m'')\left[(m' + m'')^k - 2(m')^k\right]\mathrm{d}m''\mathrm{d}m' \tag{16}$$

Equations (14) and (15) represent the loss integrals in the stochastic collision equations written for the corresponding moments of cloud droplets and raindrops, while equation (16) represents the gain integral showing the rate of raindrop production.

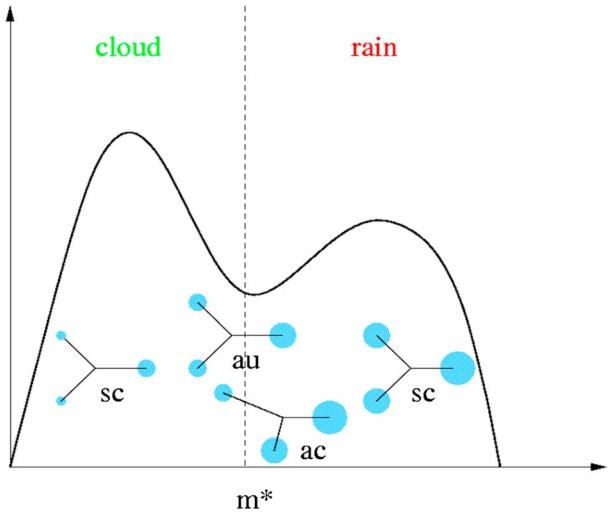

Figure 8. Schematic separation of drop spectrum into cloud droplets and raindrops and definition of collision processes components: "sc" - self collection, "au" - autoconversion, "ac" - accrétion. The m^* is the mass separating cloud droplets and raindrops. (Fom *Beheng* [2012], Jerusalem Workshop; courtesy of Dr. Beheng.)

A major difficulty is found in writing down the autoconversion term in a closed analytical form under a bulk formulation [cf. *Yano and Bouniol*, 2010]. Thus, the following discussion also addresses this process. More difficulties are encountered when a mixed phase is considered, as is further discussed in section 4.3.2. On the other hand, it is relatively straightforward to write the accretion term in a closed analytical form, and the self collection term is usually not considered in bulk approaches.

Kessler [1969] proposed the first empirical parameterization of the process of autoconversion. This was subsequently used in a great number of bulk parameterization schemes. According to *Kessler* [1969], the rate of rain mass production due to droplet collisions is proportional to cloud droplets mixing ratio (or cloud water content, CWC) q_c:

$$\left(\frac{\partial M^{(1)}}{\partial t}\right)_{au} = \frac{\partial q_r}{\partial t} = \begin{cases} k(q_c - q_{cr}), & \text{if } q_c > q_{cr} \\ 0 & \text{otherwise} \end{cases} \tag{17}$$

In equation (17) q_c and q_r are cloud and rain water contents, k and q_{cr} are model parameters to be calibrated to simulate rain formation in different clouds. The threshold value q_{cr} is often chosen equal to values from 0.5 to 1gcm^{-3}; $k = 10^{-3}\text{s}^{-1}$ [*Straka*, 2009]. Despite the fact that this formula does not take into account the shape of the DSD, it is widely used in bulk parameterization schemes [*Lin et al.*, 1983; *Reisner et al.*, 1998]. Equation (17) predicts similar raindrop production rates when the CWCs are the same, even if different DSDs are assumed. At the same time, as has been shown in many studies, rain production dramatically depends on DSD parameters, even under the same CWC. For instance, when aerosol concentration is high, cloud droplets are small, but the CWC is also high. In this case, the rain production should be low despite the high CWCs, because collisions between small droplets are inefficient and because a very high number of collisions are required to form a raindrop. To parameterize effects of aerosols when using equation (17), it is necessary to apply high values of q_{cr} for polluted clouds and low values of q_{cr} for clouds developing in a clean atmosphere. The Kessler formula is both simple and amenable to such utilization. At the same time, the linear expression (17) is completely unrelated to the solution of nonlinear SCE (12). Specifically, this scheme makes the incorrect assumption that fixed collection efficiency is independent of droplet size. Several Kessler-type schemes have been developed to improve the original Kessler parameterization. For instance, *Liu et al.* [2006] generalized equation (17) to explicitly account for the droplet concentration and relative dispersion of cloud DSD.

In most two-moment bulk parameterization schemes, the rate of autoconversion is calculated using expressions based on the work of *Berry and Reinhardt* [1974b]. These researchers derived their parameterization by analyzing the results of a limited number of numerical solutions of equation (12) using collision efficiencies presented by *Hocking and Jonas* [1970]. The latter are not currently considered very accurate. The values of the

collision efficiencies calculated in the study differ significantly from those reported by *Pinsky et al.* [2001] and *Wang et al.* [2005]. Besides, the range of conditions used by *Berry and Reinhardt* [1974b] was quite narrow. Indeed, they took the initial DSD in the form of the gamma distribution, the initial mean volume radius was varied from 10 μm to 18 μm, and LWC was taken equal to 1 gm^{-3}. During the simulations, the time Δt_{au} during which the mean drop radius reaches 50 μm was determined. The rate of autoconversion was determined as a ratio of the rainwater mass to Δt_{au}. As emphasized by *Beheng and Doms* [1986], the Berry and Reinhardt autoconversion relation does not discriminate between autoconversion and accretion.

Since the parameterization is based on comparatively few simulations that were performed using only one value of LWC, *Berry and Reinhardt* [1974b] stressed that extrapolation of their results to other cases should be made with care. This gave rise to the development of more than 10 Berry and Reinhardt-like parameterizations [*Gilmore and Straka*, 2008]. These parameterizations differ in regard to their assumptions concerning the initial DSD shape and in the use of different definitions of the characteristic time scale of the formation of the first raindrops [*Cohard and Pinty*, 2000; *Milbrandt and Yau*, 2005a, 2005b]. Despite the fact that most formulae for autoconversion are applicable to the initial stage of the first raindrop formation only, the rates predicted by these formulae differ by orders of magnitude [*Gilmore and Straka*, 2008]. These large differences between predictions can be attributed to the highly nonlinear nature of the SCE, where rates depend on DSD shape, its change over time, and on mass content.

To the best of our knowledge, only *Seifert and Beheng* [2001] have developed a scheme that treats raindrop production at later time instances when raindrop diameter exceeds ~80 μm. To take into account the time evolution of the autoconversion process during a typical rain event, as well as to use a more realistic collision kernel, these researchers introduced "universal functions" that vary with the fraction of rain drop mass within the total LWC. The universal functions were derived by comparison with the exact solution of SCE when using a specific type of collision kernel, known as the Long kernel [*Long*, 1974]. If other kernels are used, the expressions for the universal functions should be reconsidered.

The RAMS model solves the full stochastic collection equations, rather than making use of continuous growth assumptions or some of the other approaches just described. The evolution of the representation of droplet collisions within the bin-emulating bulk scheme of the RAMS model is rather interesting and is described in detail by *Saleeby and Cotton* [2004]. *Verlinde et al.* [1990] showed that analytical solutions to the collection equation were possible for the predictions of hydrometeor mixing ratios and number concentrations if the collection efficiencies are held constant, an approximation that is also made in those bulk schemes based on *Kessler* [1969]. *Walko et al.* [1995] and *Meyers et al.* [1997] implemented this approach in the earlier single- and double-moment versions of RAMS, respectively. The computational efficiency afforded by the use of lookup tables demonstrated that it was no longer necessary to assume constant or average collection efficiencies, and hence, that the full stochastic collection equations could be solved using the bin scheme within the Lagrangian parcel model, as described above. The lookup tables were calculated using the collection kernels of *Long* [1974] and *Hall* [1980]. *Feingold et al.* [1999] demonstrated that the closest agreement was found between full-bin representation of microphysics and the bulk scheme in simulations of marine stratocumulus clouds, when collection and sedimentation were represented using this bin-emulating approach.

As mentioned above, the collision kernels vary with the height and the intensity of turbulence, that is, they vary with time and in space. Effects of turbulence on the collision kernels in a bulk parameterization scheme were taken into account by *Seifert et al.* [2010]. The following procedure was used. A long set of simulations with a bin microphysics model was carried out in which the SCE equation was solved using the *Ayala et al.* [2008] kernel under different values of dissipation rate, that is, cloud water content, mean radius of cloud droplets and shape parameter ν in equation (1). In total, more than 10,000 simulations were performed. The rates of autoconversion were calculated for each simulation. A complicated expression for the autoconversion rate-enhancement factor was derived from a comparison of autoconversion rates calculated in turbulent and gravitational cases. Thus, to change the collision kernel in the bulk parameterization schemes, it was necessary to derive a new parameterization of autoconversion using numerous simulations obtained with a bin microphysics model.

4.3.2. Collisions in Mixed-Phase and Ice Clouds

Collisions in mixed-phase clouds determine the formation and growth of aggregates (snow), graupel, and hail. Hence, these collisions are responsible for precipitation in mixed-phase clouds.

4.3.2.1. Spectral Bin Microphysics

Collisions in mixed-phase clouds in the BM and MMM models are based on equation (12) (or on its analogs written for the PSD moments in each category) extended to collisions between hydrometeors of different types. Typically, droplet-ice collisions are the most important process in the formation of graupel and hail in mixed-phase convective clouds. In many studies using BM [e.g., *Khain and Sednev*, 1996; *Khain et al*., 2004a, 2013; *Fan et al*., 2009, 2012a, 2012b; *Iguchi et al*., 2008, *Iguchi et al*., 2012a, 2014; *Ovchinnikov et al*., 2013] the collision kernels between drops and ice particles of different densities are assumed to be equal to those between two spheres of corresponding densities. These kernels were calculated by solving the problem of the hydrodynamic interaction between particles within a wide range of Reynolds numbers [*Khain et al*., 2001]. The collection kernels between ice crystals and water drops are taken from *Pruppacher and Klett* [1997]. The collision kernels between ice crystals in these studies are calculated under the simplifying assumption that particles fall with their maximum cross-section oriented perpendicular to the direction of their fall. In recent studies [e.g., *Benmoshe et al*., 2012; *Phillips et al*., 2014, 2015], collision kernels are calculated taking into account the dependence of fall velocities of ice particles on the amount of rimed or liquid fractions as well as on the roughness of the particle surface. *Li et al*. [2010] compared the results of the GCE/SBM with Tropical Rainfall Measuring Mission (TRMM) observations and introduced corrections into the density and terminal fall velocity of aggregates. A breakup scheme for large aggregates was introduced. As a result, a substantially better agreement with observations was achieved. This study showed that long-term satellite observations, especially those with multiple sensors, can be very useful in constraining model microphysics.

As mentioned above, equation (12) is strictly valid only when the concentration of particles in each bin is sufficiently large. At the same time, the concentration of large hail can be quite small. In this case, *Bott*'s [1998] procedure of solving equation (12) is reduced to solving the equation of continuous growth that is suitable under low concentrations of large particles.

4.3.2.2. Bulk Parameterizations

Collisions in mixed-phase clouds represent especially complicated problems for bulk parameterization schemes. In mixed-phase clouds, the collision of particles belonging to hydrometeors of type X and Y can lead either to the formation of particles of type Z ($X+Y\rightarrow Z$) or to type X ($X+Y\rightarrow X$). Examples of the collisions $X+Y\rightarrow Z$ are those between snow and raindrops resulting in graupel formation. Examples of collisions $X+Y\rightarrow X$ are collisions between graupel and drops that lead to graupel growth (riming). Equations for the time evolution of the moments of PSDs of collecting particles $M_x^{(k)}$, collected particles $M_y^{(k)}$, and resulting hydrometeor $M_z^{(k)}$ can be written as [*Seifert and Beheng*, 2006a]

$$\left(\frac{\partial M_x^{(k)}}{\partial t}\right)_{x+y->z} = -\int_0^\infty\int_0^\infty K_{xy} f_x(m_x) f_y(m_y) m_x^k \mathrm{d}m_x \mathrm{d}m_y \tag{18}$$

$$\left(\frac{\partial M_y^{(k)}}{\partial t}\right)_{x+y->z} = -\int_0^\infty\int_0^\infty K_{xy} f_x(m_x) f_y(m_y) m_y^k \mathrm{d}m_x \mathrm{d}m_y \tag{19}$$

$$\left(\frac{\partial M_z^{(k)}}{\partial t}\right)_{x+y->z} = \int_0^\infty\int_0^\infty K_{xy} f_x(m_x) f_y(m_y) (m_x+m_y)^k \mathrm{d}m_x \mathrm{d}m_y \tag{20}$$

where the collision kernel is given by equation (13). The integrals (18) and (19) describe a decrease in concentration ($k=0$) and mass content ($k=1$) of hydrometeors of X and Y types. Equation (20) represents the rate of the increase in the concentration and in the mass contents of hydrometeors of type Z. The integrals 18–20 are analogs of equations (14)–(16) written for drop collisions.

In different bulk parameterization schemes, the integrals 18–20 (as well as equations (14)–(16)) are treated differently. Since these integrals cannot be solved analytically, several simplifications (or approximations) are used. The first simplification is that the collection efficiencies E_{xy} are replaced by a mean value $\bar{E}_{xy}$, that is, an averaged or effective collection efficiency between hydrometeors of types X and Y. This value can then be moved in front of the integrals. The second simplification is that the difference in fall velocities needed for calculation of collision kernels is also replaced by a mean value

Table 5. Expressions for Calculation of $\overline{|\Delta V_{xy}|}$ Used by Different Authors[a]

Number of Formula	References	Expressions for $\overline{\lvert\Delta V_{xy}\rvert}$
F1	*Cotton et al.* [1986]	$\overline{V_x}$
F2	*Wisner et al.* [1972] and *Cotton et al.* [1986]	$\lvert\overline{V}_x - \overline{V}_y\rvert$
F3	*Murakami* [1990], *Milbrandt and Yau* [2005a, 2005b], and *Morrison et al.* [2005a, 2005b]	$\sqrt{(\overline{V}_x - \overline{V}_y)^2 + 0.04\overline{V}_x\overline{V}_y}$
F4	*Mizuno* [1990]	$\sqrt{(1.2\overline{V}_x - 0.95\overline{V}_y)^2 + 0.08\overline{V}_x\overline{V}_y}$
F5	*Murakami* [1990], *Mizuno* [1990], and *Seifert and Beheng* [2006a, 2006b]	$\left[\frac{1}{F_n}\int_0^\infty\int_0^\infty [V_x(m_x) - V_y(m_y)]^2 D_x^2 D_y^2 f_x(m_x) f_y(m_y) m_y \mathrm{d}m_x \mathrm{d}m_y\right]^{1/2}$ where $F_n = C_n N_x N_y D_x^2(\overline{m}_x) D_y^2(\overline{m}_y)\overline{m}_x$; C_n is a constant.
F6	*Flatau et al.* [1989] and *Ferrier* [1994]	$\left\{\frac{1}{F_n} N_x N_y \overline{m}_x \left[C_1\overline{V}_x^2 - 2C_2\overline{V}_x\overline{V}_y + C_3\overline{V}_y^2\right]\right\}^{1/2}$ where $F_n = \int_0^\infty\int_0^\infty (D_x(\overline{m}_x) + D_y(\overline{m}_y))^2 f_x(m_x) f_y(m_y) m_x \mathrm{d}m_x \mathrm{d}m_y$

[a] D_x and D_y are particle diameters; constants C_n, C_1, C_2, and C_3 in Table 5 depend on parameters of PSDs [*Straka*, 2009].

$\overline{|\Delta V_{xy}|}$. This value can then be removed from the integral as well. As a result, equations (18)–(20) are simplified. For example, equation (20) can eventually be written as

$$\left(\frac{\partial M_z^{(k)}}{\partial t}\right)_{x+y->z} = \frac{\pi}{4}\overline{|\Delta V_{xy}|}\overline{E}_{xy}\int_0^\infty\int_0^\infty f_x(m_x) f_y(m_y)(m_x + m_y)^k \left(D_x^2 + D_y^2\right)\mathrm{d}m_x \mathrm{d}m_y \tag{21}$$

The diameters of particles in equation (19) must be expressed as functions of mass. It can be seen that the rates of conversions 18–20 depend on the values of $\overline{|\Delta V_{xy}|}$. Different bulk parameterization schemes use different formulas to calculate $\overline{|\Delta V_{xy}|}$ (see Table 5). To ease these calculations, it is often assumed that the fall velocity of the collector particle is much higher than that of the collected particles, so that the velocity of collected particles can be neglected. For instance, the fall velocity of the collected drops during riming is often neglected as compared to the fall velocity of ice particles [e.g., *Cotton et al.*, 1986]. In this case $\overline{V}_y \ll \overline{V}_x$, and one can use the approximated formula (F1) in Table 5. Such a simplification is typically used in one-moment bulk parameterization schemes, where $\overline{V}_x$ and $\overline{V}_y$ are mass weighted fall velocities.

In some schemes [e.g., *Wisner et al.*, 1972; *Cotton et al.*, 1986] it is assumed that $\overline{|\Delta V_{xy}|}$ is equal to the absolute value of the difference between the mass-weighted or concentration-weighted fall velocities (equation (F2) in Table 5). This expression, used in many bulk parameterization schemes, is not only a mathematically crude approximation but it also leads to the physical paradox of vanishing in the case of self collisions. According to this formula, there are no collisions between hydrometeors belonging to the same type. Since large snowflakes have an average fall velocity close to the average fall velocity of small raindrops, utilization of this expression also may erroneously discount snow-raindrop collisions, in spite of the fact that for particular snow-raindrop pairs the fall speeds of colliding particles are different and collisions can take place. To avoid this problem, many bulk parameterization schemes [e.g., *Milbrandt and Yau*, 2005a; *Morrison et al.*, 2005a, 2005b] use the formula proposed by *Murakami* [1990] (equation (F3) in Table 5). The coefficient of 0.04 in formula (F3) is introduced to avoid the physical paradox of vanishing of collisions in case $\overline{V}_x = \overline{V}_y$. The terms with the coefficient 0.04 in (F3) as well as with the coefficient 0.08 in (F4) characterize the value of dispersion of fall velocities within the particles belonging to hydrometeors of the same type. *Mizuno* [1990] proposed a similar approximation of $\overline{|\Delta V_{xy}|}$ (equation (F4) in Table 5). To get a better approximation of the collision rate, *Seifert and Beheng* [2006b] use r.m.s values instead of mean absolute values (equation (F5) in Table 5). *Flatau et al.* [1989] and *Ferrier* [1994] calculated $\overline{|\Delta V_{xy}|}$ using equation (F6) that has the same meaning as (F5). The advantage of the last two parameterizations is that they take into account specific forms of PSDs, obtained in current model calculations. The substitution of the expressions for PSDs with exponential or gamma-type relations into collision integrals like equation (21) lead to quite complicated expressions for collision rates [e.g., *Seifert and Beheng*, 2006a, 2006b].

Significant problems arise in the application of the bulk parameterization approach to the case of self collection of the type $X + X \rightarrow X$ (e.g., snowflakes) because in this case there is no difference between the averaged fall

velocities. One can expect that the application of different representations of $\overline{|\Delta V_{xx}|}$ in bulk parameterization schemes will lead to a great deal of variability in results of the bulk parameterization schemes.

In bin-emulating bulk schemes (such as in RAMS) the collision integrals equations (18)–(20) are calculated numerically. To reduce the computational cost when first using the single-moment bulk scheme, *Walko et al*. [1995] assumed collection efficiencies to be constant, calculated a large number of solutions for the integrals, and compiled 3-D lookup tables. Two of the table dimensions are the characteristic diameters of colliding particles. The third dimension is the value of the integrals for particle pairs which result from collisions between the seven types of liquid and ice particles used in RAMS. As soon as the calculations are performed, the parameters of the gamma distributions are calculated using number concentration and mass content at each model grid point. In the more recent versions of RAMS, the full stochastic collection equations are solved for all of the interactions among all liquid and ice species without assuming constant collection efficiencies, as described in the previous section.

Recent measurements of the tops of convective storms provide growing evidence that electrostatically induced aggregation may play an important role in the enhanced growth of ice particles and subsequent rapid precipitation formation. Unfortunately, there are no laboratory experiments exploring this mechanism.

4.4. Sedimentation

Sedimentation determines to a large extent the microphysical structure of clouds, as it determines the sorting of hydrometeor particles with respect to their size (*size sorting*) in the vertical direction and affects other microphysical processes such as collisions and growth/evaporation. Sedimentation also determines the amount of surface precipitation.

4.4.1. Spectral Bin Microphysics

Sedimentation of all particles in SBM is calculated by solving the following equation for the PSD:

$$\frac{\partial f_{i,k}}{\partial t} = \frac{\partial V_{t\_i,k}(z) f_{i,k}}{\partial z} \tag{22}$$

where $f_{i,k}$ is the PSD of kth hydrometeor belonging to ith mass bin. Typically in BM and MMM models, fall velocity of particles $V_{t\_i,k}(z)$ of kth hydrometeor belonging to the ith mass bin depends on the hydrometeor type and on the particle mass. The dependence of the fall velocity on air density (height) is also often taken into account. In some cases [e.g., *Benmoshe et al*., 2012; *Phillips et al*., 2007b, 2014, 2015], the fall velocity also depends on particle composition (rimed fraction and liquid water fraction in ice particles) and the roughness of the particle surface (dry or wet). The size sorting is simulated automatically since particles of different masses and of different types fall with different velocities. SBM does not face the problems in the description of particle sedimentation that arise in bulk parameterization models (see below). At the same time, the numerical viscosity of finite difference schemes approximating (22) may lead to the fact that a very low number of the largest particles fall to the surface too fast.

4.4.2. Bulk Parameterization

Sedimentation in bulk parameterization schemes is performed not for single particles but for PSD moments. This process is described by equation

$$\frac{\partial M^{(k)}}{\partial t} = \frac{\partial \overline{V}_t^{(k)} M^{(k)}}{\partial z} \tag{23}$$

In equation (23) $k = 0$ corresponds to the drop concentration, $k = 1$ corresponds to the mass content, and $\overline{V}_t^{(k)} = \frac{1}{M^{(k)}} \int m^k f(m) V_t(m) \mathrm{d}m$ is the averaged fall velocity. For the moments of different order, the averaged fall velocities are different. In the case of one-moment bulk schemes, sedimentation is performed for the first moment, so that only the mass weighted fall velocity is used. Utilization of equation (23) means, for instance, that all raindrops with fall velocities varying from, say, 0.5 m/s to 10 m/s, fall with the velocity equal to that of a "mean mass" raindrop, say, 3 m/s. It is clear that such an approach does not reproduce the spatial size sorting in real clouds when larger drops fall faster than smaller ones. Better results can be achieved using two-moment bulk parameterization schemes where particle sedimentation is described using the two equations (23), one for drop concentration and one for drop mass.

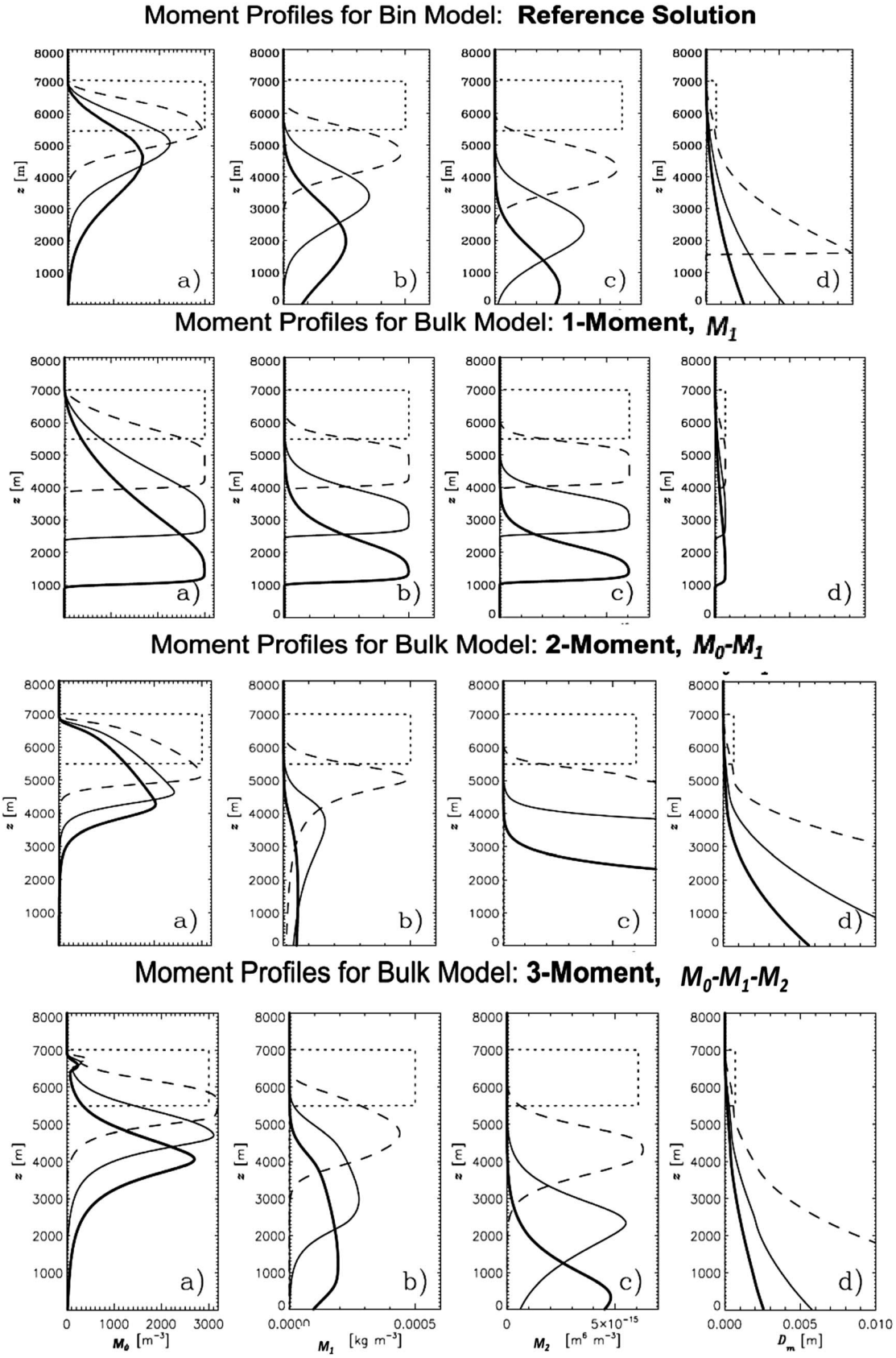

Figure 9

Note that in the case of constant fall velocity, equation (23) represents the classical equation of advection $\frac{\partial M}{\partial t} = -\overline{V}_t \frac{\partial M}{\partial z}$ (here axis z is directed downward), which has the analytical solution $M(z,t) = M\left(z - \overline{V}_t t, 0\right)$. According to this solution, the initial vertical profile of the moment is translated downward, without changing its shape. Note too that the mass averaged fall velocity should be larger than the concentration averaged one ($\overline{V}_t^{(1)} > \overline{V}_t^{(0)}$). This inequality reflects the fact that smaller particles fall more slowly than larger ones.

The difference between these velocities leads to a problem, when mass content sediments faster than number concentration. As a result, in the course of cloud simulation in one cloud area only the mass may exist at a negligible concentration, while in the cloud area located higher up, only the concentration may exist at negligible mass. Hence, the mean radii of particles turn out to be either extremely large or extremely small. In this case, the value of the radius is artificially changed to shift it into a reasonable range. Following this, the particle concentration is recalculated using the liquid water mixing ratio and the new particle size.

To decrease the number of such undesirable situations, equation (23) is typically solved using an upstream finite difference scheme with the significant computational diffusivity (upstream differences, see also *Kato* [1995]). The utilization of diffusive numerical schemes increases the overlap of the vertical profiles of the moments and leads to more reasonable values of the mean volume particle diameter. At the same time, the mean volume diameter turns out to be dependent on the diffusivity of the numerical scheme, which is determined by time step, vertical resolution, and fall velocity. This is an obvious disadvantage of such schemes. Note that one of the main microphysical effects of aerosols is a change in particle size. The artificial change of the particle size (and concentration) in the course of sedimentation may dramatically decrease the sensitivity of bulk schemes to aerosols (see sections 6 and 7). Moreover, the particle size chosen is used to determine the rate of freezing, i.e., the procedure affects other microphysical processes.

Aiming at the improvement of sedimentation representations in bulk parameterization schemes, *Milbrant and Yau* [2005a, 2005b] and *Milbrandt and McTaggart-Cowan* [2010] compared the results of sedimentation simulated by one-moment, two-moment, and three-moment bulk schemes with the solution obtained using a bin method, results of which were considered to be benchmarked. In the three-moment scheme, the additional prognostic equation for the second moment (radar reflectivity) was solved. *Milbrandt and McTaggart-Cowan* [2010] simulated sedimentation and size sorting of cloud particles initially located within the layer from 6500 m to 8000 m (Figure 9). Mass content was 0.5 gm^{-3}, and concentration was chosen 3 L^{-1}. The one-moment formulation introduces two assumptions with $N_{i0} = 8 \cdot 10^6 \mathrm{m}^{-4}$ and $\nu = 0$. The two-moment formulation only assumes $\nu = 0$. Other parameters are determined by the predicted moments. In the three-moment scheme, all PSD parameters under the gamma distribution are determined by the given three moments. Thus, this scheme does not require closure assumptions. The profiles of zeroth, first, and the second moments (directly related to radar reflectivity) and mean mass diameter D_m were calculated by solving equation (23) using a scheme similar to the upstream difference method.

It is seen (Figures 9a–9d, first row) that the peak values of higher moments sediment faster, and the amplitude of the peak decreases with time. The effect of size sorting is well seen from profiles of $D_m(z)$. The mean size of particles increases with a decrease of altitude that reflects the fact that the fall velocities of large particles is higher than small ones.

Analysis shows that the profiles calculated using the one-moment scheme dramatically differ from the benchmark solution. The one-moment scheme is not able to simulate size sorting; the mean mass particle diameters are unrealistically small and practically do not depend on height. Despite the fact that the profiles produced by the two-moment scheme were more realistic than those of the one-moment scheme, the size sorting was significantly stronger than that in the benchmark method. Simulations showed that the errors of two-moment scheme depend on the choice of the moments to be used for simulation of sedimentation. Utilization of the three-moment scheme considerably reduces errors. Accordingly, *Milbrandt and Yau* [2005b]

Figure 9. Vertical profiles of (first column) zero, first (second column), and second (third column) moments of particle size distributions as well as of (fourth column) mean mass particle diameter. (first row) Profiles calculated using bin method (benchmark) are presented and (second, third, and fourth rows) profiles calculated using one-moment, two-moment, and three-moment schemes are presented, respectively. (Compiled from Milbrandt and McTaggart-Cowan [2010], courtesy of the American Meteorological Society.)

and *Milbrandt and McTaggart-Cowan* [2010] proposed using a three-moment bulk parameterization scheme in which the equation for radar reflectivity is used in addition to equations for concentration and mass content. The same conclusion was reached by *Loftus and Cotton* [2014a].

Milbrandt and McTaggart-Cowan [2010] also proposed an approach to improve the reproduction of sedimentation in two-moment bulk schemes. In this approach, the slope parameter was parameterized as a function of the ratio of the two moments calculated during solving equation (23). The values of the shape parameter recommended for the calculation of fall velocity differ from those used in the rest of the bulk parameterization scheme. Note that all simulations were performed using the diffusive numerical scheme.

In the bin-emulating method of RAMS, the PSD given in the form of a gamma function is discretized into several tens of bins before the sedimentation time substep [*Feingold et al.*, 1998; *Cotton et al.*, 2003]. Then, the sedimentation algorithm is applied to each bin. After sedimentation, the values of the mass and the concentration calculated in different grid points are used to restore the parameters of the gamma distributions. Bin-emulating schemes have a greater computational cost than regular bulk schemes. To decrease the computational time of bin-emulating schemes, lookup tables are used to calculate fall distances of particles belonging to a particular bin. It is widely accepted that such an approach produces results closer to the benchmark solution, as compared to those based on the sedimentation of moments according to equation (23).

Morrison [2012] showed that the results of the bin-emulating approach yield a vertical distribution of moments similar to that yielded by bulk parameterization schemes, in which sedimentation is described using equation (23). Morrison concludes that improvement in the representation of sedimentation in bulk parameterization schemes can be achieved only in two- or three-moment bulk schemes in which the effects of the change of PSD distribution (e.g., the shape parameters of the PSD) during sedimentation are taken into account, as done by *Milbrandt and Yau* [2005b], *Wacker and Lupkes* [2009], and *Milbrandt and McTaggart-Cowan* [2010]. These effects should be taken into account regardless of whether bin-emulating or classic bulk schemes are employed. Note that in the SBM approach, the change in the PSD shape during sedimentation is taken into account automatically.

4.5. Other Microphysical Processes

Cloud microphysics includes many other microphysical processes, such as freezing/melting, ice multiplication, and raindrop breakup. The conversion of particles of one hydrometeor type into particles belonging to other hydrometeor types is of major importance. Practical problems sometimes require the calculation of particle salinity, charge, etc. Space constraints preclude a comprehensive discussion of this issue. Thus, we shall treat only a selection of topics.

4.5.1. Spectral Bin Microphysics

A wide range of approaches may be taken to represent different microphysical processes such as melting and freezing in SBM models. For instance, in some cases, immediate melting at the melting level was assumed [*Reisin et al.*, 1996a, 1996b; *Khain and Sednev*, 1996], while in other cases, melting was calculated in a simplified way by specifying a characteristic melting time for ice particles of different sizes, as was done by *Fan et al.* [2012a] in 3-D WRF simulations. There are SBM schemes wherein detailed melting is included by tracing the history of liquid water within melting particles and the advection of liquid water mass within ice particles [*Phillips et al.*, 2007b]. In recent versions of 2-D HUCM, liquid water fractions of snowflakes, graupel ,and hail are calculated. This means that three additional size distributions are treated in the scheme. Substantial differences also exist in the description of the process of heterogeneous freezing of drops. In most schemes, semiempirical formulae determining the probability of freezing are used [*Reisin et al.*, 1996a, 1996b; *Khain and Sednev*, 1996]. In more comprehensive schemes recently implemented into HUCM, two-step freezing is considered when the very short adiabatic stage is followed by time-dependent freezing based on the calculation of the heat balance within the freezing drops. The freezing drops were introduced as a new hydrometeor type [*Phillips et al.*, 2014, 2015; *Kumjian et al.*, 2014]. Freezing drops are converted to hail when the liquid water fraction reaches zero. Time-dependent freezing of accreted water was also implemented when riming of graupel and hail was considered. In these studies, as well as in *Phillips et al.* [2007b], shedding of liquid water is taken into account. The process of shedding is described using the expressions for maximum thickness of liquid film obtained in laboratory experiments. The drops formed by shedding are added to the distribution of raindrops.

Flossmann and Pruppacher [1988], *Flossmann et al.* [1985], and *Respondek et al.* [1995] developed a 2-D SBM cloud model with warm microphysics for investigating the formation of acid rain in cumulus clouds. In this

model, the aerosol particle mass within water droplets is traced and is treated as a separate mass distribution function. Accordingly, the processes of aerosol mass growth within droplets and aerosol scavenging is calculated. Similarly, the effects of microphysical processes (e.g., collisions) on the salinity of drops, the rate of their growth and on aerosol size were investigated in 2-D Lagrangian trajectory ensemble BM model of stratiform clouds [*Magaritz et al*., 2009, 2010; *Shpund et al*., 2011].

4.5.2. Bulk Microphysics Parameterizations

Similar to collisions, the rates of melting in bulk parameterization schemes are calculated by averaging the basic thermodynamic equations for melting over particle-sized spectra [*Milbrandt and Yau*, 2005a, 2005b; *Seifert and Beheng*, 2006a, 2006b]. Typically, these equations are treated in a simplified form, say, in neglecting collisions and in the assumption of an immediate shedding of all melted water. This approach is often reduced to the evaluation of characteristic time scales of melting for ice hydrometeors of different types. Serious simplifications are taken during averaging of these equations. The process of drop freezing is typically calculated using spectral-averaged semiempirical formulas. According to many such formulae, the rate of freezing is proportional to drop mass; that is, it is strongly size dependent.

Note that most microphysical processes such as diffusional growth, sedimentation, melting, and freezing may be expected to lead to deviations of the PSD from the gamma distribution, even if the initial distribution was gamma in shape. For instance, condensation leads to the appearance of a minimum particle size that differs from zero. In contrast, evaporation may lead to the appearance of a maximum concentration in the vicinity of zero size. Being proportional to the drop mass, drop freezing should lead to a disappearance of the tail of largest drops in the raindrop distribution. In this sense, the assumption that after each microphysical process the PSD remains a gamma distribution (even with other parameters) may lead to errors in the representation of the microphysical structure of clouds.

In summary, the utilization of a few moments of the PSD instead of the PSD themselves leads to uncertainties in treating different microphysical processes. This is because the rates of these processes are highly dependent upon particle size. Different approximations of these processes in different bulk schemes may lead to a great deal of variability in the results of simulations of the same atmospheric phenomena (see section 6).

5. Uncertainties in Numerical Cloud Microphysics

5.1. Types of Uncertainties

Uncertainties in numerical simulations of cloud microphysics are related to uncertainties in the form of the basic equations, uncertainties in the parameters and coefficients in these equations, and uncertainties in the observations. Here we briefly discuss these problems.

Uncertainties in the basic equations. As we saw in section 3, all numerical cloud microphysical approaches are based on the same system of equations for PSDs. In this regard, a number of questions arise: How accurately do these equations describe the behavior of the specified parameters? What is the accuracy to be targeted in the numerical simulations? What are the limiting environmental conditions restricting the application of these equations? Do those equations provide a complete description of the specific variable's impact on other environmental parameters?

We note that (a) Cloud microphysics deals with colloidal systems (i.e., gaseous environments filled with suspended liquid and/or solid particles), the description of which remains subject to many theoretical problems. The discussion of these problems is beyond the scope of this survey. Regarding this matter, we refer the reader to *Pruppacher and Klett* [1997].

(b) Many uncertainties are related to the fact that microphysical processes take place in a turbulent medium, where stochastic fluctuations of different parameters exist. The theory of stochastic condensation attempts to explain the PSD formation and broadening by turbulent fluctuations of supersaturation related to turbulent fluctuations of vertical velocity in cloud volumes. This approach has many theoretical problems, and the system of equations describing stochastic growth of cloud particles is solved only for some specific cases.

Despite the wide utilization of SCE (equation (12)) in the SBM and for the calculation of collision rates in bulk parameterization schemes, the strict justification of this equation under cloudy conditions is still absent. We refer readers to *Voloshuk and Sedunov*'s [1975] classic work for a detailed analysis of the conditions under which the SCE is valid. When PSDs are defined on mass grids, the use of the kinetic equation to describe collision is a

strictly valid if there are many particles belonging to each mass bin (or category). For this to occur, the air volume must be both large enough and sufficiently homogeneous. Since the atmosphere is inhomogeneous at any scale, it is even questionable whether such a scale exists. Current models (both bulk and bin) have grid spacing too large to assume that the process of collisions is "homogeneous" within such volumes.

In addition, equation (12), called the "stochastic collection equation," is actually not stochastic. When the collection kernel is prescribed a priori (as in the case of gravitational coagulation) there is nothing random in this equation. In clouds, turbulence is ubiquitous, and thus, the collision kernels are random values with a comparatively wide probability distribution function [*Pinsky et al*., 2008b]. In some models that take into account the turbulent effects on particle collisions, only an averaged PDF collision enhancement factor is applied [e.g., *Ayala et al*., 2008; *Seifert et al*., 2010; *Benmoshe et al*., 2012; *Benmoshe and Khain*, 2014]. Thus, information about the PDF of the collision kernel is not used, and it is not clear how the SCE for the case of a random kernel should be formulated.

One important problem is related to the effect of turbulence and turbulent mixing on the evolution of cloud microstructure. According to many studies, turbulence and mixing affect the size and concentration of drops and may result in enhanced rain formation. The role of turbulent mixing and its effects remains poorly understood, despite a great deal of research effort [*Paluch*, 1979; *Siebert et al*., 2006; *Burnet and Brenguier*, 2007; *Andrejczuk et al*., 2009; *Lehmann et al*., 2009; *Jarecka et al*., 2013; *Magaritz-Ronen et al*., 2014; *Korolev et al*., 2013b]. To date, no reliable equations describing the mixing of nonconservative quantities like PSDs in turbulent media have been formulated.

(c) Lack of knowledge of ice aggregation. There are many examples of complicated nonregular shapes of aggregates, in which different parts (ice crystals) are connected by a thin neck [*Heymsfield and Iaquinta*, 2000]. The nature of the forces that keep these crystals (or parts of ice crystals) together in turbulent clouds is unknown. The stability of the shape of such aggregates may indicate the existence of electrostatic forces that keep different parts of crystals together. Nothing is known about the role of this electrostatic mechanism in ice-ice collisions [*Stith et al*., 2002].

5.1.1. Uncertainties Related to Parameters in the Basic Equations

Diffusion Growth Equation. Laboratory experiments [e.g., *Reinike and Beheng*, 1996] show large scattering in the measurements of the condensation coefficient, which ranges from approximately 0.01 to 1. To date, there is no consensus on the value of the condensation coefficient.

Particle Collisions. There is significant uncertainty in the collection kernel for collisions between ice crystals, as well as between ice crystals and droplets. These collection kernels vary with air temperature, the sizes and fall velocities of ice particles, and collection efficiencies. Collection efficiencies vary with the porosity of ice particles, but this problem is far from solved. Besides, the fall velocity of ice crystals having the same mass is related to ice particle shape, rate of riming, intensity of turbulence etc. (i.e. *Siewert et al.* [2014]).

Aerosols. The discrimination between aerosol particles and CCN is not stringent. Due to their chemical complexities, single aerosol particles may contain both soluble and insoluble components; thus, they may serve both as CCN and IN. The insoluble component is often characterized by its principal composition, e.g., soot, mineral, and organic matter [*Phillips et al*., 2008]. These characteristics control the concentrations of droplets and ice crystal but are not well understood.

Ice Production. Despite many field programs and laboratory investigations, primary ice nucleation and secondary ice production remain the most poorly understood processes of mixed-phase and ice clouds. According to theory [*Khvorostyanov and Curry*, 2000, 2004, 2005]. aerosol particles contain soluble and insoluble fractions and serve as CCN or ice nuclei (IN) depending on their size and composition, as well as on environmental conditions. The practical application of the theory is complicated by the lack of information pertaining to many parameters, including the shape of the IN, wettability, and the distributions of the contact angles. In addition, other mechanisms of ice initiation have been proposed, such as contact nucleation with its numerous modes of gravitational contact, diffusiophoresis, thermophoresis [*Pruppacher and Klett*, 1997], contact nucleation inside out [*Sastry*, 2005; *Shaw et al*., 2005], and perhaps most importantly for tropical maritime convection, a secondary ice production process [*Hallett and Mossop*, 1974].

In light of the uncertainties of ice production processes, different empirically based parameterizations have been developed [e.g., *Meyers et al*., 1992; *DeMott et al*., 2010; *Phillips et al*., 2013]. Their parameterization is easy

to use in both bulk and SBM models and has already been implemented into the RAMS microphysics scheme [*Saleeby and van den Heever* [2013], GCE [*Zeng et al*., 2011], and WRF/SBM [*Fan et al*., 2014]. *Phillips et al*. [2013] devised a four-aerosol-species-dependent scheme, resolving their differing ice-nucleating abilities. However, given that the variability of observed concentration of ice crystals is very large, the differences between the ice concentrations predicted by empirical formulas and the observed ice crystal concentrations can be very large.

Ice Crystal Shape. Ice crystal habits (shapes) and related properties are marked by significant uncertainty. *Westbrook et al*. [2008], *Sulia and Harrington* [2011], and several others found that the nonsphericity of ice crystals during diffusional growth may substantially affect ice-liquid partitioning in numerical models of mixed-phase stratocumulus clouds. Indeed, the shape of ice crystals strongly influences their diffusional growth rates. Also, when ice crystal sediments, they are carried through different habit-dependent growth regimes, complex crystal shapes (e.g., capped columns) can develop.

The Conversion of Hydrometeors. There are also uncertainties related to the conversion of hydrometeors from one type to another in mixed-phase clouds as a result of collisions (riming, aggregation, etc.). In real clouds, the process of riming leads to an increase in the density of rimed snow and its conversion to graupel. Riming of graupel fosters the conversion of graupel to hail. Thus, a continuing increase of particle density (affecting fall velocity) should be taken into consideration.

5.1.2. Uncertainties Related to Observations

Measurements of CCN. Droplet concentration and other cloud quantities depend on CCN size distributions, which can be derived from CCN activity spectra, that is, from the relationship between CCN concentration and supersaturation. According to *Pruppacher and Klett* [1997], a continuous growth of CCN concentration takes place at supersaturations as high as 5–10%. However, CCN probes tend to measure only CCN concentrations at supersaturations that do not exceed 0.6% [*Prabha et al*., 2011]. At such supersaturations, the smallest CCN remain nonactivated and cannot be identified. This leads to uncertainties in the concentrations of the smallest CCN, which as was mentioned in section 4, can play a very important role in cloud microphysics leading to in-cloud nucleation.

Another problem is the lack of reliable measurements for the concentration of giant CCN (GCCN). Due to their low number concentrations, we cannot rely on existing CCN counters to accurately measure GCCN concentrations. Many modeling studies suggest a high sensitivity of cloud microphysics and precipitation to GCCN [*Feingold et al*., 1999; *Laird et al*., 2000; *van den Heever et al*., 2006; *van den Heever and Cotton*, 2007; *Carrió et al*., 2007; *Khain et al*., 2012].

Uncertainties in the Local PSD. Many in situ measurements are performed at a frequency of 1 Hz, over scales ranging from 100 to 200 m, which may not be adequate to resolve small-scale mixing and its effect on droplet/drop size distributions. Measurements at higher spatial resolution (~10–20 m) reveal many adiabatic volumes within clouds that play a principal role in initial raindrop formation, as was shown by *Khain et al*. [2013].

Early airborne measurements suggested that the number concentration of ice particles in ice clouds is essentially always dominated by small ice particles. Recently, it was found that the effect of shattering in exiting particle probes mainly affects particles with $D<500\ \mu m$ [*Korolev et al*., 2011, 2013a]. The effect of shattering can be mitigated by (a) the use of processing algorithms [*Korolev and Isaac*, 2003; *Field et al*., 2006] and (b) modification of the probes' inlets and the use of antishattering probe tips [*Korolev et al*., 2011]. As a result of this problem and the improvements gained by these new methods, the PSDs measured by imaging probes reported prior to 2011 cannot be relied upon, especially in the size subrange with $D<200\ \mu m$.

In situ measurements of hail in severe storms are, with rare exceptions, totally absent. In the 1970s and 1980s, an aircraft of the South Dakota School of Mines and Technology sampled deep convective clouds, and graupel and hail growth processes were documented [*Heymsfield and Hjelmfelt*, 1984; *Musil et al*., 1986; *Heymsfield and Miller*, 1988]. However, more detailed data are required.

Supersaturation in Clouds. The supersaturation in clouds is an unmeasured parameter. Estimations of quasi-stationary supersaturation values can be found in *Prabha et al*. [2011].

The list of such gaps in our knowledge goes on. Note, however, that different uncertainties have different "weights" and importance. The role of the uncertainties in one or another microphysical process depends on the particular problem under investigation. For instance, a great number of numerical studies indicate a comparatively low sensitivity of precipitation from deep convective clouds to the presence of ice crystals, their shape, etc. At the same time, the sensitivity of the microphysical structure of mixed-phase stratiform

clouds to ice concentration and particle shape is high, and to get realistic results, the ice crystal concentration is often adjusted to the observed values (see section 6).

In section 5.2 the possible effects of some uncertainties listed in this section are discussed.

5.2. Decrease in the Uncertainties

Uncertainties in the values of the accommodation coefficient and the ventilation coefficients in equations for diffusional droplet growth were discussed by *Kogan et al*. [1984] and *Davis* [2006]. They pointed out that the effect of these uncertainties is leveled to a significant extent by negative feedback: an increase in the rate of diffusion drop growth leads to a decrease in supersaturation, which in turn decreases the rate of diffusion growth. Thus, following these researchers, this uncertainty does not appear to play an important role when the equations for supersaturation and diffusion growth are solved together. Some evidence that accurate results can be obtained in the presence of this uncertainty is presented in section 5.3.

Regarding the uncertainties of turbulent effects on droplet collisions, significant progress has been made during the past decade. Using a long series of drop arriving times in about 50 cumulus clouds, *Pinsky and Khain* [2001, 2003] found the turbulent-induced 1 cm drop concentration clusters predicted by theory and simulated numerically [e.g., *Grits et al*., 2006]. They evaluated the amplitude of drop concentration fluctuations as a function of turbulent intensity.

Dramatic convergence of the values of the collision enhancement factor calculated using different approaches (direct numerical simulations, theoretical studies, and laboratory experiments) has been achieved [*Ayala et al*., 2008; *Pinsky et al*., 2008b; *Devenish et al*., 2012]. It was found that the collision enhancement factor varies from 1 to about 10, depending on the sizes of colliding drops and on the intensity of turbulence.

In spite of the high values of collision enhancement factors, sensitivity simulations performed by *Seifert et al*. [2010], *Benmoshe et al*. [2012], and *Lee et al*. [2008] showed that turbulence accelerates the formation of rain in cumulus clouds by only several minutes and decreases the altitude of the first rain formation by only 100–300 m, depending on the aerosol concentration. The sensitivity of the microphysical structure of simulated deep convective clouds to the turbulence-induced enhancement of the collision rate between ice-ice and ice-liquid hydrometeors has also been investigated by *Benmoshe and Khain* [2014]. In spite of the significant effects of turbulence on the rates of different microphysical processes, the difference in accumulated rain from deep convective clouds in "no-turbulence" and "turbulence" simulations performed with 50 m × 50 m resolution typically did not exceed 20%, and changes in the time of surface precipitation onset were found to be 5–10 min, depending on aerosol concentration.

It is clear, then, that a better understanding of the SCE of random collision kernels is essential for improving the accuracy of cloud simulations. At the same time, we do not anticipate any significant changes in the current estimations of turbulence effects, since the effect of PDF-averaged collision enhancement factors are well known and are the dominant processes in turbulent-cloud microphysics. It seems that turbulence does not affect precipitation onset as strongly as it was once thought [*Jonas*, 1996].

As was mentioned above, a relatively large number of particles within each size bin is essential for accurate results when the SCE is used. Sometimes, the concentration of hail or large raindrops is too low to use the SCE. The unique feature of the Bott scheme used in the SBM to calculate collisions between particles is that it reduces to the method of continuous growth when the number of collectors is low and almost no collisions between collectors and smaller particles take place.

With regard to uncertainties in the process of ice crystal nucleation, simulations of Arctic clouds carried out using the SAM/SBM represented the observed 2.5 power law relationship between the ice water content and the ice number concentration [*Yang et al*., 2013]. This 2.5 power law relationship was found in the observations of these clouds during the Indirect and Semi-Direct Aerosol Campaign (ISDAC). As mentioned by those researchers, this finding introduces the intriguing possibility that models could serve as a bridge between complex field observations, cloud modeling, and relatively idealized laboratory investigations of stochastic ice nucleation to investigate the nature of the ice nucleation process.

The substantial uncertainty in the concentration of ice nuclei (IN) in deep convective clouds does not make the simulations of such clouds meaningless because, as numerous sensitivity simulations show, while increasing IN concentrations may have an initial impact on convective storm characteristics [*van den Heever*

et al., 2006], the overall effect of an increase in the IN number concentration on the dynamics of deep convective clouds, as well as on precipitation, is relatively small [*Carrió et al*., 2007; *Lebo and Seinfeld*, 2011].

Significant progress has also recently been achieved in detailing the processes of the mutual conversion of hydrometeor types. In some studies, the conversion from one class of hydrometeors to another is performed according to calculated particle densities [*Morrison and Grabowski*, 2010; *Khain et al*., 2012; *Phillips et al*., 2014, 2015], who calculate densities of hydrometeors during riming. *Khain et al*. [2012] and *Phillips et al*. [2014, 2015] implemented the rimed fraction to calculate the bulk density of snow. Such improvement required the implementation of a new size distribution for rimed mass within snow that enhanced the sophistication of the scheme.

There are several ways to reduce uncertainty in the description of microphysical processes. At present, the indirect criterion for the choice of collision kernels in the models is the production of reasonable amounts of aggregates. In this respect, the problems are related to sticking efficiencies and getting stuck. Combining bin microphysical models with data from polarimetric radars is a good way to make progress in this direction.

The performance of laboratory experiments also reduces uncertainty. Laboratory experiments on ice nucleation [*Roberts and Hallett*, 1967; *Durant and Shaw*, 2005], secondary ice nucleation [*Hallett and Mossop*, 1974], efficiency of collisions, aerosol scavenging and riming [*Mitra et al*., 1990, 1992], turbulent effects on droplet growth [*Vohl et al*., 1999], investigations of turbulent cloud structures via digital holography (R. Shaw, NSF project), high accuracy measurements of aerosols [e.g., *Rissler et al*., 2006] and other laboratory studies have substantially contributed to our knowledge of microphysical processes. Many laboratory findings have been implemented into advanced cloud microphysical models. The theory of wet hail growth developed recently by *Phillips et al*. [2014] was validated by a comparison with laboratory measurements conducted by *Garcia-Garcia and List* [1992].

The particulars of the shapes of ice have a profound impact not only on the subsequent growth of the ice itself but also on the latter's interaction with the radiation process (by scatter of visible light by crystals). In most microphysical schemes, these computations are performed assuming relatively simple hexagonal shapes or a combination of them for ice. In reality, ice crystals hardly ever follow the pristine forms listed in textbooks but rather they exhibit an infinite variety of irregular shapes [*Korolev et al*., 1999]. If ice crystal shapes matter a great deal, we need very careful computations of ice crystal growth in order to assess correctly ice growth rate. The implication is tantalizing, because if this argument is correct, we not only need to introduce enough bins but also bins with a sufficient number of ice-shape types. Note that the equation system for microphysical processes used in SBM schemes allows for the easy assimilation of new knowledge about ice nucleation or collisions between ice particles.

Examples of such results are presented in sections 5.3 and 6.

5.3. The Reliability of the Basic Equations

Despite the existing uncertainties, many qualitatively and quantitatively important results have been obtained using cloud-resolving models with advanced microphysics. For instance, the correct representation of the droplet concentration in clouds as a result of diffusion growth of aerosol and droplets can be used to justify the corresponding growth equations. It is noteworthy that the more accurate the method used for solving the diffusion growth equation, the better the agreement with the observed data. This agreement is especially good in the parcel and Lagrangian models, where the equation of diffusion growth is solved using movable mass grids, and the process of aerosol growth is described explicitly [e.g., *Pinsky and Khain*, 2002; *Segal et al*., 2004; *Segal and Khain*, 2006; *Magaritz et al*., 2009]. Errors in the reproduction of the observed liquid water mixing ratio and droplet concentration in maritime stratocumulus clouds by such models do not exceed 5–10 % [e.g., *Magaritz et al*., 2009, 2010; L. Magaritz-Ronen et al., The effective radius vertical profile in stratocumulus clouds, *Journal of the Atmospheric Sciences*, in revision, 2015] (Figure 10). The same accuracy is reached in the reproduction of the DSD, effective and mean volume radii, and Z-LWC relationships in these clouds. An analysis based on observations with a helicopter-borne measurement platform and a SBM parcel model allowed *Ditas et al*. [2011] to simulate the values of in situ measured droplet concentration in Sc clouds with an accuracy of 5%.

Numerous simulations show that accurate solutions to the equations of diffusion growth and SCE allow for accurate simulations of the DSD in convective clouds. For example, using the Tel Aviv University rain shaft model with MMM, including drop breakup and evaporation, *Levin et al*. [1991] showed a strong agreement

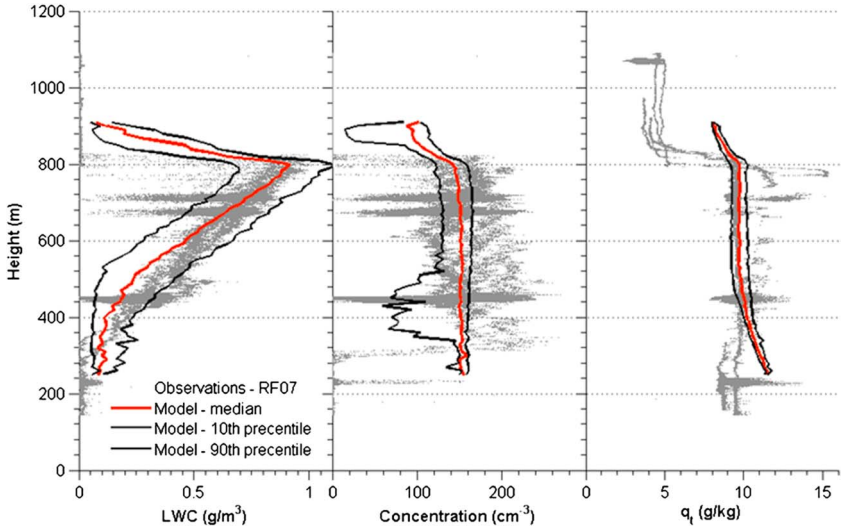

Figure 10. Vertical profiles of liquid water content, droplet concentration, and total water mixing ratio measured in a maritime stratocumulus cloud during DYCOM II, research flight RF07, and the vertical profiles of the horizontally averaged values simulated by the Lagrangian Model of the stratocumulus cloud (red lines). Black lines represent the 10th and 90th percentiles. Gray dots are measured data (L. Magaritz-Ronen et al., in revision, 2015).

between the calculated raindrop size distribution and that measured at the top and bottom of Mount Rigi in Switzerland. Similarly, the HUCM SBM model accurately simulated DSDs and their changes with height under different aerosol loadings. Figure 11 compares simulated DSDs with in situ measured DSDs during a LBA-SMOCC 2002 (Large-Scale Biosphere-Atmosphere Experiment in Amazonia-Smoke, Aerosols, Clouds, Rainfall, and Climate) field experiment in the Amazon region. Clouds developing under different aerosol concentrations were divided into Blue Ocean (BO) clouds (clean atmosphere), Green ocean (GO) clouds (intermediate aerosol concentration) and Smoky clouds (S) developing in a very polluted atmosphere with

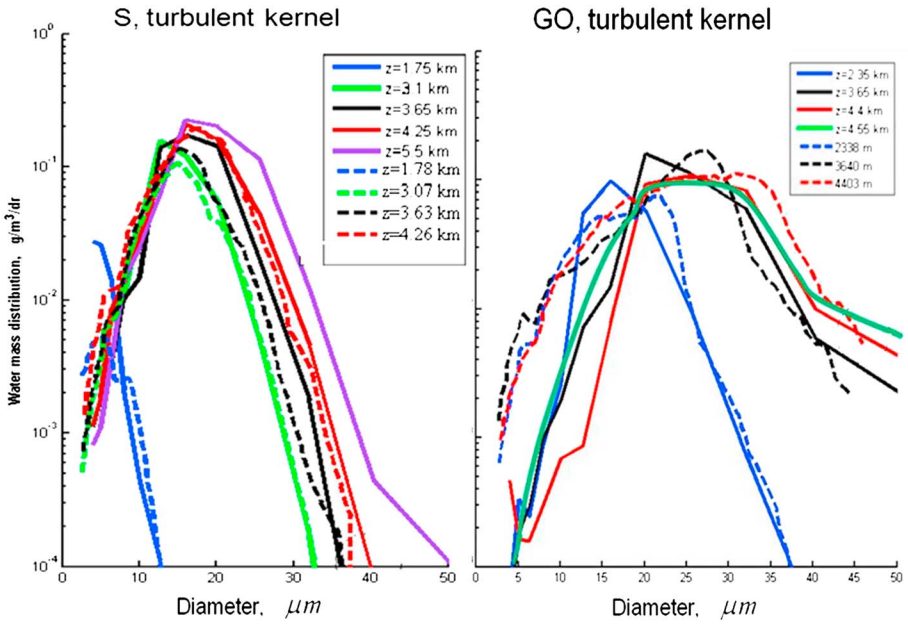

Figure 11. The mass distributions measured in situ on 5 October 2002 up to height of 4.2 km (dashed lines) [from *Andreae et al.*, 2004] and calculated using HUCM (solid lines). (left) Developing S clouds and (right) developing GO clouds. (middle) The CCN concentration at 1% of supersaturation is 5000 cm^{-3} in S and 1000 cm^{-3} in GO cases. The values of ε and Re_λ were calculated using the equation for turbulent kinetic energy at each time step and in each model grid point. (From *Benmoshe et al.* [2012]; courtesy of the American Geophysical Union.)

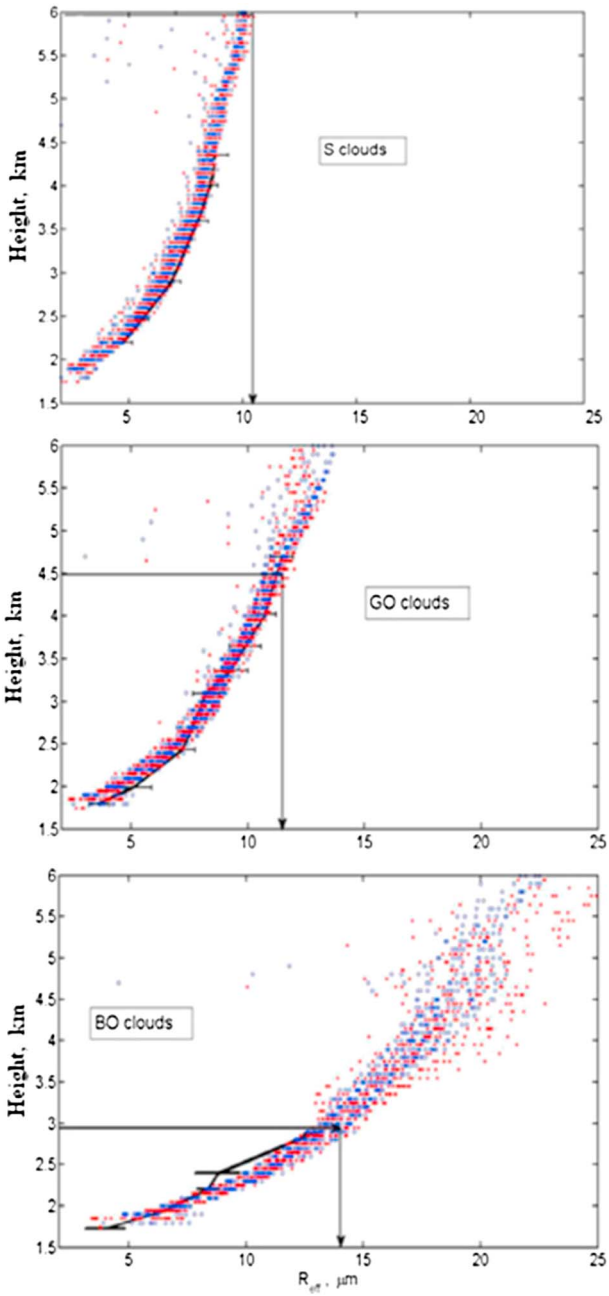

Figure 12. Height dependence of the effective radius in (top) S, (middle) GO, and (bottom) BO clouds. Simulations with gravitation collision kernel are marked by blue circles; red asterisks denote simulations with turbulent collision kernels. Solid lines show the observed data. The levels of the first rain formation found in the simulations are plotted by the horizontal arrows. (From *Benmoshe et al.* [2012]; courtesy of the American Geophysical Union.)

CCN concentrations of about $10^4\,cm^{-3}$ [*Rissler et al.*, 2006]. Sounding data from *Andreae et al.* [2004] were used for verification purposes. Figure 11 shows DSDs at different heights in GO and S clouds during the earlier stages of cloud development, before the formation of the first raindrops. These DSDs were obtained by averaging the observed DSDs over the traverse within clouds. In simulations the effects of turbulence on cloud droplets collisions were taken into account [*Benmoshe et al.*, 2012]. Figure 11 shows that the model reproduces the evolution of DSD in clouds quite well. The DSDs in GO clouds are wider than in S clouds and centered at 12–14 μm, as compared with 10 μm in S clouds.

An effective radius r_{eff} is an important microphysical characteristic of clouds that reflect their ability to produce raindrops. Raindrop formation takes place if r_{eff} exceeds 14 μm in cumulus clouds developing in comparatively clean air and 10–11 μm in clouds developing in polluted atmosphere [*Freud et al.*, 2008; *Freud and Rosenfeld*, 2012]. Figure 12 shows the vertical profiles of the effective radius, r_{eff}, calculated for BO (bottom), GO (middle), and S clouds (top). The figures were plotted for the period of cloud development when the cloud top heights grew from 2 to 6 km in the BO and GO clouds and to 6.5 km in the S clouds. The vertical profiles of r_{eff} calculated using in situ observations in many clouds during the LBA-SMOCC are presented as well.

The vertical arrows show the values of r_{eff} corresponding to the formation of the first raindrops. One can see good agreement of the model results with observations: the first raindrops form at $r_{eff} = 14$ μm in BO, at 12 μm in the GO, and at 10.5–11 μm in highly polluted S clouds. The heights of the first raindrop formation marked in Figure 12 are also in good agreement with the observations to a precision of about 100–200 m. Very accurate reproductions of the observed vertical profile of r_{eff} with low dispersion was reported in the simulation of deep convective clouds using the System Atmospheric Modeling (SAM) model with the SBM [*Khain et al.* [2013]]. It was found in the above mentioned study that in nonprecipitating developing convective clouds, $r_{eff}(z) = 1.08 r_v$, where r_v is the mean volume radius. The same relationship was found by *Freud and Rosenfeld* [2012] in numerous flights in different regions, as well as by Prabha in the field experiment CAIPEEX in India [*Khain et al.*, 2013].

Very accurate representations of radar reflectivity, as well as signatures of dual polarimetric radars in hailstorms using a SBM model, were reported recently by *Kumjian et al*. [2014].

These examples show that SBM models are able to reproduce fine features of the PSD determined by high-order PSD moments. The reliability of the existent system of microphysical equations also follows from the fact found in numerous studies that higher-moment bulk parameterization schemes produce results closer to observations than lower moment bulk parameterization schemes (see section 6 for detail).

6. Comparison of Results Obtained Using SBM and Bulk Parameterization Schemes

6.1. Criteria of Comparison

The comparison of microphysical schemes, including SBM and bulk schemes, is not simple. First, the variability of SBM schemes is nearly as large as that of bulk parameterization schemes. The SBM can differ not only by approach (BM and MMM) (to the best of our knowledge, these two approaches were never directly compared) but also by varying degrees of sophistication in their description of microphysical processes. That is, the schemes vary from dealing with one DSD to schemes containing PSDs for 7–10 types of hydrometeors. There are also large differences in the description of particular microphysical processes. For instance, different schemes use different collision efficiencies and different collision kernels. In some models, deposition growth is performed under the assumption that ice particles are spheres, whereas in other models the capacitance of nonspherical ice crystals is taken into account. The schemes differ in their treatment of melting, freezing, and so on. The number of bins used for the description of PSD may vary from a few tens to several hundreds and even a few thousand depending on the model. It is also necessary to take into account the model geometry and resolutions: 1-D parcel models typically use more accurate descriptions of particular microphysical processes, say, diffusion growth, but have problems calculating sedimentation of precipitating particles; 2-D models typically have more complicated microphysics than 3-D models. There is an urgent need for more systematic model comparisons.

Difficulties of comparison arise also because the model results (say, precipitation amount) are determined by many factors such as topography, parameterization of the boundary layer, and assimilation procedures which are not related to microphysics. In weather forecast problems, hundreds of forecasts must be compared in order to determine the advantage of one scheme over another. Such forecasts with SBM (as well as with many bulk parameterization schemes) have never been performed, and it is unlikely that they will be performed in the near future. At the same time, the drive to improve weather forecasts and a great number of different research problems (including those related to the local and global climate) trigger a strong aspiration in scientists to improve the representation of microphysical processes in mesoscale models using both bulk parameterizations and SBM.

When comparing SBM and bulk schemes, one must establish the criteria of the comparison and the parameters to be compared. The choice of approach (SBM or bulk parameterization) depends on the problem to be solved. Currently, the following four main approaches are undergoing intercomparisons.

In the first approach, the rates of separate microphysical processes (e.g., various autoconversion and sedimentation schemes) are compared [*Beheng*, 1994; *Seifert and Beheng*, 2001; *Milbrandt and Yau*, 2005a, 2005b; *Wood*, 2005; *Suzuki et al*., 2011; *Kumjian and Ryzhkov*, 2012; *Kumjian et al*., 2012]. Schemes describing particular microphysical processes are considered as "elementary" units of the entire microphysical schemes. In these studies, the bin approach is typically considered to be the more exact, or the benchmark scheme. It aims at testing and tuning particular elementary microphysical units against solutions obtained using basic microphysical equations. Some examples of this approach were discussed in previous sections. Such an approach has been used widely both for the modification of existing and for the development of new bulk parameterization schemes.

The second approach is to use dynamic-kinematic models with prescribed velocity fields, thereby allowing for the advective and gravitational transport of hydrometeors [*Szumowski et al*., 1998; *Stevens et al*., 2005; *Morrison and Grabowski*, 2007; *Ackerman et al*., 2009; *Fridlind et al*., 2012; *Shipway and Hill*, 2012; *Ovchinnikov et al*., 2013, 2014]. The prescribed kinematic framework allows for the comparison of microphysical parameters simulated by different schemes under the same dynamical conditions. This approach also allows for the identification of a better combination of elementary units to design a better bulk parameterization scheme.

Note that even strong agreement between bulk and bin schemes in the case of prescribed dynamics does not guarantee consonance when the mutual effects of microphysics and dynamics are taken into account.

The third approach is to compare bulk and bin schemes within the same dynamical framework, but taking into account all mutual influences of model microphysics and dynamics [*Seifert et al*., 2006; *Li et al*., 2009a, 2009b; *Lebo and Seinfeld*, 2011; *Fan et al*., 2012a; *Adams-Selin et al*., 2013]. It is more difficult to get agreement within observations as well as between results of bulk and bin schemes in this approach, as compared to the first two approaches noted.

Finally, the fourth approach is to compare different microphysical schemes using different models, but simulating the same well-documented case study [e.g., *Noppel et al*., 2010a]. We present below several examples of such comparisons of bulk and SBM schemes using different approaches, beginning with simulations of particular microphysical processes and ending with tropical cyclones.

In some examples, we compare the responses of different microphysical schemes to variation in aerosol concentration. The ability to represent aerosol effects on clouds, precipitation, heat, and radiation, balance is now considered a measure of suitability of one or another model to investigate local and global climatic changes. Reviews of a great number of studies and concepts of aerosol effects on clouds and precipitation can be found in *Levin and Cotton* [2009], *Rosenfeld et al*. [2008], *Khain* [2009], and *Tao et al*. [2012]. The interest in aerosol effects on cloudiness and precipitation has triggered a great number of investigations of sources of aerosol, size distribution of aerosols, their solubility and chemical composition, and so forth. A large number of measurements were classified so as to derive typical aerosol size distributions for different climatic zones (e.g., maritime continental, urban) [*Ghan et al*., 2011].

Numerical models with SBM made it possible to reproduce observed drop-aerosol concentration dependencies [*Segal and Khain*, 2006; *Ghan et al*., 2011; *Pinsky et al*., 2012]. Aerosols affect DSD, and through this all microphysical cloud properties. The similarity in the response of bulk models and of SBM to changes in the CCN concentration would provide a solid basis to account for these effects in large-scale models. Below, we offer several examples aimed to give an idea of the abilities of bulk parameterizations and SBM to simulate different atmospheric phenomena of different spatial and time scales. The main thrust is to show how such a comparison may help further the development of the representation of microphysics in cloud models rather than simply contrast one method with another.

6.2. Comparison of Effects of Individual Microphysical Processes

The representation of the process of sedimentation of particles using different microphysical scheme were illustrated in section 4 and Figure 9. As an example showing the importance of accurate reproduction of sedimentation for calculations of polarimetric radar returns, we present the results of *Kumjian and Ryzhkov* [2012]. In this study, polarimetric radar signatures produced by raindrops falling from a 3 km altitude within an atmospheric layer with horizontal wind shear of 6 ms^{-1} km^{-1} were calculated using the BM approach, as well as single two- and three-moment bulk parameterization schemes. Raindrop size distributions were assumed to have a Marshall-Palmer distribution at an altitude of 3 km. The results are illustrated in Figure 13, showing the fields of radar reflectivity Z and the differential radar reflectivity Zdr calculated using these approaches. The differential radar reflectivity is the difference in the reflectivities in the vertical and horizontal planes and is zero for spherical particles and close to zero for particles rapidly rotating during their motion. This value is extremely important in distinguishing between large hail particles, which reflect as spherical particles and have a Zdr close to zero, and large raindrops which are not spherical and have a Zdr as high as 4–5 dB. One can see substantial differences in the values of Z and Zdr obtained in the bin approach (benchmark) and a single-moment scheme. While in the bin approach large values of Z and Zdr extend to the surface, a single-moment scheme dramatically underestimates these values below 1.5 km level. So, in accordance with the conclusions of the present section 4, *Kumjian and Ryzhkov* [2012] concluded that "one-moment parameterizations are incapable of simulating size sorting." This inability to reproduce size sorting results in large errors in the Zdr calculated from the resulting DSDs. Despite the fact that errors introduced by the two-moment and three-moment schemes are relatively small, two-moment schemes with fixed-shape parameters suffer from excessive size sorting. This leads to a dramatic overestimation of Zdr (by several dB), Z, and other parameters in large zones of a simulated rain shaft encountering wind shear, as well as beneath newly precipitating clouds. Use of a diagnosed shape parameter in a two-moment scheme,

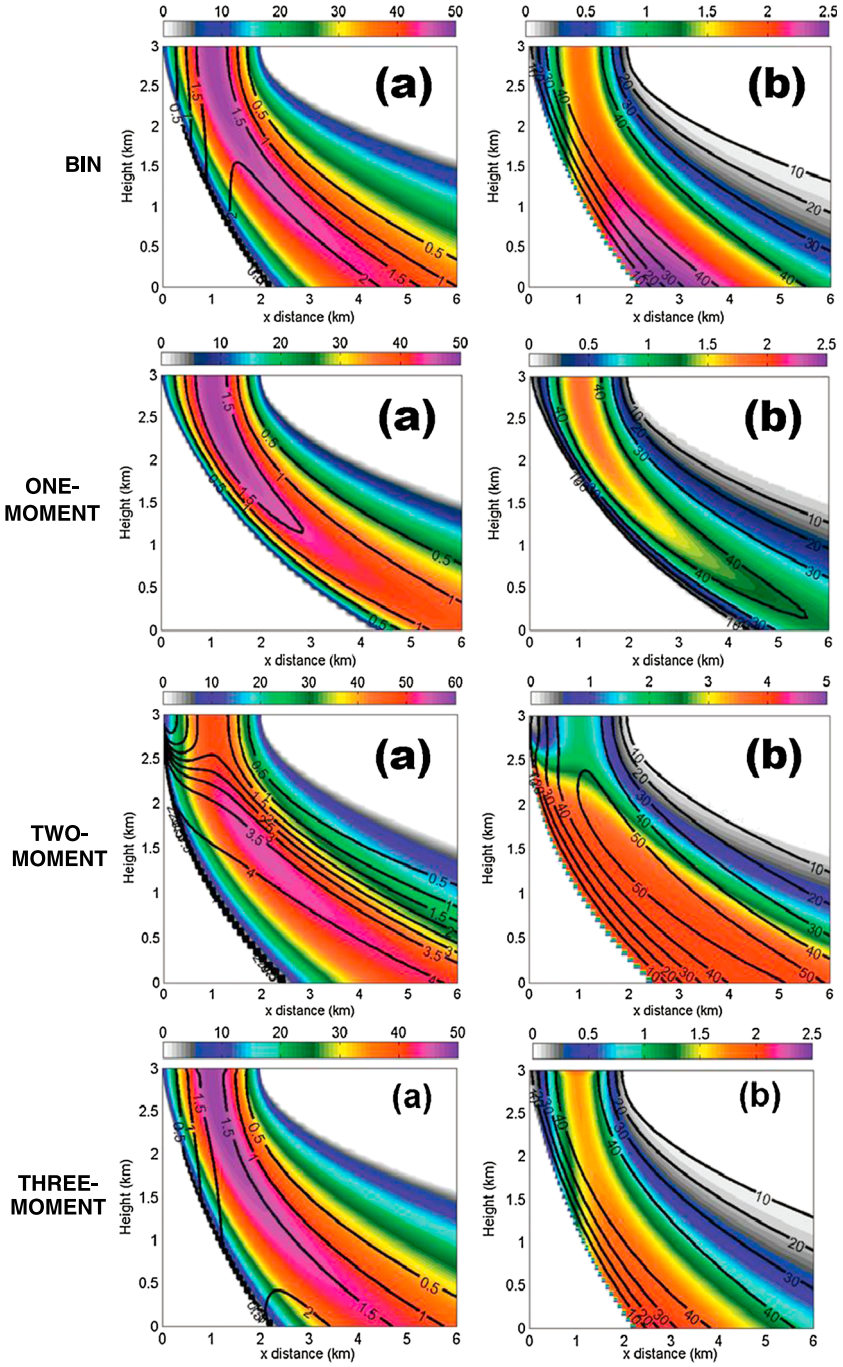

Figure 13. Results from the two-dimensional wind shear model obtained using different schemes of sedimentation. Panels show the 2-D fields of (a) *Z*H and (b) *Z*dr. Overlaid in Figure 13a are the *Z*dr contours (0.5–2.5 dB in 0.5 dB increments); Figure 13b has *Z*H contours (10–40 dB*Z*, in 10 dB*Z* increments) overlaid. For *Z*H of 0 dB*Z*, all fields are set to zero. Note that the color scales of *Z*H and *Z*dr for two-moment scheme differ from those in other panels. (From *Kumjian and Ryzhkov* [2012]; courtesy of the American Meteorological Society.)

or of a calculated shape parameter in a three-moment scheme, largely mitigates the errors associated with size sorting. Figure 13 shows that the three-moment bulk parameterization scheme provides the best agreement with the results of the bin approach. Nonetheless, even the three-moment scheme did not manage to simulate high *Z*dr near the surface in large falling raindrops (at *x* values of 2 to 4 km) (Figure 13).

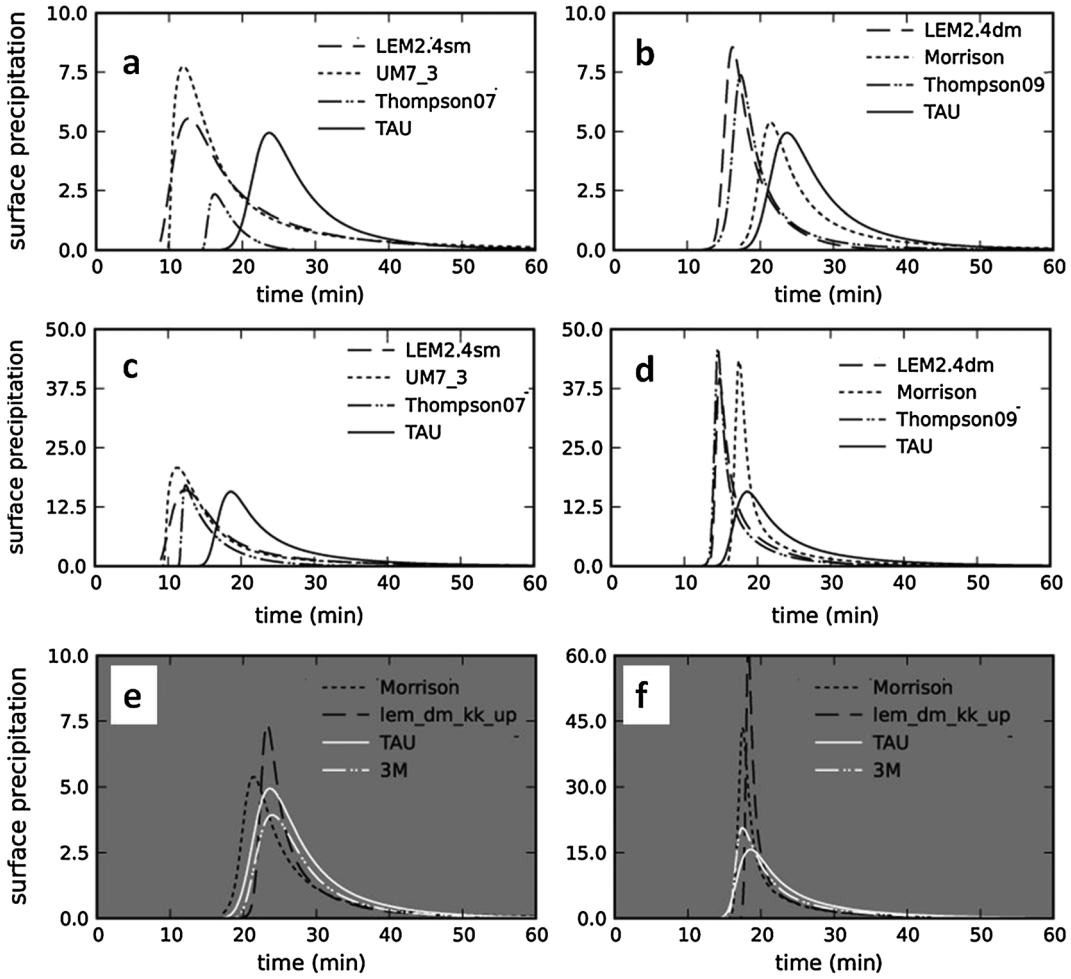

Figure 14. Time dependencies of precipitation rate (mm h^{-1}) in simulations with kinematic model using different bulk parameterization schemes and with MMM scheme. (a, b, and e) Simulations with vertical velocity of 2 m/s and (c, d, and f) the results of simulations with vertical velocity 3 m/s. Figures 14a and 14c show results of 1M schemes: LEM2.4sm [*Swann*, 1998], Thompson07 (modified from *Thompson et al.* [2004]), and UM7_3 [*Tripoli and Cotton*, 1980]. Figures 14b and 14d show results of 2M schemes LEM2.4dm [*Swann*, 1998], Thompson09 (modified from *Thompson et al.* [2004]), and Morrison [*Morrison et al.*, 2011].

Shipway and Hill [2012] compared rates of diffusional growth, collisions, and sedimentation, as well as surface precipitation in bulk microphysical schemes and in the MMM method of Tel Aviv University (TAU) [*Tzivion et al.*, 1987] using the 1-D Kinematic Driver Model (KiD) with a prescribed vertical velocity that evolves over time. KiD was developed at the UK Met Office to facilitate a consistent intercomparison of the microphysics parameterizations employed in a number of different cloud-resolving models and numerical weather prediction models. Among the bulk parameterization schemes, there were three one-moment schemes, three two-moment schemes, and one three-moment scheme. The warm microphysical processes were calculated. The results obtained using the MMM method (with 34 mass categories for drops) were considered to be benchmarked. The schemes tested produced very different surface precipitation rates and onset timing, as well as accumulated surface precipitation. The early onset of precipitation was shown to be a persistent feature of single-moment schemes (Figure 14). Two moment schemes exhibit better comparison with the MMM results. However, the peak of precipitation rate was larger than that in the MMM. The best agreement with the MMM results were reached using the three-moment scheme. Figure 14 shows that bulk schemes produce sharp and narrow peaks of precipitation as compared to the MMM scheme, which produced weaker precipitation that, over time, covered a larger area than the bulk parameterization schemes. This is a typical feature of many bulk parameterization schemes.

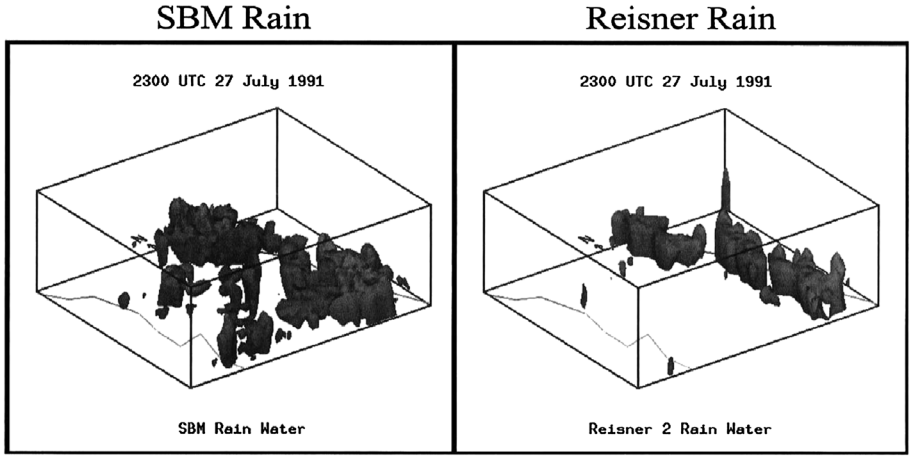

Figure 15. Three-dimensional structure of rainwater content in SBM FastM and in Reisner2 at 2300 UTC. Solid line denotes land-sea boundary. (From *Lynn et al.* [2005b]; courtesy of the American Meteorological Society.)

Below we present several examples intended to illustrate the abilities of bulk parameterizations and SBM to simulate different atmospheric phenomena of different spatial and time scales.

6.3. Mesoscale Rain Event

Lynn et al. [2005a, 2005b] appear to be the first study in which a SBM scheme was used in a mesoscale model (the fifth-generation Pennsylvania State University-NCAR Mesoscale Model (MM5)) [*Grell et al*., 1994] to simulate the evolution of a mesoscale convective system. The rain event over Florida on 27 July 1991, during the Convection and Precipitation Electrification Experiment was simulated. A 3 km resolution grid was used to simulate the mesoscale event for a comparatively long period of time and over a significant area. The rain event was simulated in experiments with both low and high CCN concentrations. The SBM results were compared to those obtained using different one-moment bulk parameterization schemes. All simulations produced more rain at certain locations than found in observations. While the SBM simulates well observed large areas of stratiform rain, the bulk schemes tended to underestimate the area of weak and stratiform rain (Figure 15).

Figure 16 shows time dependencies of the area average and maximum rain amounts. SBM produces results close to observations. The one-moment bulk models produced unrealistically large rain rates within a comparatively narrow line of cumulus clouds. One possible reason for such an effect is an incorrect representation of precipitation sedimentation. This example illustrates the substantial limitations of one-moment bulk parameterization schemes, even in the simulation of the most general characteristics such as structure of cloud ensemble and precipitation rates.

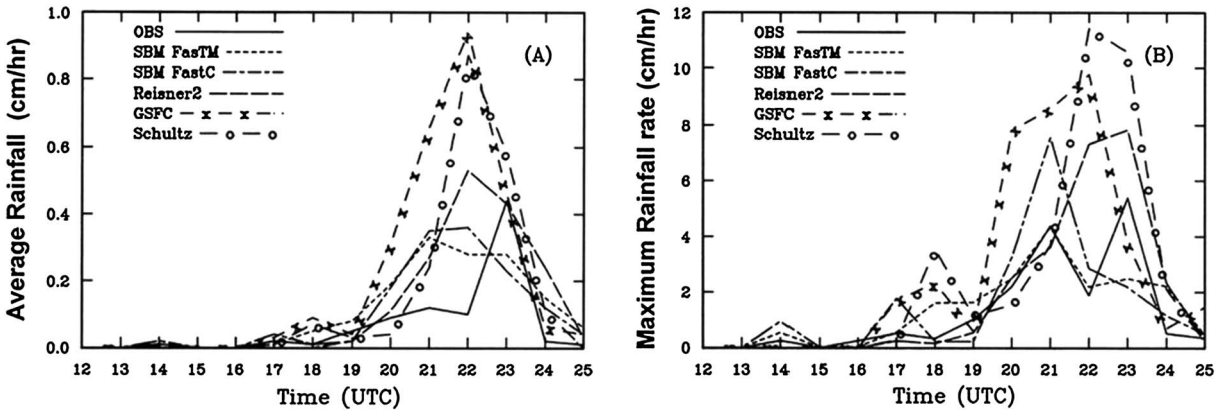

Figure 16. (a) Average and (b) maximum rainfall rates obtained from observations and model simulations. Notations: Reisner2 [*Reisner et al*., 1998], "GSFC" (Goddard Space Flight Center) [*Tao et al*., 2003], and "Schultz" [*Schultz*, 1995]. (From *Lynn et al*. [2005b]; courtesy of the American Meteorological Society.)

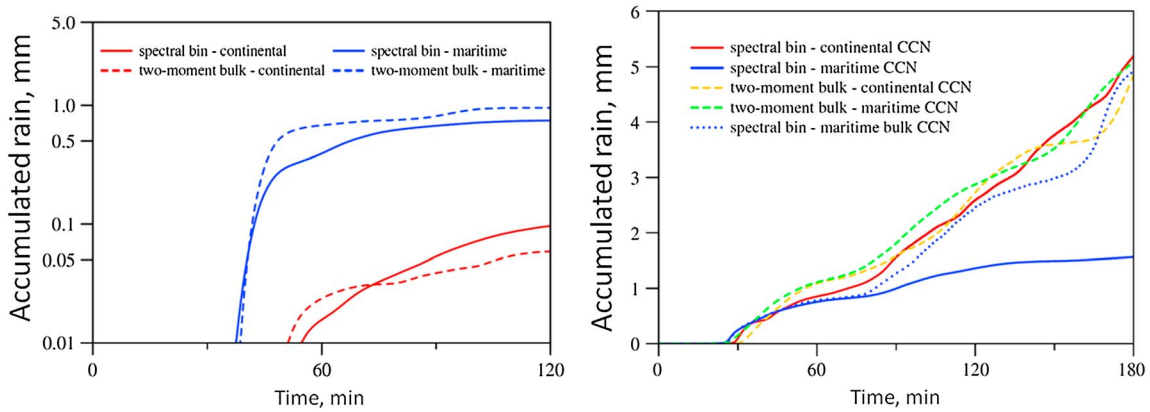

Figure 17. Time series of grid-averaged, accumulated surface precipitation from (left) the four simulations of continental clouds typical of Texas case and from (right) the five simulations of maritime clouds under GATE thermodynamic conditions using bin and two-moment bulk microphysics. In the simulations, high (continental) and low (maritime) CCN concentrations were used. (From *Seifert et al.* [2006]; courtesy of Elsevier.)

Lynn and Khain [2007] simulated the same storm using a larger computational area. They compared the results of SBM simulations with those obtained using bulk parameterization schemes other than those used in *Lynn et al.* [2005a]. Specifically, they used the Thompson scheme [*Thompson et al.*, 2006], the Reisner-Thompson scheme, which is a modified version of the Reisner2, and the two-moment scheme described by *Seifert et al.* [2006]. The results obtained are quite similar to those shown in Figure 15: all bulk schemes overestimated by a factor of 2–3 the averaged and maximum rain rates as compared to the observations. The two-moment scheme predicted rain rates better than the one-moment schemes. The SBM scheme overestimated the maximum rain rate by about 20%.

6.4. Cumulus and Stratocumulus Clouds

Morrison and Grabowski [2007] used a 2-D kinematic model with preset dynamics to compare the microphysical structure of warm stratocumulus clouds and warm cumulus clouds simulated using the *Morrison et al.* [2005b] two-moment bulk scheme with a bin scheme under different aerosol loadings. Three different parameterizations for the coalescence process were tested: B1994 [*Beheng*, 1994], SB2001 [*Seifert and Beheng*, 2001], and KK2000 [*Khairoutdinov and Kogan*, 2000]. Simulations showed that utilization of different schemes led to differences in horizontally averaged values of RWC, as well as mean raindrop diameters.

It is interesting that the difference in the accumulated rain produced by different schemes was comparatively low (up to 10–20%). This result suggests that accumulated rain is determined to a large extent by general properties of the atmosphere, such as environmental humidity and the dependence of saturating water vapor pressure on temperature, which is similar in all schemes. However, precipitation rates can vary quite dramatically in different schemes.

Morrison and Grabowski [2007] showed that results of one-moment schemes were much worse than those of two-moment schemes. They found that in order to adjust the results of one-moment schemes to those in two-moment ones, the intercept parameter N_0 should be changed in height by 5 orders of magnitude. Taking into account the strong sensitivity of the results to the value of the intercept parameter, they concluded that one-moment schemes are not suitable for use in regional or global climate simulations using cloud-resolving models.

A detailed comparison of bulk and bin approaches in the simulations of structure and precipitation of continental clouds (Texas clouds) and tropical maritime clouds (GATE 1974) was done by *Seifert et al.* [2006]. Toward this goal, the two-moment scheme by *Seifert and Beheng* [2006a, 2006b] was implemented into the HUCM. Simulations were performed for two aerosol loadings: a high CCN concentration of 1260 cm^{-3} and a low CCN concentration of 100 cm^{-3}. It was found that the most important factor in achieving a reasonable agreement between concentrations and mass contents in bulk parameterization and SBM is an accurate representation of the warm-phase autoconversion process. To obtain comparable results, the parameters of the various PSDs in the bulk scheme were calibrated. In spite of differences between PSDs in the bin and bulk

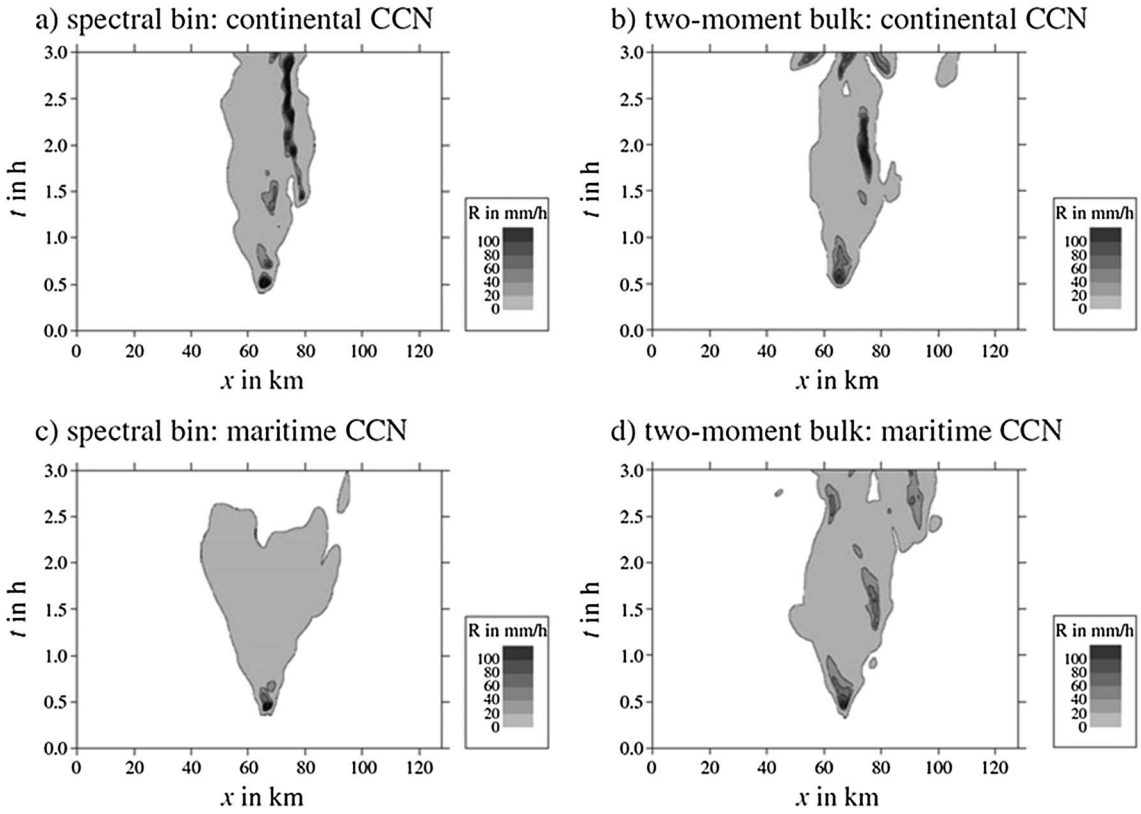

Figure 18. Hovmöller diagrams showing the surface precipitation in mm/h from the four GATE case simulations applying (a, c) spectral bin versus (b, d) two-moment bulk microphysics and assuming continental (Figures 18a and 18b) versus maritime CCN (Figures 18c and 18d). (From *Seifert et al.* [2006]; courtesy of Elsevier.)

simulations, the precipitation rates and accumulated precipitations turned out to be quite close, especially in the presence of high CCN concentrations (Figure 17).

The substantial difference in the accumulated rain amounts from maritime clouds at low CCN concentrations, seen in Figure 17 (right), is related to the fact that the bulk scheme did not take into account a decrease in aerosol concentration due to nucleation scavenging. Neglecting the aerosol budget in the SBM scheme led to a substantial decrease in the difference between accumulated rain amounts in the SBM and in the bulk scheme (see curve spectral bin-maritime bulk CCN in Figure 17). The neglect of such cloud-aerosol feedback led to a difference in the time dependencies of precipitation rates, as shown in Figure 18. In particular, one can see the formation of secondary convective clouds in the bulk parameterization simulation with low CCN (Figure 18d), while no such secondary convective clouds arose in the SBM simulation when most CCN were scavenged.

Fan et al. [2012a, 2012b] and *Wang et al.* [2013] reported a significant improvement of the two-moment *Morrison and Grabowski* [2007] bulk parameterization scheme when nucleation aerosol scavenging was taken into account. *Thus, to improve representation of cloud-aerosol interaction in atmospheric models using bulk parameterization schemes, the schemes should include the aerosol budget, aerosol transport and the process of nucleation scavenging.*

Sensitivity experiments performed by *Fan et al.* [2012a, 2012b] and *Wang et al.* [2013] using four different types of autoconversion schemes revealed that errors in predicting cloud water content could be traced largely to saturation adjustment employed in calculating condensation/evaporation in bulk schemes. Last, it was found that rain evaporation in bulk schemes was too fast, as compared to the SBM. This effect was also found by *Li et al.* [2009b] and *Shipway and Hill* [2012].

Saleeby and van den Heever [2013] showed that in bulk parameterization schemes that represent aerosol budgeting, transport, and nucleation scavenging, the reproduction of microphysical parameters appears to be significantly improved. Sensitivity experiments done using four different types of autoconversion schemes

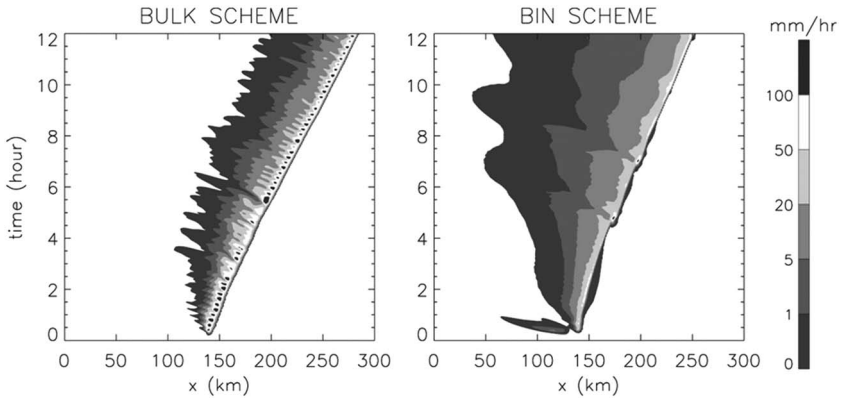

Figure 19. The time-domain diagram of surface rainfall for the (left) bulk and (right) bin scheme simulations. (Adopted from *Li et al*. [2009a]; courtesy of the American Meteorological Society.)

reveal that the saturation adjustment employed in calculating condensation/evaporation in bulk schemes is largely responsible for the major discrepancies in predicting cloud water content. Thus, *an explicit calculation of the diffusion growth with predicted supersaturation (such as is included in the bin-emulating bulk scheme of the RAMS model) is a promising way to improve bulk microphysics schemes.*

The results again indicated that two-moment schemes have significant advantages over one-moment ones.

Noteworthy is that the implementation of nucleation scavenging by *Wang et al*. [2013] doubled the required computer time. As a result, the computer time-cost ratio of SBM/Bulk decreased in this particular case from ~12 to ~6–7. The implementation of equations for diffusion growth of droplets requires substantial changes in bulk schemes and will lead to further increases in computational time.

6.5. Squall Lines

Squall lines are a vivid example of mesoscale convective systems in which convective clouds form a line of several hundred kilometers in length. The front of a squall line represents an elongated thunderstorm characterized by heavy rain, hail, and lightning. The width of the leading updraft core of a squall line typically ranges from 10 to a few tens of kilometers. A wide zone of light precipitation forms behind the convective zone. The light precipitation zone, caused largely by aggregates, has a width of a few hundred kilometers. Squall lines represent a typical type of severe weather phenomenon both over land and over sea. However, over the sea squall lines represent the dominant type of mesoscale convective systems. The lifetime of squall lines can be as long as 10 h, as compared to about 1 h of isolated clouds. The formation of squall lines and their longevity have been well investigated [*Heymsfield and Schotz*, 1985; *Rotunno et al*., 1988; *Tao et al*., 1993].

Li et al. [2009a, 2009b] simulated a squall line typical of continental conditions observed during the Preliminary Regional Experiment for Storm-scale Operational and Research Meteorology 1985 (PRE-STORM) [*Rutledge et al*., 1988; *Zhang et al*., 1989; *Braun and House*, 1997]. Simulations were performed using the 2-D anelastic version of the Goddard Cumulus Ensemble model (GCE) with two types of microphysical schemes, namely, a one-moment bulk microphysical scheme based on *Lin et al*. [1983] with prognostic equations for mixing ratios of cloud water, rain, ice, snow, and graupel/hail, and SBM [*Khain et al*. 2004; *Phillips et al*., 2007b]. The model resolution in the zone of interest was 1 km; time step was 6 s. Figure 19 shows the surface rainfall time-domain plots obtained in these simulations.

Figure 19 shows that the squall line simulated by the SBM had a much larger trailing stratiform area than the squall line simulated using the bulk parameterization scheme. These results accord well with those shown in Figure 14. The SBM indicates a much larger contribution of light rain to the total surface rainfall. The SBM actually did not generate rain rates higher than 90 mm/h. During the mature stage, about 20% of the total surface rainfall was stratiform in the SBM, compared with only 7% in the bulk simulation. According to *Johnson and Hamilton* [1988], about 29% of the surface rain came from the stratiform region. This means that the SBM describes the partitioning of rain into convective and stratiform better than the one-moment bulk parameterization scheme.

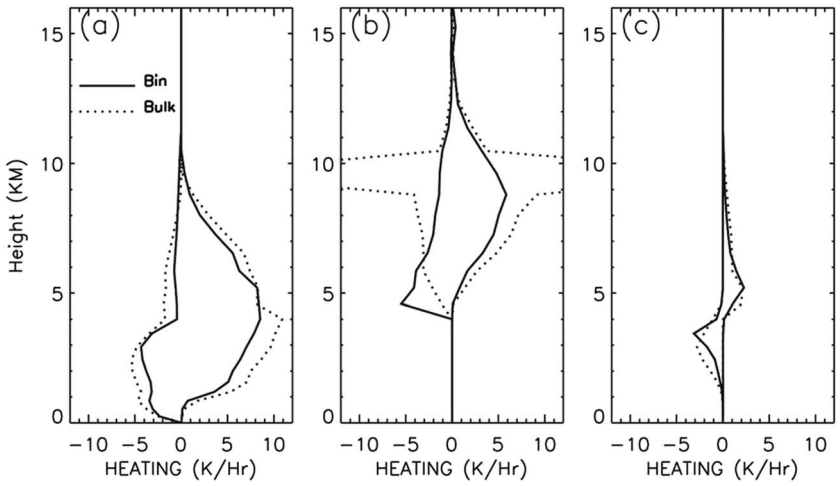

Figure 20. Components of the microphysical heating profiles simulated by the bulk (dashed lines) and bin (solid lines) schemes: (a) condensation and evaporation, (b) deposition and sublimation, and (c) melting and freezing. (Adopted from *Li et al*. [2009a]; courtesy of the American Meteorological Society.)

Another significant difference between structures of a squall line simulated by the bulk parameterization scheme, on the one hand, and by the SBM and observations, on the other, is the formation of high rainfall rate streaks in the bulk parameterization scheme, which extend from the leading convection well into the stratiform region, and the lack of them in the SBM simulations and in the observations. These high surface rainfall streaks manifest themselves as propagating convective cells, as seen well rearward into the trailing stratiform region.

The appearance of a multicell structure within simulated squall lines using bulk parameterization runs is attributed by *Li et al*. [2009a, 2009b] to errors in both the evaporation rate of (i.e., to cooling at low levels), as well as in the fall velocity of graupel in bulk parameterization schemes. Tuning these values made the results obtained using the bulk scheme closer to those of the SBM.

Figure 20 shows the vertical profiles of the heat budget items related to different microphysical processes. The budgets were calculated for the entire computational area. Bulk parameterization leads to higher condensation and stronger evaporation than the SBM and to similar rates of freezing and melting. In general, despite very different local precipitation rates and spatial precipitation distributions, the accumulated rain was nearly the same, namely, the average area rain rate was 2.7 mm/h and 2.4 mm/h in the bulk parameterization and in the SBM, respectively. We draw attention to the large spikes in both deposition and sublimation at around 10 km in the bulk simulation seen in Figure 20. These spikes are produced artificially by limitations in the saturation adjustment scheme in the bulk scheme. Although these two spikes largely cancel out each other and have little effect on the total energy budget, the related heating and cooling can substantially affect the structure of the squall line in the bulk parameterization.

Morrison et al. [2009a] simulated an idealized squall line similar to that simulated by *Li et al*. [2009a, 2009b] using a 2-D version of WRF. The two-moment bulk parameterization scheme described by *Morrison et al*. [2005b] and *Morrison and Grabowski* [2007] was used. This scheme includes prognostic variables for the mixing ratio and the number concentration of graupel. The results of the simulations were compared to those obtained using a single-moment scheme. The single-moment scheme was formed from the two-moment one, except that the number concentrations of the precipitation species were preset, not predicted. Thus, the intercept parameters were specified for rain, snow, and graupel. The Hovmöller plot of surface rainfall rate for the two-moment and one-moment simulations is presented in Figure 21. The squall lines simulated in this study were much more intense than those in the simulations performed by *Li et al*. [2009a, 2009b]. The widths of convective precipitation zones exceeded 50 km, and the fraction of light rain was much less than in the SBM.

The main finding of the study was that the two-moment scheme produced a much wider and prominent region of trailing stratiform precipitation, relative to the single-moment scheme. This difference was attributed to a decrease in the rain evaporation rate in the stratiform region in the two-moment scheme as

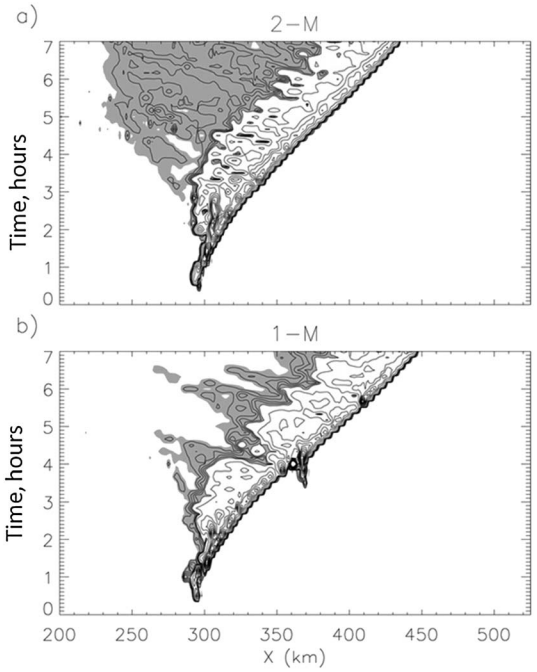

Figure 21. Hovmöller plot of the surface rainfall rate for the (a) two-moment and (b) one-moment simulations. Contour interval is every 1 mm h^{-1} for rates between 0 and 5 mm h^{-1} and every 10 mm h^{-1} for rates greater than 10 mm h^{-1}. To highlight the stratiform rain precipitation region, moderate precipitation rates between 0.5 and 5 mm h^{-1} are shaded gray. (From *Morrison et al.* [2009a]; courtesy of the American Meteorological Society.)

compared to that in the one-moment scheme. The difference in rain evaporation rates reflects the difference in the shape of raindrop distribution, expressed in the values of the intercept and slope parameters. In the two-moment scheme where the intercept parameter was calculated, it ranged from 10^5 to $10^7 m^{-4}$ in the stratiform region and from 10^7 to 10^9 m^{-4} in the convective region, compared with a constant value of 10^7 m^{-4} specified in the single-moment scheme. Larger values of the intercept parameter in the convective region are related to higher collision rates. At the same time, rain in the stratiform region was primarily produced by melting snow. The key point is that no single value of the intercept for raindrops in the one-moment scheme was able to reproduce the results of the two-moment scheme. These results show again that the two-moment scheme produced more realistic results vis-à-vis the spatial distribution of precipitation than the single-moment one. They also show that spatial precipitation distribution depends dramatically on the way in which parameters determining the shape of PSDs are calculated.

Baldauf et al. [2011] carried out many simulations using the COSMO weather forecast model. These researchers found the more sophisticated two-moment scheme advantageous in cases of strong squall line situations.

Finally, *Khain et al.* [2009] simulated the same squall line as *Morrison et al.* [2009a] but used the WRF with two microphysical schemes: the SBM scheme similar to that used by *Khain et al.* [2004a] and *Li et al.* [2009a, 2009b] and a two-moment bulk parameterization scheme [*Thompson et al.*, 2004, 2008] (see Table 2). Simulations were carried out with different CCN (and cloud droplet) concentrations. The dynamical and microphysical structure of the squall line simulated with the WRF/SBM is quite similar to that simulated by *Li et al.* [2009a, 2009b] using GCE/SBM. The bulk scheme produced substantially lower CWC in cases of low CCN concentration and substantially lower RWC in cases of higher CCN concentration than that found in the SBM. The overlapping differences in the structure of the squall lines were reported by *Li et al.* [2009a, 2009b], where another bulk scheme was used. Accumulated rain predicted by the SBM scheme was close to that predicted by the SBM scheme in *Li et al.* [2009a, 2009b], but twice as low as *Thompson et al.*'s [2008] bulk parameterization scheme. Both schemes predicted substantially lower rain rates than those obtained by *Morrison et al.* [2009a].

These results support the conclusion that two-moment bulk parameterization schemes predict the spatial structure of rain in squall lines better than single-moment ones, but the spatial distribution depends heavily on parameters determining the DSD shape.

6.6. Supercell Storms

Khain and Lynn [2009] simulated a supercell storm with a 2 km resolution WRF using SBM [*Khain et al.*, 2004a], as well as the Thompson (2004) bulk parameterization scheme. The computational area was 252 km × 252 km, and the maximum time step was 10 s. The simulations were performed under clean, semipolluted, and polluted conditions. To show that aerosol effects on precipitation depend on environmental conditions and to compare aerosol effects with the impact of other factors, the simulations were carried out under moderate humidity, typical of the U.S. Great Plains region and also higher relative humidity, typical of the U.S. southern Gulf coast. The difference between the relative humidity in these simulations was about 10%. Maximum vertical velocities

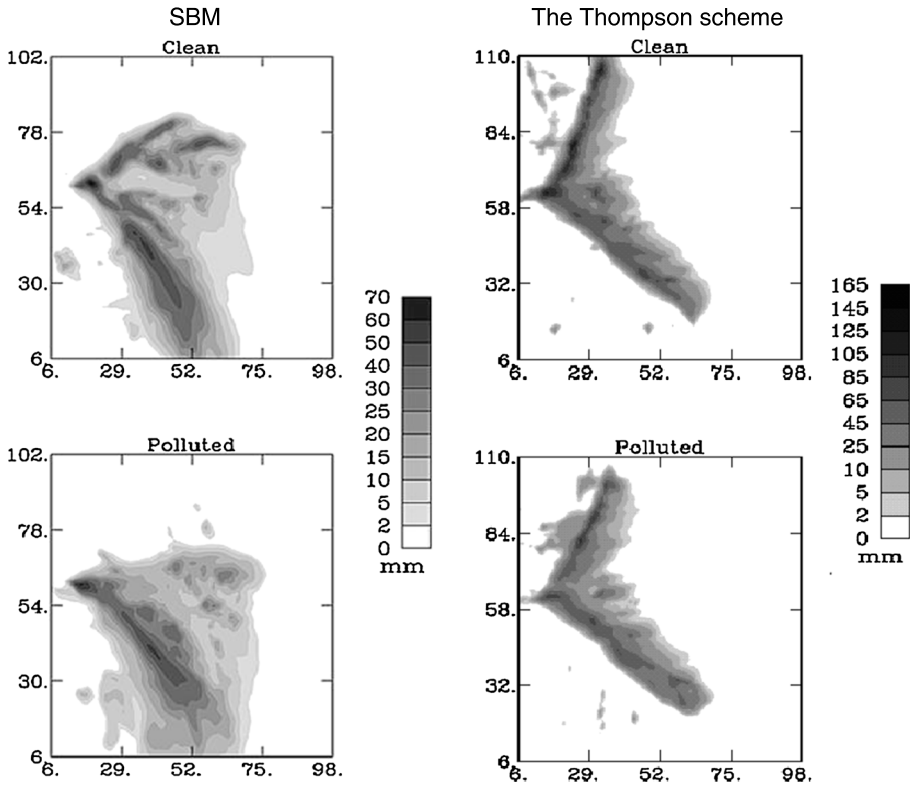

Figure 22. Accumulated surface rain simulated using the SBM and the Thompson scheme at 240 min under relatively high humidity for (top row) clean and (bottom row) polluted conditions. Grey scales for SBM and the bulk scheme are different. (From *Khain and Lynn* [2009]; courtesy of the American Geophysical Union.)

in SBM simulations ranged from 25 to 40 m/s. The Thompson scheme produced maximum vertical velocities ranging from 45 m/s to 65 m/s. Both schemes produced two branches of precipitation, the SBM simulations predicted stronger intensification of the right-hand branch, while the Thompson scheme predicted faster development of the left-hand branch of the storm (Figure 22). Analysis shows that these differences in precipitation structures are caused by differences in the vertical velocities produced by the schemes, which leads to an ascending of hydrometeors to altitudes with different directions of background flow.

The bulk parameterization scheme produced twice as much accumulated rain as the SBM. An increase in humidity leads to a dramatic change in precipitation amount and distribution (Figures 23a and 23b). A similar study dealing with the same supercell storm was carried out by *Lebo and Seinfeld* [2011]. In their study, the results obtained using the MMM scheme [*Reisin et al*., 1996a] were compared with those obtained using the double-moment bulk scheme developed by *Morrison et al*. [2005a]. Figures 23c and 23d show the domain average cumulative surface precipitation for these simulations. The cumulative surface rain was similar in the SBM and the MMM at both high and low relative humidities. The bulk parameterization scheme by *Morrison et al*. [2005a] produced twice the amount of accumulated rain as in the bin schemes. The accumulated rain responded in opposite ways to changes in the CCN concentration in the bulk scheme, on one hand, and the bin schemes, on the other.

6.7. Hailstorms

Hailstorms pose a serious threat to agriculture and property across the globe. The hail-induced damage rapidly increases with hail size. Since hail grows largely by accretion of supercooled water, the mass of supercooled water would be expected to substantially affect the size of hail particles. Hail suppression hypotheses suggest that in order to prevent the growth of initial hail embryos to hailstone size, the amount of supercooled water should be decreased [*Krauss*, 1999; *Wisner et al*., 1972; *Heymsfield*, 1982]. Since an increase in CCN concentration typically leads to an increase in supercooled water content, one can expect a substantial effect of the CCN on the mass and the size of hail particles.

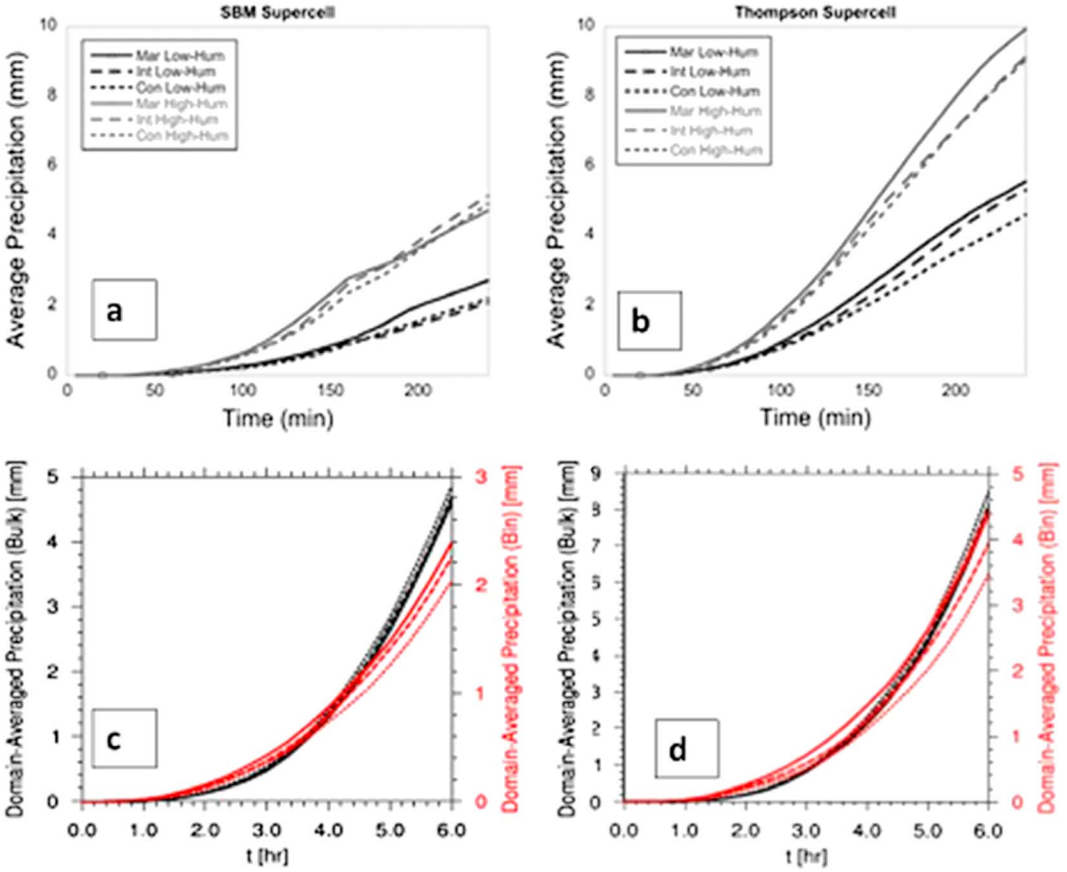

Figure 23. Cumulative surface precipitationin simulations of a supercell storm: (a) the SBM and (b) the two-moment bulk parameterization scheme. (Adopted from *Khain and Lynn* [2009].) Domain-averaged cumulative precipitation in simulations: (c) with the low RH and (d) with high RH using the bulk (black) and bin (red) microphysics models. The simulations were performed for the "clean" (solid), "semipolluted" (dashed), and "polluted" (dotted) scenarios (Adopted from *Lebo and Seinfeld* [2011]; courtesy of the American Geophysical Union.)

Simulation of large hail requires an accurate reproduction of the tail of a hail PSD. *Wisner et al*. [1972] developed a hybrid bulk-bin parameterization model in which hail was described using a significant number of bins. Here we compare the results of three advanced microphysical models that were used for simulation of hailstorms producing hailstones with diameters up to 5 cm and radar reflectivity up to 70 dB*Z*. A hailstorm in Villingen-Schwenningen, southwest Germany, on 28 June 2006 was simulated using two models: the 2-D SBM model HUCM [*Khain et al*., 2011; *Kumjian et al*., 2014] and the 3-D weather prediction model COSMO with *Seifert and Beheng*'s [2006a, 2006b] two-moment bulk microphysical scheme. To simulate large hail, a special hydrometeor class of large hail was introduced into the bulk parameterization scheme [*Noppel et al*., 2010b].

Although both models were able to reproduce the hailstorm, the parameters of the simulated hailstorms turned out to be quite different. The radar reflectivity field simulated by HUCM with high CCN concentrations accords well with the observations: the maximum radar reflectivity reaches 70 dB*Z*, and high values of reflectivity reach altitudes of 10–11 km (not shown). The SBM-simulated maximum reflectivity in the case of high CCN concentrations is substantially higher than in the case of low CCN concentrations. In contrast, the COSMO model with bulk parameterization predicts higher values of reflectivity and larger areas of high reflectivity in the case of clean air. In the simulations using bulk parameterization, the radar reflectivity rapidly decreases with height above 6 km.

Both in a study by *Khain et al*. [2011] and in the simulations of the same storm using a new version of HUCM with explicit treatment of wet growth of hail [*Khain et al*., 2014b; E. Ilotoviz et al., Effect of aerosols on freezing drops, hail and precipitation in a mid-latitude storm, *Journal of the Atmospheric Sciences*, in revision, 2015], the

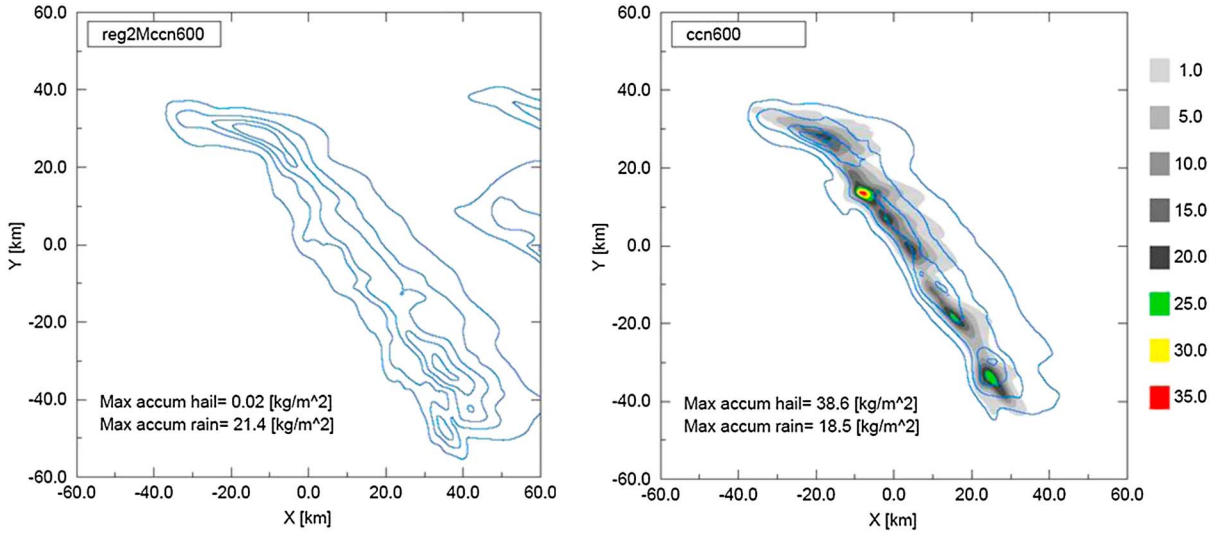

Figure 24. Surface accumulated amounts of hail (shaded contours) and rain (blue contours) at end of simulation (210 min) for (left) REG2M and (right) 3MHAIL schemes. Contour values are 1, 5, 10, 15, 20, 25, 30, and 35 kg m^{-2}. The CCN concentration is 600 cm^{-3}. (From *Loftus and Cotton* [2014b] with changes; courtesy of Dr. Cotton.)

diameter of hailstones in the case of high CCN concentrations reached 5 cm. This is in agreement with the observations. In the clean case, the diameter of hail particles was typically lower than 2 cm.

In SBM simulations, the hail shaft at the surface was much higher in the polluted case than in the clean one. In the clean case, hail particles are small and melt before reaching the surface. In contrast, in simulations with two-moment schemes, the hail shaft in the clean air case was substantially larger than in the polluted case.

Actually, the SBM- and the two-moment bulk schemes simulate different mechanisms of hail growth. While in the SBM at high CCN concentrations hail grows largely by the accretion of high supercooled water content in the area of cloud updraft, in the two-moment bulk scheme hail forms mostly by freezing raindrops at comparatively low distances above freezing level.

To improve the representation of hail using bulk parameterization schemes, *Loftus et al.* [2014] developed a 3MHAIL bulk parameterization (see Table 2) in which hail evolution was described using three PSD moments, while the other hydrometeors were described using a two-moment scheme. This scheme has been implemented into RAMS. A supercell storm that occurred over northwest Kansas on 29 June 2000 during the Severe Thunderstorm and Electrification and Precipitation Study was simulated. The results of the 3MHAIL scheme were compared to two different two-moment schemes, one of which is the two-moment bin-emulating scheme (REG2M) used in RAMS [*Cotton et al.*, 2003]. The second one is obtained by a simplification of the 3MHAIL scheme.

All schemes managed to simulate the formation of strong hailstorms. All models simulated maximum velocities up to 40 m/s. In all simulations, the integral mass of hail in clouds is maximum at lower CCN concentrations. At the same time, none of the two-moment bulk parameterization schemes were able to simulate observed high radar reflectivity at altitudes of 9–11 km. Large hail in the two-moment bulk schemes did not exceed 2 cm in diameter. Figure 24 shows surface accumulated amounts of hail and rain at the end of the simulation (210 min) in the REG2M scheme and in the 3MHAIL scheme. In Figure 24, the accumulated rain amounts are also presented. One can see that surface precipitation in the case of the three-moment bulk parameterization scheme consists largely of hailstones, while the two-moment scheme actually does not produce hail at the surface. Total (rain + hail) precipitation is substantially higher in the 3MHAIL case.

Comparison of calculated radar reflectivity, polarimetric parameters, and hail size with observations indicates that the SBM and 3MHAIL schemes simulated the microphysics of the hailstorm much better than the two-moment schemes. Both the SBM and the 3MHAIL schemes produced hailstones with diameters of several centimeters in the case of high CCN concentrations, and both schemes predict an increase in hail precipitation at the surface level in the polluted case [*Loftus and Cotton*, 2014b; E. Ilotoviz et al., in revision, 2015]. Simulations

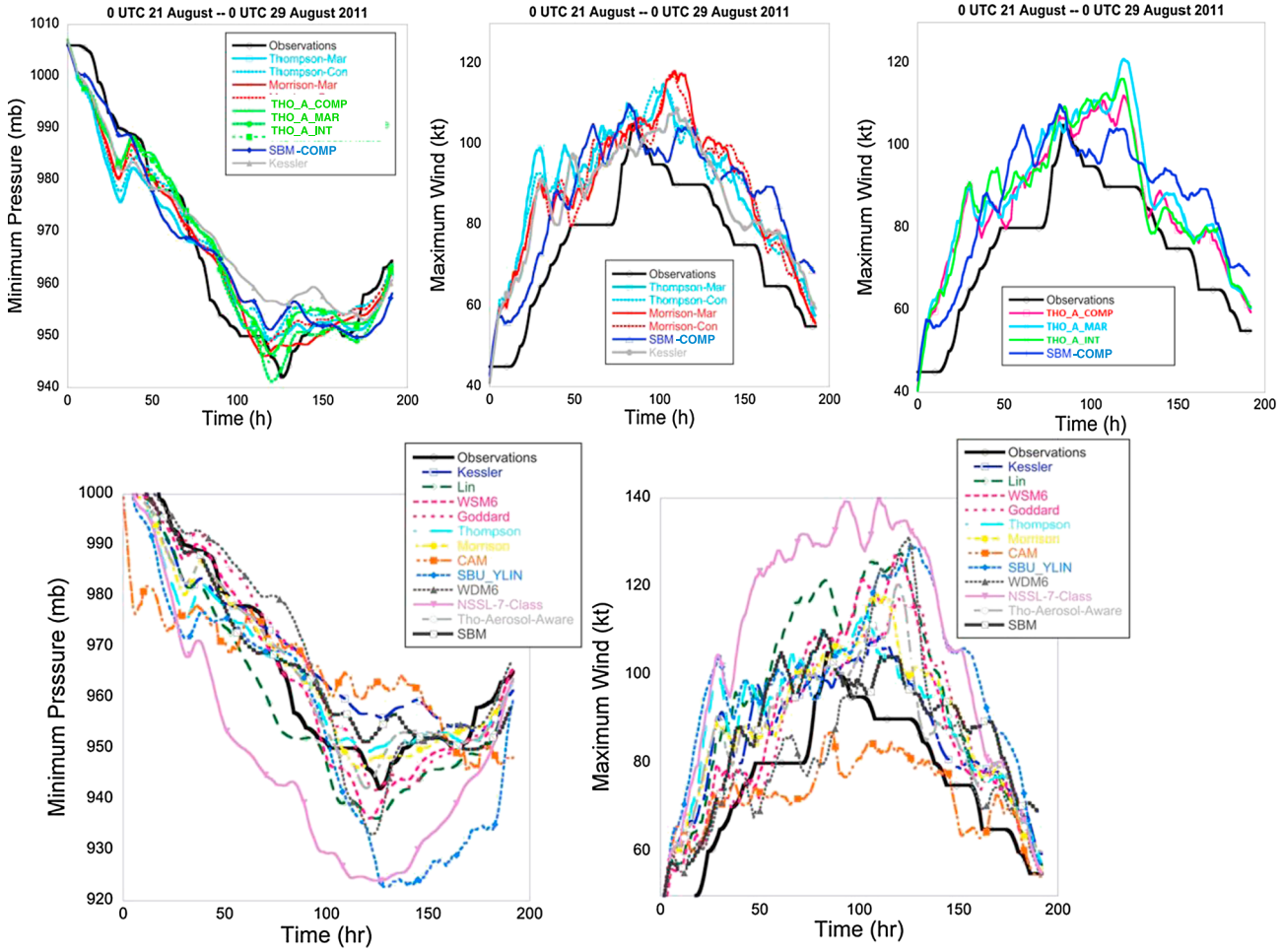

Figure 25. (top row) Time dependencies of the minimum pressure (left) and maximum wind velocity (middle and right) in simulations carried out with SBM and schemes by Morrison and Thompson allowing changes of aerosol or droplet concentrations. The results obtained using the simplest warm rain Kessler parameterization, as well as observed dependencies are presented for comparison. (bottom row) Time dependencies of minimum pressure and maximum wind speeds in WRF simulations of Hurricane Irene (2011) using different bulk parameterization schemes. Most bulk schemes are described in Table 2. Notations: Simulations with low CCN (or droplet) concentrations are denoted as MAR. Simulations with high CCN (or droplet) concentrations are denoted as CON. The scheme denoted as "Thompson" is described by *Thompson et al.* [2004]. The scheme denoted as "Morrison" is described by *Morrison et al.* [2005a]. The scheme denoted as "Tho-Aerosol-Aware" is described in *Thompson and Eidhammer* [2014] [from *Khain et al.*, 2014a, also in revision, 2015)].

of a hailstorm using a three-moment bulk scheme [*Milbrandt and Yau*, 2006] supported the ability of the three-moment schemes to simulate large hail stones.

The results of these studies show that the simulation of such phenomena as large hail requires an accurate description of the PSD tail and necessitates the utilization of at least three moments of hail PSD to simulate the formation of hail of several centimeters in diameter. At the same time, the location of precipitation, as well as the approximate accumulated rain mass, can be described using two-moment bulk parameterization schemes.

6.8. Hurricanes

The intensity of a hurricane depends on its rate of latent heat release, as well as on its spatial distribution. Taking into account the dominant role of latent heat release, tropical cyclones are ideal phenomena to test and to compare different microphysical parameterizations [e.g., *Tao et al.*, 2011]. We illustrate the effects of microphysical parameterizations on the intensity of a model tropical cyclone (TC) using as an example a simulation of Hurricane Irene, which moved northward along the U.S. coast during the second half of August 2011. The resolution of the finest nested grid over the area of 500 km × 500 km was taken as 1 km, and TC-ocean coupling was taken into account. Two aerosol scenarios were considered. In the first scenario, the aerosol concentration was assumed to be low (100 cm^{-3} at S = 1%) over the entire computational area, including North

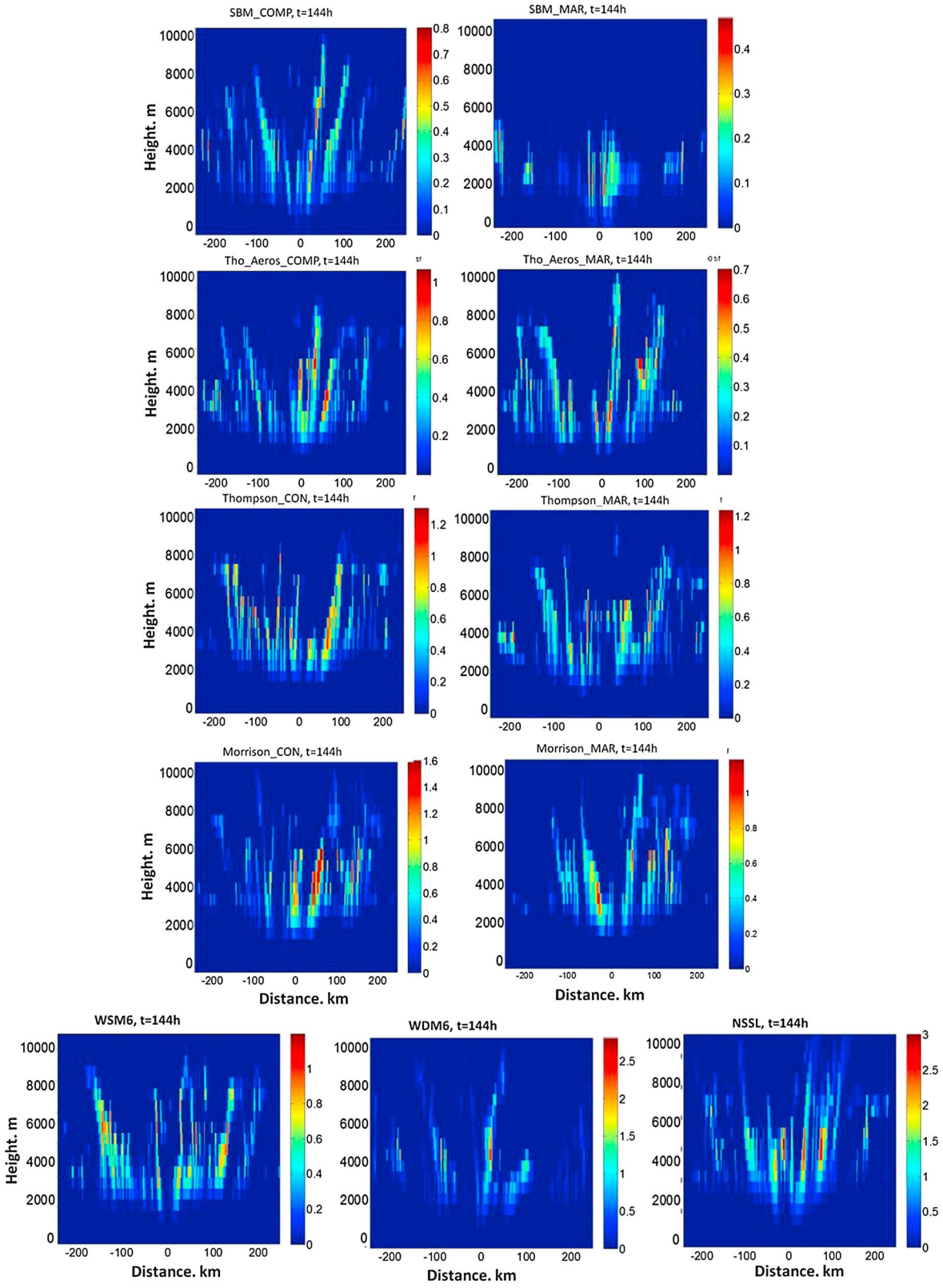

Figure 26. Vertical east-west cross sections in the fields of the cloud water mixing ratio (in gkg^{-1}) in simulations of Hurricane Irene. (first to fourth rows) The fields calculated with microphysical schemes allowing for different droplet concentrations as input. Panels in the left column correspond to simulations with higher droplet concentrations. The cross sections in the right column show the results of the simulations with low maritime droplet concentrations. (fifth row) The WSD6, WDM6, and NSSL bulk parameterization schemes which do not contain droplet concentration as an input parameter. (From A. Khain et al., in revision, 2015.)

America and the Atlantic. In the second scenario, the concentration of aerosols over land was increased to ~2000 cm^{-3}. Simulations with low CCN concentrations are denoted as "MAR," simulations with high CCM concentrations over land are denoted as "COMP" and simulations with bulk-schemes using high (continental) droplet concentrations over the entire area are denoted as "CON." Figure 25 shows the time dependencies of minimum pressure and maximum wind speeds in WRF simulations using different bulk parameterization schemes mostly described in Table 2. Figure 25 (top row) shows time dependencies of the minimum pressure (left) and maximum wind velocity (middle and right) in simulations carried out with SBM and schemes by Morrison and Thompson allowing changes of aerosol or droplet concentrations. Among the bulk parameterization schemes, the Thompson and Morrison schemes produce the best agreement with observations. Figure 25 (bottom row) shows the time dependencies calculated in all simulations with different bulk schemes. The great variation in time dependencies suggests a substantial sensitivity of TC intensity to the treatment to cloud microphysics. The variability of minimum pressure and maximum wind predicted by different bulk schemes is great: up to 40 mb and 60 kt (30 m/s), respectively. *Tao et al.* [2011] also obtained a high variability of intensity of model TCs simulated by using different bulk schemes. Figure 25 suggests the major importance of a correct description of microphysical processes.

A specific feature of Hurricane Irene was a 4 h time shift between the maximum wind speed and the minimum surface pressure. This effect is related to an increase in the TC size, caused, as was shown by *Khain et al.* [2014a, also in revision, 2015] and *Lynn et al.* [2014], by aerosols that penetrated to the TC and fostered formation of secondary eyewall at larger distance from the TC center. Figure 25 (top row) shows that only SBM was able to simulate such a time shift. The good simulation of maximum wind-minimum pressure dependencies by the WRF/SBM model indicates the importance of high-quality microphysical schemes for prediction of TC intensity.

It is well known that the cloud-water mixing ratio or cloud-water content (CWC) is acutely sensitive to aerosol concentration and significantly affects the rates of both warm and cold processes. To compare the sensitivity of different microphysical schemes to aerosols, in Figure 26 we present vertical east-west cross sections of CWC obtained by SBM and bulk schemes. The first to fourth rows show the CWC fields simulated by bulk schemes in which initial aerosols or droplet concentrations were high, as in continental clouds (left column), and low, as in clean maritime air. Note first that the maximum values of the CWC in these simulations are close, which is in keeping with the fact that these schemes simulated tropical cyclones of similar intensity. CWC is substantially larger and reaches higher levels in the COMP case than in the MAR case with SBM. The difference in the fields of CWC in the bulk schemes with high and low aerosol (or droplet) concentrations is much less pronounced. The ratio of the maximum values of CWC in the SBM_COMP and the SBM_MAR exceeds 2. At the same time, the ratio in the bulk schemes is typically below 1.5. In the SBM_MAR, no CWC occurred above an altitude of about 5 km, yet in all of the simulations with bulk schemes, a significant amount of supercooled CWC reached 9 km, and occasionally the level of homogeneous freezing (~10 km). Actually, the cross sections in the CWC fields in the bulk-MAR are much more similar to the CWC cross sections of the SBM_COMP than to the SBM_MAR. So, Figure 26 shows a much lower sensitivity of bulk schemes to aerosols than SBM, in agreement with the results of the simulations of TC intensity.

The CWC cross sections plotted for the simulations with WSM6, WDM6, and NSSL (see Table 2) bulk schemes also showed that supercooled CWC reaches the level of homogeneous freezing, which is to be expected in the presence of high CCN concentrations. The cross sections of CWC in WDM6 and, especially in NSSL, indicate much higher CWC maxima than when using the other microphysical schemes. The very high CWC in the NSSL run was in accordance with a very high TC intensity predicted by this scheme (Figure 25, bottom row).

Figure 27 shows the maximum wind-minimum pressure dependencies in the 1 km ocean coupling simulations of Irene with different bulk parameterization schemes and using WRF/SBM. The observed dependence is also presented. One can see that the WRF/SBM simulates the observed dependence well. Other schemes show substantial differences with observations. These deviations are closely related to the failure of the bulk schemes to predict the time shift between the maximum wind and minimum pressure caused by aerosol effects. Circles in the figure denote the points of the minimum pressure and maximum wind. All of the bulk schemes predicted the minimum pressure and the maximum wind in one time instance, which is denoted by one circle of the maximum wind-minimum with pressure dependencies. The SBM predicts maximum wind and minimum

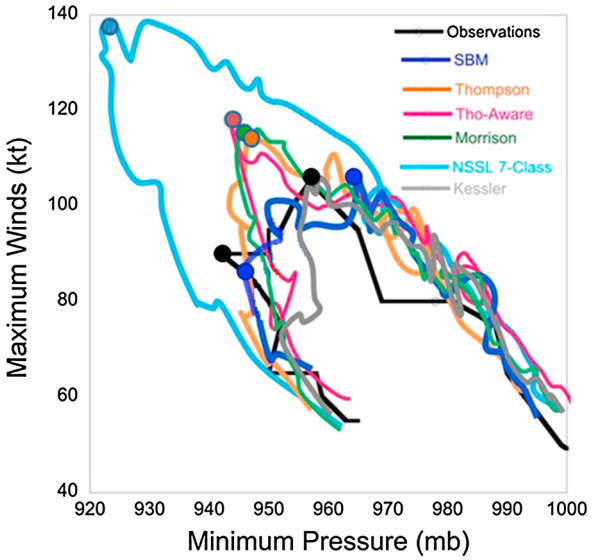

Figure 27. The maximum wind-minimum pressure dependencies calculated in the 1 km resolution simulations of Irene using the WRF model with the TC-ocean coupling taken into account. The dependencies are plotted for different microphysical schemes. The dependence calculated using observed data is presented as well. Circles denote the points of minimum pressure and maximum wind. All bulk schemes predict the minimum pressure and maximum wind in one time instance, which is denoted by one circle of the maximum wind-minimum pressure dependencies. The SBM predicts the maximum wind and minimum pressure at different time instances, which is denoted by two circles. The results of SBM agree well with observations. (From *Lynn et al.* [2014], with changes.)

pressure at different time instances, which is denoted by two circles on the corresponding curve. The results of SBM agree well with observations.

The simulations of hurricanes show that the intensity of tropical cyclones in numerical models depends strongly on the microphysical schemes used. The improvement of model resolution requires a better model microphysics to simulate the observed TC behavior. The utilization of SBM allows for better simulation of TC intensity and structure than the more simple bulk parameterization schemes.

Simulations of hurricanes performed using different aerosol concentrations (not shown) indicate that an increase in CCN concentration at the TC periphery leads to TC weakening [*Zhang et al.*, 2007, 2009; *Cohen and Khain*, 2009; *Khain et al.*, 2010; *Carrió and Cotton*, 2010; *Rosenfeld et al.*, 2012; *Cotton et al.*, 2012; *Hazra et al.*, 2013; *Lynn et al.*, 2014], while an increase in aerosol concentration at the inner TC core leads to TC intensification [*Herbener et al.*, 2014; *Lynn et al.*, 2014, A. Khain et al., in revision, 2015]. To take these effects into account, as well as the effects of aerosols on lightning within TCs [*Khain et al.*, 2008b, 2011], it is necessary to advect aerosols within a TC. One may then predict the location of the zones of enhanced and reduced CCN concentrations.

6.9. Microstructure of Mixed-Phase Clouds and Cloud Systems

A significant number of studies have been dedicated to the development of retrieval algorithms and to the investigation of radiation and microphysical processes using atmospheric models of different complexity from 1-D SBM models [e.g., *Kumjian et al.*, 2012] to mesoscale and large-scale models [e.g., *Tao et al.*, 2003; *Sato and Okamoto*, 2006; *Iguchi et al.*, 2008, 2012a, 2012b, 2014; *Li et al.*, 2010; *Saito et al.*, 2007; *Suzuki et al.*, 2010, 2011; *Alexandrov et al.*, 2012]. Many of these studies use cloud-resolving atmospheric models in which bin microphysics is employed. In some of these studies, the results obtained using SBM are compared with those obtained using bulk parameterization schemes, while in others, various bulk schemes are compared against observations. Below we will focus on two studies from the above list.

Iguchi et al. [2012a] simulated three precipitation events using the Japan Meteorological Agency Nonhydrostatic Model (JMA-NHM). These events were also observed by shipborne and by spaceborne W-band cloud radars of the CloudSat, a polar-orbiting satellite. The SBM [*Khain et al.*, 2004a] and single-moment bulk cloud microphysics [*Lin et al.*, 1983] schemes were employed for comparison. Figure 28 shows the Contoured Frequency Altitude Diagrams (CFADs) representing the normalized reflectivity-height histograms obtained during the period 1200 UTC 22 May to 1200 UTC 23 May 2001. One can see that SBM simulates observed vertical distribution of radar reflectivity much better than the bulk parameterization scheme. The first simulations with SBM showed that to improve representation of dBZe-height histograms by SBM, it was necessary to take into account an increase of fall velocity of snow due to riming (Figure 28c), which was done in next versions of HUCM.

This example shows that model microphysics, in our case the SBM, can be improved with regard to the representation of poorly understood processes such as ice-ice and aggregate-drop collisions using available radar data.

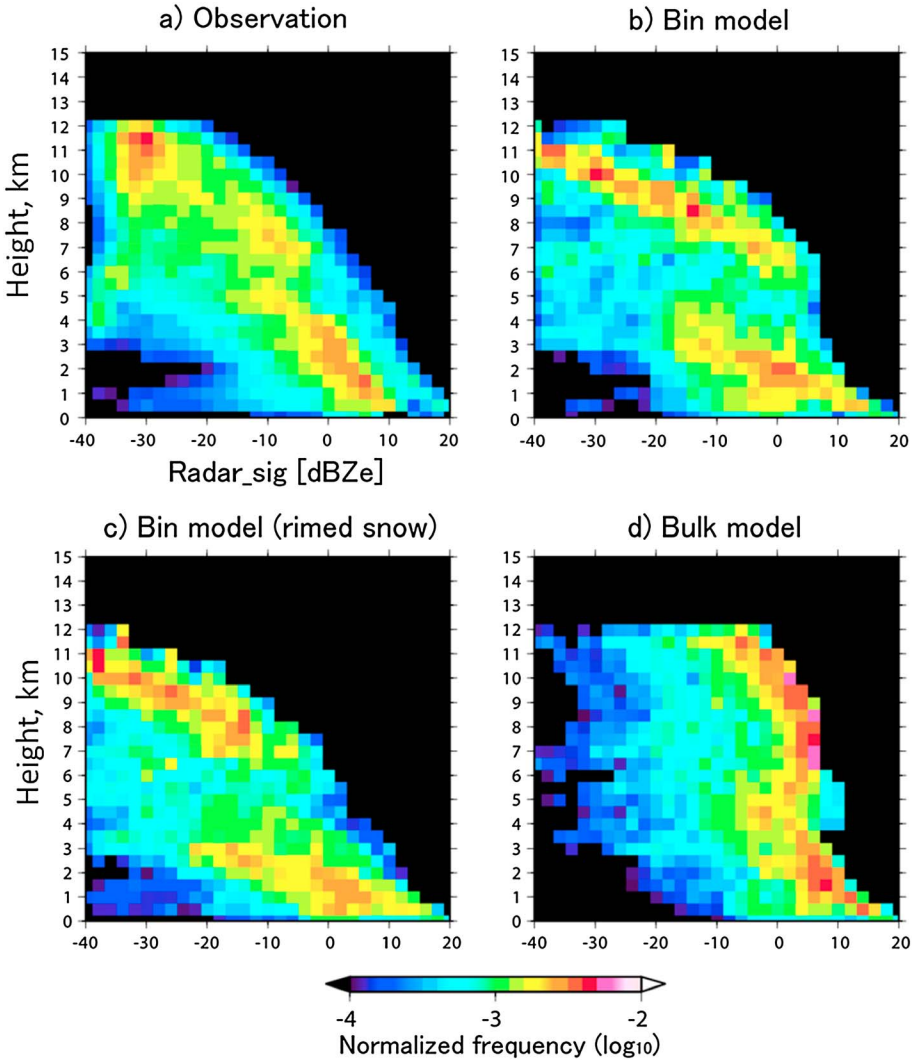

Figure 28. The Contoured Frequency Altitude Diagrams (CFADs) showing normalized dBZe-height histograms constructed from (a) the radar measurement and the simulations by (b) the bin (control), (c) the bin (rimed snow), and (d) the bulk model during the period 1200 UTC 22 May to 1200 UTC 23 May 2001. (From *Iguchi et al.* [2012a]; courtesy of the American Meteorological Society.)

Suzuki et al. [2011] compared various warm rain process rates obtained from the single-moment scheme in the Nonhydrostatic Icosahedral Atmosphere Model (NICAM), the two-moment scheme in the RAMS model, and observational data from the CloudSat cloud precipitation radar and Moderate Resolution Imaging Spectroradiometer. Three precipitation categories, namely, no precipitation, drizzle, and rain were defined according to nonattenuated, near-surface radar reflectivity. The fractional occurrence of these precipitation categories and the probability of precipitation were then examined as a function of various cloud characteristics including droplet size, liquid water path, and droplet number concentration for both schemes and observations. The analysis was facilitated through model radar simulators. An example of the results of this analysis is shown in Figure 29. It is evident that both NICAM and RAMS tend to convert cloud water to larger hydrometeors more rapidly than the observations suggest. The drizzle-to-rain transition in RAMS appears to be more realistic than in NICAM, and the RAMS ultimately produces rain fraction better than NICAM. However, ultimately, both bulk schemes make errors in simulating the cloud-to-rainwater conversion processes: too-rapid conversion of cloud water to rain when compared with observations appears to be a common problem with bulk schemes.

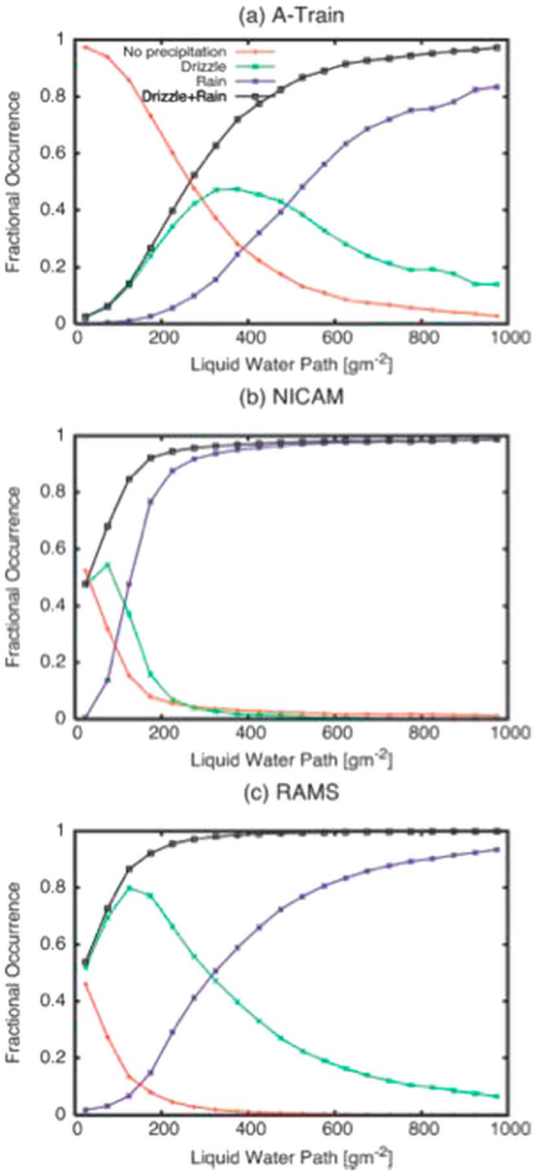

Figure 29. Fractional occurrence of no precipitation (red), drizzle (green), and rain (blue) categories as a function of cloud LWP obtained from (a) satellite measurements (A-Train) [*Stephens et al*., 2002], (b) NICAM-SPRINTARS, and (c) RAMS. Shown in black is the sum of contributions from drizzle and rain categories (after *Suzuki et al*. [2011]; courtesy of the American Meteorological Society).

6.10. Simulation of Microstructure of Stratiform Arctic Clouds

The microphysical properties of Arctic stratiform clouds have been the object of a great deal of scholarly interest. This is so due to the fact that these clouds play a leading role in the radiative budget and climate [*Shupe and Intrieri*, 2004; *Zuidema et al*., 2005; *Prenni et al*., 2007; *Verlinde et al*., 2007; *Fridlind et al*., 2007; *Morrison et al*., 2008]. The degree of sensitivity of phase composition of such clouds to the concentration of IN varies between the models. The model intercomparison studies [*Luo et al*., 2008; *Klein et al*., 2009; *Morrison et al*., 2009b, 2011; *Muhlbauer et al*., 2010] reveal a dramatic dispersion of results of different models in the prediction of the liquid-ice partitioning under the same environment conditions. Among the results obtained using sophisticated LES models, the best agreement with observations was obtained by *Avramov and Harrington* [2010] using the LES model Distributed Hydrodynamic Aerosol and Radiative Modeling Application (DHARMA) bin with *Ackerman et al*.'s [2009] SBM scheme.

Ovchinnikov et al. [2014] performed an intercomparison of seven LES models with different microphysical parameterizations. The models were used to simulate Arctic clouds observed during the Indirect and Semi-Direct Aerosol Campaign (ISDAC) [*Avramov et al*., 2011; *McFarquhar et al*., 2011]. Among the models used for intercomparison, only two models used SBM, namely, SAM-SBM [*Khain et al*., 2004a; *Fan et al*., 2011] and DHARMA bin (Distributed Hydrodynamic Aerosol and Radiative Modeling Application) [*Ackerman et al*., 1995]. In spite of the large uncertainty in ice nucleation (the concentration was tuned to the observed one), significant differences between models remained in depositional growth rates and precipitation fluxes, as well in the values of liquid water path (LWP) and ice water path (IWP). The remaining dispersion is related to the differences in the model representations of the basic process in mixed-phase stratiform clouds, namely, diffusion growth/deposition-evaporation/sublimation. The dispersion in the results is illustrated in Figure 30, which compares time dependencies of LWP and IWP obtained by using LES models with different microphysics in the set of simulations named ICE4 with target ice crystal concentration of 4 L^{-1}. One can see a widespread of values for the LWP. As regard the IWP, a stationary state was reached. The values of IWP in SBM simulations turned out to be substantially larger than in bulk ones.

It is interesting to note that different SBM schemes produced similar results. *Ovchinnikov et al*. [2014] found that bulk schemes provide a better agreement with bin schemes when ice-sized spectra are approximated by gamma distributions with widths comparable to those predicted by the bin schemes. The results show that to simulate the main microphysical parameters of mixed-phase stratocumulus clouds, the accurate simulation of PSD of ice crystals and droplets is required.

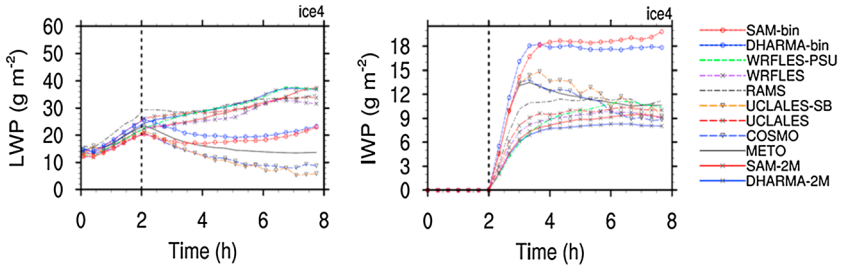

Figure 30. Time dependencies of LWP and IWP obtained using different models. Ice crystal concentration was 4 L^{-1}. Titles of the models: SAM_SBM (PNNL), SAM-2M (bulk) (PNNL), DHARMA-bin, DHARMA-2M (bulk) (NASA GISS), UCLA-LES-SU (Stockholm University), UCLA-LES (NASA Langley), COSMO (Karlsruhe University), MetOffice (Met Office UK), RAMS (Penn State), WRF_LES (NOAA), and WRF-LES-PSU (Penn State). SAM-2M, DHARMA-2M, UCLA-LES, and WRF-LES employ the same bulk microphysics scheme. (From *Ovchinnikov et al.* [2014]; courtesy of the American Meteorological Society.)

6.11. Convection on Large-Scale and Long-Term Periods

At large scales and for long durations, the properties of convection and the distribution of clouds with respect to their heights are determined by long-term forcings such as radiation forcing and aerosol forcing. According to idealized modeling, studies performed using bulk parameterization schemes and under the assumption of radiative-convective equilibrium for tropical convection, cloud fraction is not sensitive to CCN [*van den Heever et al.*, 2011; *Khairoutdinov and Yang*, 2013], and both shortwave and longwave radiative forcings at the top of the atmosphere are reduced when CCN concentration increases. In contrast, observational studies have consistently shown increased cloud top height and cloud cover and higher precipitation rates in polluted environments over large regions and globally at time scales of months and years [*Koren et al.*, 2010; *Niu and Li*, 2012; *Bell et al.*, 2008; *Koren et al.*, 2012].

Using WRF-SBM, *Fan et al.* [2013] conducted 3-D, month-long cloud-resolving simulations of summertime convection in three regions: the tropical western Pacific (TWP), southeastern China (SEC), and the U.S. southern Great Plains (SGP) to represent tropical, mid-latitude coastal, and midlatitude inland summer convective clouds, respectively (Figure 31). Computation areas were performed using a nested grid system. The outermost grids measured 1400 km, and the 2 km resolution of the innermost grids measured about 600 × 600 km. The duration of calculations allowed for the clarification of the climatic properties of convection in these regions. In the simulations radiative properties of clouds, the variations of cloud coverage were calculated at two concentrations of CCN that differed by a factor of 6 to represent the clean and polluted environments. Figure 31 shows the vertical profiles of cloud occurrence frequencies during the 1 month period from the clean and polluted simulations and observations, as well as of cloud fractions averaged over the 1 month simulation period for the TWP, SGP, and SEC regions [*Fan et al.*, 2013]. The long-term simulations using SBM-WRF captured several of the finer cloudiness features in the different regions including (a) the dominance of two zones of cloud occurrence

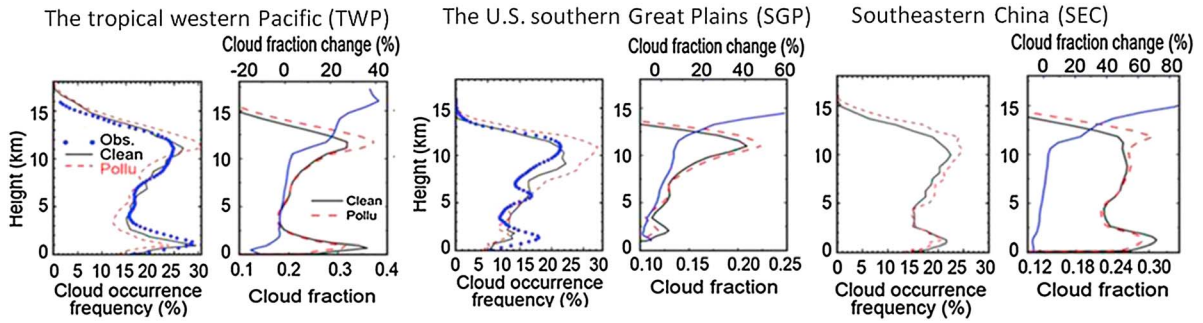

Figure 31. Vertical profiles of cloud fraction for (left) TWP, (middle) SGP, and (right) SEC regions. The left columns show the cloud occurrence frequencies during the 1 month period from the clean (Clean; black) and polluted (Pollu; red dashed) simulations and observations (Obs; blue dotted). The right columns in each panel show the vertical profiles of cloud fractions averaged over the 1 month simulation period. The percentage changes are shown as blue lines, with the secondary axis in the same plots. (From *Fan et al.* [2013], with changes, courtesy of the American Geophysical Union.)

maxima: Sc in the boundary layer and the anvils of deep convective clouds; and (b) the maximum cloud coverage caused by anvils of deep convective clouds; and (c) the increase of this coverage in a polluted atmosphere.

In the WRF/SBM, the simulations captured the observed macrophysical and microphysical properties of summer convective clouds and precipitation in the tropics and midlatitudes. These studies provided a comprehensive view of how aerosols affect cloud cover, cloud top height, and radiative forcing. Its increase in aerosol concentration led to the formation of very small cloud crystals with very low sedimentation velocity. As a result, a substantial increase in the area and depth of anvils of deep convective clouds was found in polluted conditions, in agreement with observations. In contrast, the bulk parameterization schemes did not reveal this effect. *Fan et al*. [2013] explained the difference in the results obtained using the WRF/SBM model and those using the bulk parameterization by the fact that bulk schemes, and in particular, the Morrison bulk scheme used by *Khairoutdinov and Yang* [2013], could not simulate the much reduced fall velocities of ice and snow at the upper levels from clean to polluted conditions, which is the key factor in the slow cloud dissipation and increased cloud fraction, cloud top height, and cloud thickness that are found in both ground-based multisensor and satellite measurements. According to *Fan et al*. [2013], bulk schemes cannot simulate such effects because they do not calculate a spectrum of particle-sized resolved fall speeds within each model grid box. As a result, the evaluations of the indirect CCN effect on radiative balance also turned out to be different. This example points to *the importance of simulating accurately the sedimentation velocity and sublimation rates not only of large particles affecting precipitation but also small ice crystals affecting the radiative balance of the atmosphere*.

7. Discussion and Future Directions

7.1. Summary

The current review has systematically examined how the major microphysical processes, as listed in Table 4, are represented using both bin and bulk formulations. We emphasize that the bin formulation, as compared to the bulk descriptions, can describe those microphysical processes with more consistent accuracy. When high-resolution mass grids are used, the SBM schemes accurately reproduce the observed cloud structure, PSDs and their moments as well as raindrop and drizzle formations. We consider the month-long simulations of convection performed by *Fan et al*. [2013] in different climatic zones as a significant achievement in the application of SBM to climate problems. The long-term simulations using SBM-WRF captured the observed macrophysical and microphysical properties of summer convective clouds and precipitation in the tropics and midlatitudes. These studies provide a comprehensive view of how aerosols increase cloud cover, cloud top height, and radiative forcing. None of the bulk schemes tested were able to reproduce these results.

The major limitations of SBM are related to its high computational cost. To decrease the computational cost, simplified SBM schemes with a small number of hydrometeor classes and a relatively small number of bins are often used, especially in 3-D simulations. This, of course, decreases the accuracy of the simulations. In our experience, the number of doubling mass bins (in SBM) and categories (in the MMM) should exceed ~40. Such mass grids allow the simulation of large hydrometeors (especially large hail), which play a very important role in the microphysics of convective storms. These large particles are found in the tail of PSDs and strongly affect the development of PSDs and all other processes. Despite the fact that the SBM uses basic "first principle" equations, the different microphysical processes are described in SBM schemes with different levels of detailing. One of the main conclusions of the paper is that in order to improve the description of precipitation rates, spatial precipitation variability, partitioning of convective and stratiform clouds, and the interactions of aerosols with clouds and with precipitation, the utilization of bin or hybrid bin schemes is desirable. We also emphasize the various remaining observational uncertainties, as well as the current lack of a robust understanding of some of the basic microphysical processes. Our recommendations to further develop the SBM are described in sections 7.2 and 7.3.

The main advantage of bulk schemes over the SBM is their higher computational efficiency. However, this gain is offset by a loss in accuracy and a reduction in the sensitivity to many microphysical processes such as the effects of aerosols on clouds. An analysis of observational data in different types of clouds shows that real local PSDs have a complicated shape and often cannot be well approximated by gamma or exponential distributions. Simulations of microstructure of stratiform Arctic clouds (section 6.10) show that a reasonable structure of clouds simulated by bulk schemes can be obtained if the parameters of PSDs are tuned to approximate PSDs simulated in SBM. It is also shown that in real clouds, the parameters of PSD are interrelated.

Taking into account the relationships between different parameters may substantially improve the accuracy of bulk schemes. In contrast, fixing one or several parameters in the gamma distribution may lead to substantial errors in the representation of cloud microphysics. The specific feature of various microphysical processes is a dramatic, highly nonlinear dependence of the rates of microphysical processes on particle size. The averaging of PSD over particle spectra severely reduces the sensitivity of bulk schemes to particle size. Operating with a small number of PSD moments has serious drawbacks, especially when simulating the temporal and spatial changes in the PSD. For instance, the utilization of saturation adjustment during diffusional growth introduces errors in CWC. The different approaches to the description of accretion provide rates that vary by several orders of magnitude. Especially important are errors in sedimentation that lead to errors in size sorting, i.e., in the vertical distribution of microphysical parameters. The errors in size sorting subsequently produce errors in the computation of precipitation rate and precipitation distribution on the ground. Furthermore, bulk schemes often introduce significant errors into the description of melting, freezing, and other processes.

Detailed comparisons between SBM (including MMM) and bulk parameterization schemes, as well as comparisons between various bulk parameterization schemes themselves was made. It was found that increasing the number of moments in the bulk schemes leads to better agreement with those from the SBM. Three-moment models produce much better agreement with the SBM approach and with observations than do two-moment schemes, while two-moment schemes are more accurate than one-moment parameterizations. The bin-emulating scheme, especially three-moment bin-emulating schemes, indicates larger sensitivity to aerosols. Finally, those bulk schemes that do not use saturation adjustment procedures also seem to be more sensitive to the impacts of aerosols. Improvement of bulk schemes is discussed below, in sections 7.2 and 7.3.

7.2. Areas of Application and Ways to Improve Microphysical Schemes

This overview emerged from the COST meeting (Jerusalem, November 2012) entitled "Complexity of convective microphysical schemes: *bin vs*. *bulk*." Two approaches to a description of microphysics, "bulk parameterization" and SBM, developed at nearly the same time but with two different aims: (a) to introduce microphysics into cloud-resolving simulations in an effective manner and (b) to investigate cloud microphysical processes. Originally, these directions in cloud modeling were quite distinct. Further developments were realized by interactions between these two approaches. Individual elements of all modern bulk parameterization schemes were developed and calibrated against bin analogs. Thus, it makes sense to consider this process interactive rather than competitive. A comparative stance, as taken in this overview, provides useful information about the strengths and weaknesses of each approach. Further progress should be driven by the goal of combining respective advantages.

Despite the continuously increasing "overlap" in the areas of application of bulk parameterization and SBM, there are still wide areas in which the utilization of one or another method is preferable.

Bulk microphysics parameterization schemes have been successfully fulfilling their aim of replacing traditional schemes of convection parameterization in cloud-resolving models. This "mission," however, is far from accomplished. Most large-scale models are still cloud irresolvable, and the natural first step to improve model resolution is to use bulk parameterization schemes as the more computationally efficient of the two approaches.

In cases such as the GCM as well as the operative weather forecast, the only reasonable solution at present is to use bulk parameterization schemes or to improve the traditional schemes using parameterizations coming from components of bin approaches [*Khairoutdinov and Kogan*, 2000; *Hoose et al*., 2010]. This is especially true because important parameters such as temperature, humidity, and, to some extent, precipitation can be predicted by bulk parameterization schemes with a precision that is often satisfactory from a practical point of view. Previous bulk-bin comparisons [*Seifert et al*., 2006; *Li et al*., 2009a, 2009b; *Morrison et al*., 2009a; *Wang et al*., 2013] have shown that important quantities useful for weather forecasting such as accumulated rain rate are likely determined largely by concentration and mass contents of hydrometeors, and to a lesser degree by the shape of the PSDs. At the same time, precipitation rate, type of precipitation (liquid or ice), and spatial distributions of precipitation were found to be strongly dependent on parameters of gamma distribution, that is, on PSD shape.

Current bulk parameterization schemes (especially one-moment schemes) are much less sensitive than the SBM to aerosols. There are several physical causes of such insensitivity. The application of saturation

adjustment makes the schemes insensitive to aerosols at the stage of diffusion growth, as was discussed in section 4.2. This is also true when comparing bulk schemes that do and do not utilize saturation adjustment procedures. Errors in size sorting during sedimentation dramatically decrease the sensitivity of the bulk schemes to aerosols at the later stages of cloud evolution. The application of different autoconversion schemes cannot increase sensitivity to aerosols, especially in cases when one-moment bulk schemes (which are unable to simulate size sorting) are used [*Planche et al*., 2014; *Grabowski*, 2014]. These limitations place into question the validity of the application of current one- and many two-moment bulk schemes, in large-scale models for the investigation of aerosol effects on clouds, cloud-radiation interaction, and precipitation.

A comparison of bulk parameterization schemes with their bin analogs, as well as the bulk parameterizations themselves presented in sections 4 and 6 indicates several main directions for improving the representation of microphysics in cloud-resolving models. There are several main steps to improve both the representation of microphysics in cloud-resolving models and their forecast skill. An important step toward improving the accuracy of bulk schemes would be the implementation of the diffusion growth/evaporation equation, instead of utilizing the saturation adjustment assumption, such as is currently incorporated in the bin-emulating bulk scheme of RAMS. A comparison of bulk parameterization and SBM indicates that the utilization of the saturation adjustment assumption exaggerates the intensity of latent heat release and vertical velocities and may lead to an overestimation of convective precipitation, as compared to a stratiform one. The assumption of saturation adjustment substantially simplifies the algorithm of diffusion growth, but makes new nucleated droplets indistinguishable from old cloud droplets. This latter may lead to unrealistic DSDs. Thus, avoiding the supersaturation adjustment by implementation of the diffusion growth equation is an attractive and promising direction for improving bulk parameterization schemes.

The utilization of two-moment (with variable parameters of PSDs) and, especially, three-moment schemes dramatically improves the representation of particle sedimentation and size sorting, as compared to one-moment schemes (Figure 9) [*Loftus and Cotton*, 2014a, 2014b]. Improving the representation of sedimentation and condensation/evaporation as well as deposition/sublimation is of crucial importance for a better calculation of precipitation and the radiative budget of the atmosphere. We believe that these improvements will substantially increase the sensitivity of bulk parameterization schemes to aerosols.

The improvement of the representation of autoconversion and accretion processes as well as of the melting of hydrometeors is an important step toward improving bulk schemes.

The next important step in the improvement of bulk schemes is an implementation of a calculation of the aerosol budget; that is, taking into account the processes of aerosol transport, nucleation scavenging, recycling, and regeneration. Currently, the parameters of bulk schemes tuned for particular conditions (say, continental conditions) are used over large areas where a wide range of conditions, including a great variety of aerosol concentrations, take place. The results of hurricane simulations in spatially inhomogeneous fields of aerosol concentration clearly indicate that the parameters of bulk schemes in each grid point should change spatially and with time, depending on specific local geographical and meteorological conditions. An analysis of CWC fields in simulated hurricanes showed that many bulk schemes had properties typical of continental clouds, in which supercooled liquid existed up to the level of homogeneous freezing. It is particularly important to calibrate the autoconversion rates for raindrop formation at the proper altitudes, depending on droplet concentration.

It seems that the impact of nonsoluble aerosols playing the role of IN is substantially underestimated in current bulk and SBM schemes. In fact, investigators take into account the properties of IN only if ice crystal nucleation is considered. Raindrop freezing is calculated using formulas that do not contain any information about IN. At the same time, the freezing of raindrops is caused by the immersed IN within the drops.

Thus, an important step toward the improvement of cloud microphysics is to combine diverse schemes of different microphysical processes into one physically closed block.

Recently, *Morrison and Milbrandt* [2014] reported a new bulk parameterization scheme that recalculates ice particle density in the course of riming. This approach decreases to some extent the uncertainty related to the conversion of ice particles of one hydrometeor type to another. The results of bulk parameterization schemes depend on the choice of the moment used to describe the evolution of the particle size distribution [*Milbrandt and McTaggart-Cowan*, 2010]. The optimum choice of moments is another step toward the

improvement of bulk parameterization. The utilization of better resolution and smaller time steps seems to be an important way to improve the results of models that use bulk parameterization schemes.

The development of bin-emulating schemes improves the representation of each microphysical process and their response to the presence of aerosols [*Saleeby and van den Heever*, 2013]. In principle, most microphysical processes lead to a deviation of PDF from the gamma distribution. Restoring the gamma distribution at each time step after applying bin-emulating procedures leads to a significant decrease in computational time during the advection step but may reduce the benefits of the bin-emulating algorithms.

An important way to improve models with bulk parameterization is a wider use of empirical data to tune bulk parameterization schemes to certain meteorological conditions/phenomena (e.g., hurricanes), or to eliminate biases by statistical analyses of forecasts in particular geographic regions. We believe that a substantial improvement can be reached by using a different set of governing parameters of bulk parameterization schemes in different geographical regions (e.g., sea, land, and urban). Such a calibration of parameters can be performed through comparisons, with the help of SBM schemes.

If all other conditions are similar, SBM schemes have an obvious advantage over the current bulk parameterization schemes for a wide range of research problems where knowledge of PSD shapes is of importance. Analysis of the results of observations and numerical studies shows that the shape of a local PSD often cannot be described by gamma distributions. Even in cases in which particular size distributions can be approximated by gamma or exponential distributions, all parameters of these size distributions vary dramatically in space and time during cloud evolution, so that their values in the models can be determined only approximately. The fixing of some parameters does not allow for the simulation of realistic distributions. Moreover, many microphysical processes foster deviation of the PSD from gamma or exponential distributions. At present, there is no firm physical basis for selecting a specific function (e.g., gamma or lognormal) to describe particle size distributions in numerical simulations of clouds.

The ability of SBM models to calculate PSDs made the SBM approach a powerful tool for the investigation and parameterization of cloud-microphysical processes. The potential of the current bin microphysics schemes is far from exhausted. The knowledge accumulated to date allows for further development of the schemes and their improvements. Large-eddy simulations combined with bin microphysics were used for the development of parameterization expressions for the rates of autoconversion and accretion in mesoscale and large-scale models, formulation of parameterization of haze homogeneous freezing [*Khairoutdinov and Kogan* [2000]; *Hoose et al.* [2010]], etc. The application of bin microphysical models allowed one to discover effects that were found in observations later (for instance, aerosol-induced convective invigoration, an increase in hail size in polluted clouds, the formation of first raindrops in undiluted cloud volumes in zones of maximum turbulence [*Khain et al.*, 2003, 2004a, 2011, 2013], respectively). Only SBM models were able to represent the microphysical structure of mixed-phase stratiform clouds [*Ovchinnikov et al.*, 2014].

A great number of studies investigating aerosol effects were performed using bulk parameterization schemes (largely two-moment ones). In some studies, similar responses of precipitation amount and location to varying CCN amounts were found [e.g., *Noppel et al.*, 2010a]. Nonetheless, we believe that SBM models can simulate more accurately the processes of cloud-aerosol interaction. Obtaining a response to variation of aerosol size and concentration by bulk parameterization comparable to SBM schemes is considered an improvement of bulk parameterization schemes [e.g., *Fan et al.*, 2012a; *Wang et al.*, 2013]. Increases in computing power allowed for the conducting of multiple month-long cloud-resolving simulations with spectral bin cloud microphysics that captures the observed macrophysical and microphysical properties of summer convective clouds and precipitation in the tropics and midlatitudes [*Fan et al.*, 2011, 2013]. These studies provide a comprehensive view of how aerosols affect cloud cover, cloud top height, and radiative forcing. The work of *Fan et al.* [2013] clearly indicates the ability of the SBM models to investigate some of the most intricate climatic problems. At present, the SBM can be successfully used for simulation of intensity of dangerous phenomenon such as storms, hail, and flooding.

The SBM approach is useful for the development of retrieval algorithms for remote sensing, relating Doppler and polarimetric radar data as well as data of satellite observations with cloud microphysical parameters. Importantly, radar parameters are highly sensitive to the tails of PSDs and also to their particle shape and phase composition.

Note that climate models require, in principle, a greater degree of accuracy in the description of microphysical processes than do weather prediction models. Indeed, in the case of weather prediction, the role of advective processes can be more important than that of diabatic processes. In climate models diabatic processes play a predominant role. According to the results of several numerical studies conducted over long periods of time, a substantial variation of aerosol concentrations produced changes in spatially and time-averaged precipitation of 7–10% [e.g., *Seifert et al*., 2011; *van den Heever et al*., 2011]. At small time scales, precipitation fluctuations caused by aerosols are relatively large. Besides, even if the 10% effect is not very important in weather forecasts, 7–10% variation of latent heat release (that corresponds to the variation in precipitation amounts) for climate problems is of major importance (say, in the case when the forecast of temperature change of order of 1°C per several years is required). While the utilization of SBM over the entire globe in the GCM is unlikely to take place in the foreseeable future, we believe the SBM will be used for climate studies (say, seasonal prediction of tropical cyclone activity) within limited areas or in superparameterization schemes. The SBM can be also efficiently used for development of parameterizations for large-scale models.

As discussed in section 5, further progress on both bulk and SBM schemes is contingent upon laboratory, radar, satellite, and in situ measurements that can provide new knowledge about processes in mixed-phase and ice clouds, ice nucleation, mixing, and so on. New and better particle probes are clearly required. The shattering of ice crystals is a notable issue that has been resolved only recently. Ice crystals clearly exhibit an extremely wide range of habits. It is well known that details of the shapes of ice have a profound impact not only on the subsequent growth of the ice but also on their interactions with the radiation process (by the scattering of visible light by the crystals). In almost all existing SBM and bulk schemes, a relatively simple shape (or set of shapes) of ice particles is assumed. However, ice crystals do not appear in pure, textbook forms, but rather, more often than not, deviate to some extent from these idealized shapes used in microphysical schemes. If ice crystal shapes have a profound impact, we need very careful computations of ice crystal growth in order to correctly determine ice-growth rates. The implication is tantalizing, because if this argument is correct, we not only need to introduce a sufficient number of bins, but those also with a sufficient number of ice-shape types. For certain specific goals, the utilization of more than three types of ice crystals is required.

Further progress in SBM strongly depends on obtaining in situ microphysical measurements in deep convective clouds and storms as well as mixed-phase stratiform clouds. These data should include PSDs of different hydrometeors and aerosols. In addition to in situ measurements, satellite remote sensing, and ground-based Doppler polarimetric radar measurements are of crucial importance. Since major microphysical equations are known and used in the SBM, the SBM models can assimilate new findings comparatively easy. As examples of observed data triggering the improvement of SBM, we note here three developments (among many others): (a) *Rosenfeld and Gutman* [1994] and *Freud and Rosenfeld* [2012], who triggered numerical investigations of the formation of first raindrops in cumulus clouds; (b) *Li et al*. [2010], who showed the necessity of taking into account rimed mass in aggregates and its effect on fall velocity; and (c) *Kumjian et al*. [2012], who pointed to the necessity of the application of time-dependent freezing.

Quite typically, the need to interpret remote sensing signatures triggers the further development of SBM schemes. A recent example is the development and implementation of a novel, detailed scheme of time-dependent freezing into the HUCM that allowed the simulation and explanation of detailed laboratory experiments of hail wet growth [*Phillips et al*., 2014], as well as the formation of differential reflectivity columns, which are indicators of strong hail [*Kumjian et al*., 2014].

Satellite data (as well as radar data) are useful to improve bulk parameterization schemes as well [*Matsui et al*. [2009]].

7.3. Computational Aspects

The choice of "bulk versus bin" is closely related to the compromise "computer time versus accuracy." It seems that three-moment schemes are substantially closer to the SBM than one- and two-moment schemes. It is possible that the utilization of four moments of PSD would produce the accuracy in PSD simulation similar to that obtained currently using several tens of bins. In this case, however, the computational costs in the SBM and the bulk parameterization approaches will be comparable.

In the SBM scheme, computational time demands are related not only to the calculation of PSDs, but also to the utilization of time-steps, which are typically less than 10–15 s (particular microphysical processes such as

diffusion growth/evaporation are typically calculated with time steps as short as 1 s and in some especially accurate schemes with even shorter time steps), as well as with higher model resolution. Typical time steps used in bulk schemes are of several tens of seconds, with some exceptions (for instance, the current COSMO NWP model of the German Weather Service works with a time step of 6 s and a horizontal resolution of 2.8 km). The small time steps and high spatial resolution are required not only for numerical stability but also for an accurate description of microphysical processes with small characteristic time scales.

In the present overview, we refrained from an extensive consideration of numerical aspects of comparison bulk parameterization and bin microphysics approaches. Note that it is widely, and possibly wrongly, assumed that models with bulk parameterization schemes can be integrated using time steps substantially larger than those required in SBM models.

It is an accepted practice to calculate the effects of microphysics using explicit numerical schemes by assuming that the rates of change of any microphysical value during one time step are constant. This approach can lead to serious errors in the calculation of microphysical quantities. For instance, during diffusional drop growth, supersaturation changes exponentially with a characteristic time scale equal to the drop relaxation time. The characteristic phase relaxation time in liquid and mixed-phase clouds typically varies from 1 to 10 s [*Korolev and Mazin*, 2003].

Characteristic time scales (for instance, the time scale of drop evaporation) may be quite small, so the utilization of explicit finite difference schemes using large time steps may lead to an appearance of negative values of mass contents and/or concentrations [*Sednev and Menon*, 2012]. The replacement of these negative values by zeros during the model integration would break down the mass conservation. *Sednev and Menon* [2012] calculated maximum values of time steps that can be used in different bulk parameterization schemes during descriptions of particular microphysical processes and showed that at certain mixing ratios the maximum possible time steps decrease to several seconds. Utilization of positive definite schemes also leads to distorting internal fluxes of different quantities [*Durran*, 2010] . The same is valid for other processes, such as sedimentation and collisions: too-large time steps can lead to errors in the estimation of particle size. Finally, all proposed methods for improving bulk parameterization schemes (e.g., applying more bin-emulating procedures, using more PDF moments, implementing aerosol budgets) will increase computational time.

There are several ways to decrease the SBM computational cost: (a) utilization of simplified versions, in which one mass grid is used for the description of several classes of hydrometeors. For instance, *Hall* [1980] used only one mass grid to describe ice particles. On this grid, the smallest particles were assigned to ice crystals, and the largest ones to graupel. *Khain et al*. [2009] used only two types of ice hydrometeors: low density and high density. These simplified schemes are useful for simulating specific meteorological phenomena in which ice processes are of secondary importance; (b) utilization of fewer mass bins in accordance with the nature of the particular hydrometeor. For instance, there are no micron-sized hail particles nor are there several centimeter-sized raindrops; (c) development and utilization of efficient numerical algorithms; and (d) wider utilization of lookup tables. Notably, the bin-emulating scheme of RAMS [*Saleeby and Cotton*, 2004; *van den Heever et al*., 2006, 2011; *Saleeby and van den Heever*, 2013; *Loftus et al.*, 2014; *Loftus and Cotton,* 2014a, 2014b] utilizes several hundred lookup tables for CCN activation, collisions, sedimentation, and so on; (e) proper design of parallel calculations. One of the primary ways to surmount computational problems is the proper design of parallel calculations, wherein each processor or node calculates a different area in the domain, and the tiling approach is utilized for integration.

The hybrid bin or bin-emulating schemes such as RAMS are intermediate between bulk and bin approaches in terms of simulation accuracy and computational efficiency.

7.4. Design of Microphysics in Large-Scale Models

Improvement in the representation of convection and microphysics in large-scale and climate models can be accomplished only in association with improvements in cloud representation. In the current operational models, clouds are treated by two separate schemes tagged "clouds" and "convection." The former handles the types of clouds "almost" resolved by a model, consisting mostly of stratiform-type clouds. The purpose of this scheme is to evaluate radiative and microphysical tendencies. A cloud fraction parameter is usually introduced into this scheme so that a cloud does not need to fill a whole grid. Full microphysics can easily be implemented into a cloud scheme, if resolution discrepancy is not an issue. The convective clouds are treated

separately by a convection scheme, whose main purpose is to evaluate the convective transport of total entropy and moisture. A mass flux formulation, typically adopted for this purpose, can handle the problem very well as long as these two quantities are conserved. Because a convective fraction is a rather ill-defined quantity within this formulation, nonconservative processes, including microphysics, are often treated in a rather ad hoc manner. Furthermore, under a standard quasi-equilibrium assumption [*Yano and Plant*, 2012], no convective life cycle is considered in these convective schemes. Thus, it would be rather physically inconsistent, though perhaps technically possible, to implement full microphysics that anticipate time-evolving convective dynamics. The 1-D cloud models that are used in traditional parameterization schemes for the representation of mass fluxes and the calculation of convective heating, cooling, and precipitation are very simple and often unrealistic. *Zhang* [2014] was the first to attempt to implement a reasonable description of microphysical processes into the elementary cloud models. This description incorporates elements of two-moment bulk parameterization schemes. At the same time, some properties of elementary cloud models remained from the old schemes: the cloud is assumed to be in a quasi-stationary state, and new clouds form at each time step, so the model has "no memory." Even such a simplified scheme allowed for a substantially improved representation of precipitation in a GCM. In our view, traditional convective parameterizations can be improved by calibrating the parameters of elementary cloud models by a comparison with the results of LES cloud simulations using SBM or the best bulk parameterization schemes appropriately averaged over space and time. Superparameterization as well as the Nonhydrostatic Anelastic Model with Segmentally Constant Approximations (SCA) [*Yano et al*., 2010] circumvents these difficulties. The computing cost is clearly an issue in practical implementations of superparameterization. By contrast, the SCA approach is relatively computationally cheap and practical.

Aerosol advection and cloud-aerosol interaction accompanied by aerosol scavenging due to drop activation must also be taken into account in large-scale models. Despite much effort, the representation of aerosol effects (as well as cloud microphysics altogether) in large-scale and climate models remains the main source of uncertainty [*Carslaw et al*., 2013]. The sink of cloud water in warm clouds is determined by the processes of autoconversion and accretion. While the rate of the autoconversion depends on droplet concentration, that is, is affected by aerosol concentration, the rate of accretion is determined largely by the mass contents of liquid cloud water and rainwater. Thus, the aerosol effects turn out to be dependent on the relation between the rates of autoconversion and accretion. This relation is different for stratocumulus and cumulus clouds. The effect was recently investigated by *Gettelman et al*. [2013] using a stationary bulk parameterization cloud model [*Wood et al*., 2009] mimicking the microphysics used in the GCM. Finally, it is desirable to take into account the effects of turbulence on the rate of autoconversion. A close collaboration of scientists involved in "large-scale" and "microphysical" problems is required to advance in this direction.

Some unsolved theoretical problems remain as regards to "scale dependence" of convective and microphysical processes. Among them is the problem of representation of convective processes on the meshes with grid spacing of the same order as the convective processes themselves (the so-called "grey zone"). There is also the problem of the relationship of model grid spacing and the characteristic spatial and time scales of microphysical processes. The utilization of higher resolution is desirable, but the question "what resolution ideally represents convection and microphysics?" is yet to be answered. Detailed cloud simulations indicate that the required spatial resolution is on the order of 100 m (as used in LES), which allows for a separation between convective and small-scale turbulent motions. However, the application of such grid spacing is not feasible in large-scale models in the near future. One of the possible ways to use high resolution is superparameterization, mentioned in section 1. This approach can be extended to include bin microphysics.

In the present study, we discussed the problems of the representation of microphysics in cloud-resolving models. A comparison of different methods was conducted for comparatively short times and spatial scales. For climate investigations, the averaging of such results helps to understand the corresponding effects on longer time scales and larger spatial scales. It is necessary to understand whether the differences are amplified due to internal instabilities (i.e., self-organized criticality [see *Yano et al*., 2012a]) or rather smooth out due to the self-regulatory nature of the system (i.e., homeostasis [*Yano et al*., 2012b]). This is an important question, as yet to be addressed. Many examples show that at certain environmental conditions, dissipation of one cloud creates downdrafts leading to the formation of new clouds. Note that maritime convective clouds are typically closely related. Squall lines represent classical cases of self organization of convection under certain wind conditions. There are a number of good reasons to think that self organization is a widespread

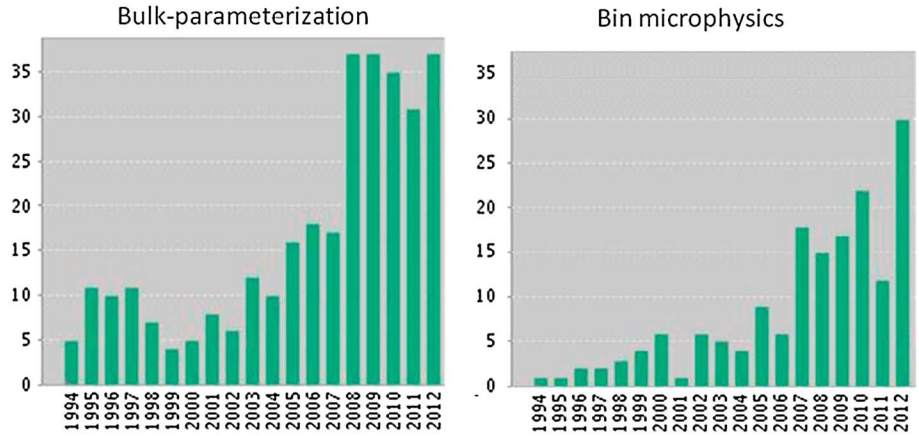

Figure 32. Annual number of publications found in Web Science using key words "bulk parameterization" and "bin microphysics."

phenomenon in the Earth's atmosphere [cf. *Yano*, 1998; *Moncrieff*, 2010]. Moreover, the development of secondary clouds during the dissipation of the primary ones can depend on aerosol loading. For instance, *Khain et al.* [2005] reported the formation of a squall line after the dissipation of a primary cloud in the high CCN concentration and the dissipation of a primary cloud without the formation of a squall line in the low CCN concentration. When aerosols trigger secondary clouds, their effects on precipitation increase substantially. In this sense, the effects of aerosols on single clouds may substantially differ from aerosol effects on cloud ensembles. Simulations of cloud ensembles indicate that aerosols tend to organize convection, intensify deep convection, and decrease the number of small clouds [*Lee et al.*, 2008]. These examples show that both self organization and homeostasis take place, with self organization apparently dominating. This problem requires further investigation. It is worth noting that in large-scale models with traditional parameterization of convection, the dynamical interaction between clouds at cloud scale is not taken into account. Simple cloud models (plumes or bubbles) used in the convective parameterization schemes do not take into account wind shear.

7.5. Some Statistics

As a last argument for the importance of the topics covered in this overview, we present basic statistical data about the growing interest in bin and bulk schemes within the research community. During the past decade, the application of both bulk parameterization and SBM models rapidly increased with increasing model resolution. Figure 32 shows the annual number of publications found in the "Web of Science" using the key words "bulk parameterization" and "bin microphysics" since 1994. The number of publications treating these topics is much larger than that shown in Figure 32, because the titles of many studies using bulk parameterization or SBM do not contain these key words.

It is clear, however, that these statistics reflect a trend of a growing publication rate on these topics. One can see a jump in 2007–2008 in both cases. Fewer publications mention SBM than bulk parameterization, but the former group has been continuously expanding, indicating, it seems, the increased application of SBM in mesoscale models.

A rapid increase in computer power has made the utilization of SBM in mesoscale studies quite routine in many scientific centers. This means that each user will be able to choose the most suitable approach for solving particular problems.

Acknowledgments
This study was supported by the European project COST095WG4. The Hebrew University group was supported by grants from the U.S. Department of Energy's (DoE), Office of Biological and Environmental Research (BER) (DE-S0006788 and DE-SC0008811) and by the Binational U.S.-Israel Science Foundation (grant 2010446). K.D. Beheng gratefully acknowledges the support of several grants made by the German Research Foundation (Deutsche Forschungsgemeinschaft) and the German Ministry of Education and Research (BMBF), by the European Community with the STREP project ANTISTORM (FP6-2003-NEST-B1) and in the framework of the joint German-Israel Cooperation in Water Technology. S.C. van den Heever is grateful for grants from the National Science Foundation, NASA, and the U.S. Department of Energy that have supported the ongoing development of various microphysical parameterization schemes within the RAMS model, as well as the investigation into microphysical and aerosol processes over the last 5 years. Vaughan Phillips was supported by two awards from the National Science Foundation (NSF) (ATM-0427128, which later became ATM-0852620), and from the Office of Science (BER) of the U.S. Department of Energy (DE-SC0007396). Alexei Korolev's work was supported by Environment Canada and Transport Canada. All data used are available through papers noted in the reference list.

The Editor on this paper was Alan Robock. He thanks three anonymous reviewers for their review assistance on this manuscript.

References

Ackerman, A. S., O. B. Toon, and P. V. Hobbs (1995), A model for particle microphysics, turbulent mixing, and radiative transfer in the stratocumulus-topped marine boundary layer and comparisons with measurements, *J. Atmos. Sci.*, *52*, 1204–1236.

Ackerman, A. S., et al. (2009), Large-eddy simulations of a drizzling, stratocumulus-topped marine boundary layer, *Mon. Weather Rev.*, *137*, 1083–1110, doi:10.1175/2008MWR2582.1.

Adams-Selin, R. D., S. C. van den Heever, and R. H. Johnson (2013), Impact of graupel parameterization schemes on idealized bow echo simulations, *Mon. Weather Rev.*, *141*, 1241–1262.

Alexandrov, M. D., B. Cairns, C. Emde, A. S. Ackerman, and B. van Diedenhoven (2012), Accuracy assessments of cloud droplet size retrievals from polarized reflectance measurements by the research scanning polarimeter, *Remote Sens. Environ.*, *125*, 92–111, doi:10.1016/j.rse.2012.07.012.

Andreae, M. O., D. Rosenfeld, P. Artaxo, A. A. Costa, G. P. Frank, K. M. Longo, and M. A. F. Silva-Dias (2004), Smoking rain clouds over the Amazon, *Science*, *303*, 1337–1342.

Andrejczuk, M., W. W. Grabowski, S. P. Malinowski, and P. K. Smolarkiewicz (2009), Numerical simulation of cloud–clear air interfacial mixing: Homogeneous versus inhomogeneous mixing, *J. Atmos. Sci.*, *66*, 2493–2500.

Andrejczuk, M., W. W. Grabowski, J. Reisner, and A. Gadian (2010), Cloud-aerosol interactions for boundary layer stratocumulus in the Lagrangian Cloud Model, *J. Geophys. Res.*, *115*, D22214, doi:10.1029/2010JD014248.

Arakawa, A. (2004), The cumulus parameterization problem: Past, present, and future, *J. Clim.*, *17*, 2493–2522.

Avramov, A., and J. Y. Harrington (2010), Influence of parameterized ice habit on simulated mixed phase Arctic clouds, *J. Geophys. Res.*, *115*, D03205, doi:10.1029/2009JD012108.

Avramov, A., et al. (2011), Toward ice formation closure in Arctic mixed-phase boundary layer clouds during ISDAC, *J. Geophys. Res.*, *116*, D00T08, doi:10.1029/2011JD015910.

Ayala, O., B. Rosa, and L. P. Wang (2008), Effects of turbulence on the geometric collisions rate of sedimenting droplets: Part 2. Theory and parameterization, *New J. Phys.*, *10*, 075016, doi:10.1088/1367-2630/10/7/075016.

Baldauf, M., A. Seifert, J. Forstner, D. Majewski, M. Raschendorfer, and T. Reinhardt (2011), Operational convective-scale numerical weather prediction with the COSMO Model: Description and sensitivities, *Mon. Weather Rev.*, *139*, 3887–3905.

Beheng, K. D. (1994), A parameterization of warm cloud microphysical conversion processes, *Atmos. Res.*, *33*, 193–206.

Beheng, K. D. (2010), The evolution of raindrop spectra: A review of microphysical essentials, in *Rainfall: State of the Science*, edited by F. Y. Testik and M. Gebremichael, AGU, Washington, D. C., doi:10.1029/2010GM000957.

Beheng, K. D. (2012), From size distributions to bulk microphysical parameterizations. Presentation at COST Workshop, COST-ES0905 - WG4 meeting, Jerusalem, 12–16 Nov.

Beheng, K. D., and G. Doms (1986), A general formulation of collection rates of cloud and raindrops using the kinetic equation and comparison with parameterizations, *Beiträge zur Phys. der Atmos.*, *59*(1), 66–84.

Bell, T. L., et al. (2008), Midweek increase in U.S. summer rain and storm heights suggests air pollution invigorates rainstorms, *J. Geophys. Res.*, *113*, D02209, doi:10.1029/2007JD008623.

Benmoshe, N., and A. P. Khain (2014), The effects of turbulence on the microphysics of mixed-phase deep convective clouds investigated with a 2-D cloud model with spectral bin microphysics, *J. Geophys. Res. Atmos.*, *119*, 207–221, doi:10.1002/2013JD020118.

Benmoshe, N., A. Khain, M. Pinsky, and A. Pokrovsky (2012), Turbulent effects on cloud microstructure and precipitation of deep convective clouds as seen from simulations with a 2-D spectral microphysics cloud model, *J. Geophys. Res.*, *117*, D06220, doi:10.1029/2011JD016603.

Berry, E. X., and R. L. Reinhardt (1974a), An analysis of cloud droplet growth by collection: Part I. Double distributions, *J. Atmos. Sci.*, *31*, 1814–1824.

Berry, E. X., and R. L. Reinhardt (1974b), An analysis of cloud drop growth by collection: Part II. Single initial distributions, *J. Atmos. Sci.*, *31*, 1825–1831.

Berry, E. X., and R. L. Reinhardt (1974c), An analysis of cloud drop growth by collection: Part III. Accretion and self collection, *J. Atmos. Sci.*, *31*, 2118–2126.

Bott, A. (1998), A flux method for the numerical solution of the stochastic collection equation, *J. Atmos. Sci.*, *55*, 2284–2293.

Bott, A. (2000), A numerical model of the cloud-topped planetary boundary-layer: Influence of the physico-chemical properties of aerosol particles on the effective radius of stratiform clouds, *Atmos. Res.*, *53*, 15–27.

Boucher, O., and U. Lohmann (1995), The sulfate-CCN-cloud albedo effect, a sensitivity study with two general circulation models, *Tellus*, *47B*, 281–300.

Braun, S. A., and R. House Jr. (1997), The evolution of the 10–11 June 1985 PRE-STORM squall line: Initiation, development of rear inflow, and dissipation, *Mon. Weather Rev.*, *125*, 478–504, doi:10.1175/1520-0493(1997)125<0478:TEOTJP>2.0.CO;2.

Brenguier, J.-L., and W. W. Grabowski (1993), Cumulus entrainment and cloud droplet spectra: A numerical model within a two-dimensional dynamical framework, *J. Atmos. Sci.*, *50*(1), 120–136, doi:10.1175/1520-0469(1993)0502.0.CO;2.

Burnet, F., and J.-L. Brenguier (2007), Observational study of the entrainment-mixing process in warm convective cloud, *J. Atmos. Sci.*, *64*, 1995–2011.

Carrió, G. G., and W. R. Cotton (2010), Investigations of aerosol impacts on hurricanes: Virtual seeding flights, *Atmos. Chem. Phys. Discuss.*, *10*, 22,437–22,467, doi:10.5194/acpd-10-22437-2010.

Carrió, G. G., S. C. van den Heever, and W. R. Cotton (2007), Impacts of nucleating aerosol on anvil-cirrus clouds: A modeling study, *Atmos. Res.*, *84*, 111–131.

Carslaw, K. S., et al. (2013), Large contribution of natural aerosols to uncertainty in indirect forcing, *Nature*, *503*, 67–71.

Cheng, C.-T., W.-C. Wang, and J.-P. Chen (2010), Simulation of the effects of increasing cloud condensation nuclei on mixed-phase clouds and precipitation of a front system, *Atmos. Res.*, *96*, 461–476.

Chen, J.-P., and S.-T. Liu (2004), Physically based two-moment bulk water parametrization for warm-cloud microphysics, *Q. J. R. Meteorol. Soc.*, *130*, 51–78.

Chen, S.-H., and W.-Y. Sun (2002), A one-dimensional time dependent cloud model, *J. Meteor. Soc. Jpn.*, *80*, 99–118.

Chen, Y.-C., L. Xue, Z. J. Lebo, H. Wang, R. M. Rasmussen, and J. H. Seinfeld (2011), A comprehensive numerical study of aerosol-cloud-precipitation interactions in marine stratocumulus, *Atmos. Chem. Phys.*, *11*, 9749–9769, doi:10.5194/acp-11-9749-2011.

Clark, T. L. (1973), Numerical modeling of the dynamics and microphysics of warm cumulus convection, *J. Atmos. Sci.*, *30*, 857–878.

Cohard, J.-M., and J. P. Pinty (2000), A Comprehensive two-moment warm microphysical bulk model scheme: I: Description and tests, *Q. J. R. Meteorol. Soc.*, *126*, 1815–1842.

Cohen, N., and A. P. Khain (2009), Aerosol effects on lightning and intensity of landfalling hurricanes, in *Chapter in the Book: Hurricanes and Climate Change*, chap. 189–212, edited by J. B. Elsner and T. H. Jagger, 419 pp., Springer, New York, doi:10.1007/978-0-387-09410-6.

Costa, A. A., C. Jacinto de Oliveira, J. C. Parente de Oliveira, and A. J.´ da Costa Sampaio (2000), Microphysical observations of warm cumulus clouds in Ceará, Brazil, *Atmos. Res.*, *54*, 167–199.

Cotton, W. R., G. J. Tripoli, R. M. Rauber, and E. A. Mulvihill (1986), Numerical simulation of the effects of varying ice crystal nucleation rates and aggregation processes on orographic snowfall, *J. Clim. Appl. Meteorol.*, *25*, 1658–1680.

Cotton, W. R., et al. (2003), RAMS 2001: Current status and future directions, *Meteorol. Atmos. Phys.*, *82*, 5–29.

Cotton, W. R., G. M. Krall, and G. G. Carrió (2012), Potential indirect effects of aerosol on tropical cyclone intensity: Convective fluxes and cold-pool activity, *Trop. Cycl. Res. Rev.*, *1*(3), 293–306.

Cramér, H. (1999), *Mathematical Methods of Statistics*, 575 pp., Princeton Univ. Press, Princeton, N. J.
Davis, E. J. (2006), A history and state-of-the-art of accommodation coefficients, *Atmos. Res*, *82*, 561–578.
De Rooy, W. C., P. Bechtold, K. Fröhlich, C. Hohenegger, H. Jonker, D. Mironov, A. Pier Siebesma, J. Teixeiraf, and J.-I. Yano (2013), Entrainment and detrainment in cumulus convection: An overview, *Q. J. R. Meteorol. Soc.*, *139*, 1–19.
Delanoë, J., A. Protat, J. Testud, D. Bouniol, A. J. Heymsfield, A. Bansemer, P. R. A. Brown, and R. M. Forbes (2005), Statistical properties of the normalized ice particle size distribution, *J. Geophys. Res.*, *110*, D10201, doi:10.1029/2004JD005405.
DeMott, P. J., A. J. Prenni, X. Liu, S. M. Kreidenweis, M. D. Petters, C. H. Twohy, M. S. Richardson, T. Eidhammer, and D. C. Rogers (2010), Predicting global atmospheric ice nuclei distributions and their impacts on climate, *Proc. Natl. Acad. Sci. U.S.A.*, *107*(25), 11,217–11,222.
Devenish, B. J., et al. (2012), Review article. Droplet growth in warm turbulent clouds, *Q. J. R. Meteorol. Soc.*, *138*(667), 1401–1429.
Ditas, F., R. A. Shaw, H. Siebert, M. Simmel, B. Wehner, and A. Wiedensohler (2011), Aerosols-cloud microphysics-thermodynamics-turbulence: Evaluating supersaturation in a marine stratocumulus cloud, *Atmos. Chem. Phys. Discuss.*, *11*, 29,777–29,805, doi:10.5194/acpd-11-29777-2011.
Dooley, A. L. (2008), Ice microphysics observations in tropical cyclones from NAMMA, MS thesis, 65 pp., Univ. of Illinois at Urbana-Champaign.
Durant, A. J., and R. A. Shaw (2005), Evaporation freezing by contact nucleation inside-out, *Geophys. Res. Lett.*, *32*, L20814, doi:10.1029/2005GL024175.
Durran, D. R. (2010), *Numerical Methods for Fluid Dynamics With Applications to Geophysics*, 2nd ed., 516 pp., Springer, New York.
Dusek, U., et al. (2006), Size matters more than chemistry for cloud-nucleating ability of aerosol particles, *Science*, *312*(5778), 1375–1378, doi:10.1126/science.1125261.
Enukashvily, I. M. (1980), A numerical method for integrating the kinetic equation of coalescence and breakup of cloud droplets, *J. Atmos. Sci.*, *37*, 2521–2534.
Fan, J., M. Ovtchinnikov, J. M. Comstock, S. A. McFarlane, and A. Khain (2009), Ice formation in Arctic mixed-phase clouds: Insights from a 3-D cloud resolving model with size-resolved aerosol and cloud microphysics, *J. Geophys. Res.*, *114*, D04205, doi:10.1029/2008JD010782.
Fan, J., S. Ghan, M. Ovchinnikov, X. Liu, P. J. Rasch, and A. Korolev (2011), Representation of Arctic mixed-phase clouds and the Wegener-Bergeron-Findeisen process in climate models: Perspectives from a cloud-resolving study, *J. Geophys. Res.*, *116*, D00T07, doi:10.1029/2010JD015375.
Fan, J., L. R. Leung, Z. Li, H. Morrison, H. Chen, Y. Zhou, Y. Qian, and Y. Wang (2012a), Aerosol impacts on clouds and precipitation in eastern China: Results from bin and bulk microphysics, *J. Geophys. Res.*, *117*, D00K36, doi:10.1029/2011JD016537.
Fan, J., D. Rosenfeld, Y. Ding, L. R. Leung, and Z. Li (2012b), Potential aerosol indirect effects on atmospheric circulation and radiative forcing through deep convection, *Geophys. Res. Lett.*, *39*, L09806, doi:10.1029/2012GL051851.
Fan J., L. R. Leunga, D. Rosenfeld, Q. Chena, Z. Lid, J. Zhang, and H. Yan (2013), Microphysical effects determine macrophysical response for aerosol impacts on deep convective clouds, *Proc. Natl. Acad. Sci. U.S.A.*, *110*(48), E4581–E4590, doi:10.1073/pnas.1316830110.
Fan, J., et al. (2014), Aerosol impacts on California winter clouds and precipitation during CalWater 2011: Local pollution versus long-range transported dust, *Atmos. Chem. Phys.*, *14*, 81–101.
Feingold, G., and A. J. Heymsfield (1992), Parameterizations of condensational growth of droplets for use in general circulation models, *J. Atmos. Sci.*, *49*, 2325–2342.
Feingold, G., S. Tzivion, and Z. Levin (1988), The evolution of raindrop spectra with altitude. 1: Solution to the stochastic collection/breakup equation using the method of moments, *J. Atmos. Sci.*, *45*, 3387–3399.
Feingold, G., S. M. Kreidenweis, B. Stevens, and W. R. Cotton (1996), Numerical simulations of stratocumulus processing of cloud condensation nuclei through collision-coalescence, *J. Geophys. Res.*, *101*(D16), 21,391–21,402, doi:10.1029/96JD01552.
Feingold, G., R. L. Walko, B. Stevens, and W. R. Cotton (1998), Simulations of marine stratocumulus using a new microphysical parameterization scheme, *Atmos. Res.*, *47–48*, 505–528.
Feingold, G., W. R. Cotton, S. Kreidenweis, and J. Davis (1999), The impact of giant cloud condensation nuclei on drizzle formation in strato-cumulus: Implications for cloud radiative properties, *J. Atmos. Sci.*, *56*, 4100–4117.
Ferrier, B. S. (1994), A double-moment multiple-phase four-class bulk ice scheme. Part I: Description, *J. Atmos. Sci.*, *51*, 249–280.
Field, P. R., R. J. Hogan, P. R. A. Brown, A. J. Illingworth, T. W. Choularton, and R. J. Cotton (2005), Parametrization of ice-particle size distributions for midlatitude stratiform cloud, *Q. J. R. Meteorol. Soc.*, *131*, 1997–2017.
Field, P. R., A. J. Heymsfield, and A. Bansemer (2006), Shattering and particle interarrival times measured by optical array probes in ice clouds, *J. Atmos. Oceanic Technol.*, *23*(10), 1357–1371.
Flatau, P., G. J. Trripoli, J. Verlinde, and W. R. Cotton (1989), The CSU_RAMS cloud microphysics module: General theory and code documentation, Colorado State Univ., Dep. of Atmospheric Science, paper 451, 88 pp.
Flossmann, A. I., and H. R. Pruppacher (1988), A theoretical study of the wet removal of atmospheric pollutants. Part III: The uptake, redistribution, and deposition of (NH4)2SO4 particles by a convective cloud using a two-dimensional cloud dynamics model, *J. Atmos. Sci.*, *45*, 1857–1871.
Flossmann, A. I., W. D. Hall, and H. R. Pruppacher (1985), A theoretical study of the wet removal of atmospheric pollutants. Part 1: The redistribution of aerosol particles captured through nucleation and impaction scavenging by growing cloud drops, *J. Atmos. Sci.*, *42*, 583–606.
Formenton, M., V. T. J. Phillips, and B. Lienert (2013a), A new snow microphysics parameterization applied to a cloud electrification model: Framework and preliminary results, 93rd AMS Annual Meeting, Austin, Tex., 6–10 Jan.
Formenton, M., G. Panegrossi, D. Casella, S. Dietrich, A. Mugnai, P. Sano`, F. Di Paola, H.-D. Betz, C. Price, and Y. Yair (2013b), Using a cloud electrification model to study relationships between lightning activity and cloud microphysical structure, *Nat. Hazards Earth Syst. Sci.*, *13*, 1085–1104, doi:10.5194/nhess-13-1085-2013.
Freud, E., and D. Rosenfeld (2012), Linear relation between convective cloud drop number concentration and depth for rain initiation, *J. Geophys. Res.*, *117*, D02207, doi:10.1029/2011JD016457.
Freud, E., D. Rosenfeld, M. O. Andreae, A. A. Costa, and P. Artaxo (2008), Robust relations between CCN and the vertical evolution of cloud drop size distribution in deep convective clouds, *Atmos. Chem. Phys.*, *8*, 1661–1675.
Fridlind, A. M., A. S. Ackerman, G. McFarquhar, G. Zhang, M. R. Poellot, P. J. DeMott, A. J. Prenni, and A. J. Heymsfield (2007), Ice properties of single-layer stratocumulus during the Mixed-Phase Arctic Cloud Experiment: 2. Model results, *J. Geophys. Res.*, *112*, D24202, doi:10.1029/2007JD008646.
Fridlind, A. M., et al. (2012), A comparison of TWP-ICE observational data with cloud-resolving model results, *J. Geophys. Res.*, *117*, D05204, doi:10.1029/2011JD016595.
Garcia-Garcia, F., and R. List (1992), Laboratory measurements and parameterizations of supercooled water skin temperatures and bulk properties of gyrating hailstones, *J. Atmos. Sci.*, *49*, 2058–2072.

Geoffroy O., J.-L. Brenguier, and F. Burnet (2010), Parametric representation of the cloud droplet spectra for LES warm bulk microphysical schemes, *Atmos. Chem. Phys.*, *10*, 4835–4848, doi:10.5194/acp-10-4835-2010.

Gettelman A., H. Morrison, C. R. Terai, and R. Wood (2013), Microphysical process rates and global aerosol-cloud interactions, *Atmos. Chem. Phys. Discuss.*, *13*, 11,789–11,825, doi:10.5194/acpd-13-11789-2013.

Ghan, S. J., R. C. Easter, J. Hudson, and F.-M. Bréon (2001), Evaluation of aerosol indirect radiative forcing in MIRAGE, *J. Geophys. Res.*, *106*, 5317–5334, doi:10.1029/2000JD900501.

Ghan, S. J., H. Abdul-Razzak, A. Nenes, Y. Ming, X. Liu, M. Ovchinnikov, B. Shipway, N. Meskhidze, J. Xu, and X. Shi (2011), Droplet nucleation: Physically based parameterizations and comparative evaluation, *J. Adv. Model. Earth Syst.*, *3*, M10001, doi:10.1029/2011MS000074.

Gilmore, M. S., and J. M. Straka (2008), The Berry and Reinhardt autoconversion parameterization: A digest, *J. Appl. Meteorol. Climatol.*, *47*, 375–396.

Golovin, A. M. (1963), The solution of the coagulation equation for cloud droplets in a rising air current, *Izv. Akad. Nauk. SSSR. Ser. Geofiz.*, *5*, 783–791.

Grabowski, W. W. (2001), Coupling cloud processes with the large-scale dynamics using the Cloud-Resolving Convection parameterization (CRCP), *J. Atmos. Sci.*, *58*, 978–997.

Grabowski, W. W. (2003), Impact of cloud microphysics on convective-radiative quasi-equilibrium revealed by cloud-resolving convection parameterization (CRCP), *J. Clim.*, *16*, 3463–3475.

Grabowski, W. W. (2006), Comments on "Preliminary tests of multiscale modeling with a two-dimensional framework: Sensitivity to coupling methods" by Jung and Arakawa, *Mon. Weather Rev.*, *134*, 2021–2026.

Grabowski, W. W. (2014), Untangling microphysical impacts on deep convection applying a novel modeling methodology, *J. Atmos. Sci.*, in press.

Grabowski, W. W., and P. K. Smolarkiewicz (1999), CRCP: A cloud resolving convection parameterization for modeling the tropical convecting atmosphere, *Phys. D*, *133*, 171–178, Special Issue: Predictability: Quantifying uncertainty in models of complex phenomena, 18th Annual Conference of the Center for Non-linear studies, Los Alamos, N. M., 11–15 May, 1998.

Grell, G., J. Dudhia, and D. R. Stauffer (1994), A description of the fifth generation Penn State/NCAR Mesoscale Model (MM5), *Tech. Note NCAR/TN-398+STR*, 121 pp.

Grits, B., M. Pinsky, and A. P. Khain (2006), Investigation of small-scale droplet concentration inhomogeneities in a homogeneous turbulent flow, *Meteorol. Oceanic Phys.*, *92*, 191–204.

Hall, W. D. (1980), A detailed microphysical model within a two-dimensional dynamic framework: Model description and preliminary results, *J. Atmos. Sci.*, *37*, 2486–2507.

Hallett, J., and S. C. Mossop (1974), Production of secondary ice crystals during the riming process, *Nature*, *249*, 26–28.

Handwerker, J., and W. Straub (2011), Optimal determination of parameters for gamma-type drop size distributions based on moments, *J. Atmos. Oceanic Technol.*, *28*, 513–529.

Hashino, T., and G. J. Tripoli (2007), The Spectral Ice Habit Prediction System (SHIPS). Part I: Model description and simulation of the vapor deposition process, *J. Atmos. Sci.*, *64*, 2210–2237.

Hashino, T., and G. J. Tripoli (2008), The Spectral Ice Habit Prediction System (SHIPS). Part II: Simulation of nucleation and depositional growth of polycrystals, *J. Atmos. Sci.*, *65*, 3071–3094, doi:10.1175/2008JAS2615.1.

Hashino, T., and G. J. Tripoli (2011), The Spectral Ice Habit Prediction System (SHIPS). Part IV: Box model simulations of the habit-dependent aggregation process, *J. Atmos. Sci.*, *68*, 1142–1161, doi:10.1175/2011JAS3667.1.

Hazra, A., P. Mukhopadhyay, S. Taraphdar, J. P. Chen, and W. R. Cotton (2013), Impact of aerosols on tropical cyclones: An investigation using convection-permitting model simulation, *J. Geophys. Res. Atmos.*, *118*, 7157–7168, doi:10.1002/jgrd.50546.

Herbener, S. R., S. C. van den Heever, G. G. Carrió, S. M. Saleeby, and W. R. Cotton (2014), Aerosol indirect effects on idealized tropical cyclone dynamics, *J. Atmos. Sci.*, *71*, 2040–2055.

Heymsfield, A., C. Schmitt, and A. Bansemer (2013), Ice cloud particle size distributions and pressure-dependent terminal velocities from in situ observations at temperatures from 0° to −86°C, *J. Atmos. Sci.*, *70*, 4123–4154.

Heymsfield, A. J. (1982), A comparative study of the rates of development of potential graupel and hail embryos in High Plains storms, *J. Atmos. Sci.*, *39*, 2867–2897.

Heymsfield, A. J., and J. Iaquinta (2000), Cirrus crystal terminal velocities, *J. Atmos. Sci.*, *57*, 916–938.

Heymsfield, A. J., and K. M. Miller (1988), Water vapor and ice mass transported into the Anvils of CCOPE thunderstorms: Comparison with storm influx and rainout, *J. Atmos. Sci.*, *45*(22), 3501–3514.

Heymsfield, A. J., and R. M. Sabin (1989), Cirrus crystal nucleation by homogeneous freezing of solution droplets, *J. Atmos. Sci.*, *46*, 2252–2264.

Heymsfield, A. J., A. Bansemer, P. R. Field, S. L. Durden, J. L. Stith, J. E. Dye, W. Hall, and C. A. Grainger (2002), Observations and parameterizations of particle size distributions in deep tropical cirrus and stratiform precipitating clouds: Results from in situ observations in TRMM field campaigns, *J. Atmos. Sci.*, *59*, 3457–3491.

Heymsfield, A. J., A. Bansemer, G. Heymsfield, and A. O. Fierro (2009), Microphysics of maritime tropical convective updrafts at temperatures from −20°C to −60°C, *J. Atmos. Sci.*, *66*, 3530–3565.

Heymsfield, A. J. M., and R. Hjelmfelt (1984), Processes of hydrometeor development in Oklahoma convective clouds, *J. Atmos. Sci.*, *41*, 2811–2835.

Heymsfield, G. M., and S. Schotz (1985), Structure and evolution of a severe squall line over Oklahoma, *Mon. Weather Rev.*, *113*, 1563–1589.

Hill, A. A., S. Dobbie, and Y. Yin (2008), The impact of aerosols on non-precipitating marine stratocumulus. I: Model description and prediction of the indirect effect, *Q. J. R. Meteorol. Soc.*, *134*, 1143–1154.

Hocking, L. M., and P. R. Jonas (1970), The collision efficiency of small drops, *Q. J. R. Meteorol. Soc.*, *96*, 722–729.

Hong, S.-Y., and J. O. J. Lim (2006), The WRF single-moment 6-Class microphysics scheme (WSM6, *J. Korean Meteorol. Soc.*, *42*(2), 129–151.

Hong, S.-Y., J. Dudhia, and S.-H. Chen (2004), A revised approach to ice microphysical processes for the bulk parameterization of clouds and precipitation, *Mon. Weather Rev.*, *132*, 103–120.

Hoose, C., J. E. Kristjansson, J.-P. Chen, and A. Hazra (2010), A classical-theory-based parameterization of heterogeneous ice nucleation by mineral dust, soot, and biological particles in a global climate model, *J. Atmos. Sci.*, *67*, 2483–2503.

Igel, A., S. C. van den Heever, C. Naud, S. M. Saleeby, and D. Posselt (2013), Sensitivity of warm frontal processes to cloud-nucleating aerosol concentrations, *J. Atmos. Sci.*, *70*, 1768–1783.

Igel, A. L., and S. C. van den Heever (2014), Aerosol impacts in shallow convection as simulated by bin and bulk schemes in RAMS, The 94th American Meteorological Society Annual Meeting, AMS, Atlanta, Ga, 2–6 Feb.

Iguchi, T., T. Nakajima, A. P. Khain, K. Saito, T. Takemura, and K. Suzuki (2008), Modeling the influence of aerosols on cloud microphysical properties in the east Asia region using a mesoscale model coupled with a bin-based cloud microphysics scheme, *J. Geophys. Res.*, *113*, D14215, doi:10.1029/2007JD009774.

Iguchi, T., T. Nakajima, A. Khain, K. Saito, T. Takemura, H. Okamoto, T. Nishizawa, and W.-K. Tao (2012a), Evaluation of cloud microphysics in JMA-NHM simulations using bin or bulk microphysical schemes through comparison with cloud radar observations, *J. Atmos. Sci.*, *69*, 2566–2586, doi:10.1175/JAS-D-11-0213.1.

Iguchi, T., T. Matsui, J. J. Shi, W.-K. Tao, A. P. Khain, A. Hou, R. Cifelli, A. Heymsfield, and A. Tokay (2012b), Numerical analysis using WRF-SBM for the cloud microphysical structures in the C3VP field campaign: Impacts of supercooled droplets and resultant riming on snow microphysics, *J. Geophys. Res.*, *117*, D23206, doi:10.1029/2012JD018101.

Iguchi, T., T. Matsui, W. Tao, A. Khain, V. Phillips, C. Kidd, T. L'Ecuyer, S. Braun, and A. Hou (2014), WRF-SBM simulations of melting layer structure in mixed-phase precipitation events observed during LPVEx, *J. Appl. Meteorol. Climatol.*, *53*, 2710–2731, doi:10.1175/JAMC-D-13-0334.1.

Ikeda, K., R. Rasmussen, C. Liu, G. Thompson, and L. Xue (2008), Investigation of the dependence of squall line structure and dynamics on microphysical parameterization, 15th International Conference on Clouds and Precipitation, Cancun, Mexico, July.

Illingworth, A. J., and T. M. Blackman (2002), The need to represent raindrop size spectra as normalized gamma distributions for the interpretation of polarization radar observations, *J. Appl. Meteorol.*, *41*, 286–297.

Jarecka, D., H. Pawlowska, W. W. Grabowski, and A. A. Wyszogrodzki (2013), Modeling microphysical effects of entrainment in clouds observed during EUCAARI-IMPACT field campaign, *Atmos. Chem. Phys. Discuss.*, *13*, 1489–1526, doi:10.5194/acpd-13-1489-2013.

Jiang, H., H. Xue, A. Teller, G. Feingold, and Z. Levin (2006), Aerosol effects on the lifetime of shallow cumulus, *Geophys. Res. Lett.*, *33*, L14806, doi:10.1029/2006GL026024.

Johnson, R. H., and P. J. Hamilton (1988), The relationship of surface pressure features to the precipitation and airflow structure of an intense midlatitude squall line, *Mon. Weather Rev.*, *16*, 1444–1472.

Jonas, P. R. (1996), Turbulence and cloud microphysics, *Atmos. Res.*, *40*, 283–306.

Kato, T. (1995), A box-Lagrangian rain-drop scheme, *J. Meteorol. Soc. Jpn.*, *73*, 241–245.

Kessler, E. (1969), On the distribution and continuity of water substance in atmospheric circulations, Meteor. Monogr., No. 10, *Am. Meteorol. Soc.*, *84*(59), 3457–3491.

Khain, A., D. Rosenfeld, and A. Pokrovsky (2005), Aerosol impact on the dynamics and microphysics of convective clouds, *Q. J. R. Meteorol. Soc.*, *131*, 2639–2663, doi:10.1256/qj.04.62.

Khain, A., B. Lynn, and J. Dudhia (2010), Aerosol effects on intensity of landfalling hurricanes as seen from simulations with the WRF model with spectral bin microphysics, *J. Atmos. Sci.*, *67*, 365–384, doi:10.1175/2009JAS3210.1.

Khain, A., T. V. Prabha, N. Benmoshe, G. Pandithurai, and M. Ovchinnikov (2013), The mechanism of first raindrops formation in deep convective clouds, *J. Geophys. Res. Atmos.*, *118*, 9123–9140, doi:10.1002/jgrd.50641.

Khain, A. P. (2009), Notes on state-of-the-art investigations of aerosol effects on precipitation: A critical review, *Environ. Res. Lett.*, *4*, 015004, doi:10.1088/1748-9326/4/1/015004.

Khain, A. P., and B. Lynn (2009), Simulation of a super cell storm in clean and dirty atmosphere, *J. Geophys. Res.*, *114*, D19209, doi:10.1029/2009JD011827.

Khain, A. P., and I. Sednev (1996), Simulation of precipitation formation in the eastern Mediterranean coastal zone using a spectral microphysics cloud ensemble model, *Atmos. Res*, *43*, 77–110.

Khain, A. P., M. Ovchinnikov, M. Pinsky, A. Pokrovsky, and H. Krugliak (2000), Notes on the state-of-the-art numerical modeling of cloud microphysics, *Atmos. Res.*, *55*, 159–224.

Khain, A. P., M. B. Pinsky, M. Shapiro, and A. Pokrovsky (2001), Graupel-drop collision efficiencies, *J. Atmos. Sci.*, *58*, 2571–2595.

Khain, A. P., D. Rosenfeld, and A. Pokrovsky (2003), Simulation of aerosol effects on convective clouds developed under continental and maritime conditions, Geophys. Res. Abstracts, 5, 03180, European Geophysical Society. *Nice, Assembly of WMO*, 6–11 April.

Khain, A. P., A. Pokrovsky, M. Pinsky, A. Seifert, and V. Philips (2004a), Simulation of effects of atmospheric aerosols on deep turbulent convective clouds by using a spectral microphysics mixed-phase cumulus cloud model. Part I: Model description and possible applications, *J. Atmos. Sci.*, *61*, 2963–2982.

Khain, A. P., V. Arkhipov, M. Pinsky, Y. Feldman, and Y. Ryabov (2004b), Rain enhancement and fog elimination by seeding with charged droplets. Part 1: Theory and numerical simulations, *J. Appl. Meteorol.*, *43*(10), 1513–1529.

Khain, A. P., N. Benmoshe, and A. Pokrovsky (2008a), Factors determining the impact of aerosols on surface precipitation from clouds: Attempt of classification, *J. Atmos. Sci.*, *65*, 1721–1748, doi:10.1175/2007JAS2515.1.

Khain, A. P., N. Cohen, B. Lynn, and A. Pokrovsky (2008b), Possible aerosol effects on lightning activity and structure of hurricanes, *J. Atmos. Sci.*, *65*, 3652–3667.

Khain, A. P., L. R. Leung, B. Lynn, and S. Ghan (2009), Effects of aerosols on the dynamics and microphysics of squall lines simulated by spectral bin and bulk parameterization schemes, *J. Geophys. Res.*, *114*, D22203, doi:10.1029/2009JD011902.

Khain, A. P., D. Rosenfeld, A. Pokrovsky, U. Blahak, and A. Ryzhkov (2011), The role of CCN in precipitation and hail in a mid-latitude storm as seen in simulations using a spectral (bin) microphysics model in a 2D dynamic frame, *Atmos. Res.*, *99*(1), 129–146, doi:10.1016/j.atmosres.2010.09.015.

Khain, A. P., V. Phillips, N. Benmoshe, and A. Pokrovsky (2012), The role of small soluble aerosols in the microphysics of deep maritime clouds, *J. Atmos. Sci.*, *69*, 2787–2807, doi:10.1175/2011JAS3649.1.

Khain, A. P., E. Ilotoviz, N. Benmoshe, V. Phillips, A. V. Ryzhkov, and M. R. Kumjian (2014a), 14-th conference on cloud physics, Westin Copley Place, Boston, Mass, 7–11 July.

Khain, A., B. Lynn, and J. Dudhia (2014b), WRF with spectral bin microphysics: Now part of the WRF software depository, The Conference of WRF users, June.

Khairoutdinov, M., and Y. Kogan (2000), A new cloud physics parameterization in a large-eddy simulation model of marine stratocumulus, *Mon. Weather Rev.*, *128*(1), 229–243.

Khairoutdinov, M. F., and D. A. Randall (2001), A cloud resolving model as a cloud parameterization in the NCAR Community Climate System Model: Preliminary results, *Geophys. Res. Lett.*, *28*, 3617–3620, doi:10.1029/2001GL013552.

Khairoutdinov, M. F., and C. E. Yang (2013), Cloud-resolving modelling of aerosol indirect effects in idealised radiative-convective equilibrium with interactive and fixed sea surface temperature, *Atmos. Chem. Phys.*, *13*(8), 4133–4144.

Khairoutdinov, M. F., D. A. Randall, and C. DeMotte (2005), Simulations of the atmospheric general circulation using a cloud-resolving model as a super-parameterization of physical processes, *J. Atmos. Sci.*, *62*, 2136–2154.

Khvorostyanov, V. I., and J. A. Curry (2000), A new theory of heterogeneous ice nucleation for application in cloud and climate models, *Geophys. Res. Lett.*, *27*, 4081–4084, doi:10.1029/1999GL011211.

Khvorostyanov, V. I., and J. A. Curry (2004), The theory of ice nucleation by heterogeneous freezing of deliquescent mixed CCN. Part I: Critical radius, energy, and nucleation rate, *J. Atmos. Sci.*, *61*, 2676–2691.

Khvorostyanov, V. I., and J. A. Curry (2005), The theory of ice nucleation by heterogeneous freezing of deliquescent mixed CCN. Part II: Parcel model simulation, *J. Atmos. Sci.*, *62*, 261–285.
Khvorostyanov, V. I., A. P. Khain, and E. L. Kogteva (1989), A two-dimensional non stationary microphysical model of a three-phase convective cloud and evaluation of the effects of seeding by a crystallizing agent, *Soviet Meteorol. Hydrol.*, *5*, 33–45.
Klein, S. A., et al. (2009), Intercomparison of model simulations of mixed phase clouds observed during the ARM Mixed-Phase Arctic Cloud Experiment. I: Single-layer cloud, *Q. J. R. Meteorol. Soc.*, *135*, 979–1002, doi:10.1002/qj.416.
Kogan, Y., I. P. Mazin, B. N. Sergeev, and V. I. Khvorostyanov (1984), *Numerical Cloud Modeling*, 183 pp., Gidrometeoizdat, Moscow.
Kogan, Y. L. (1991), The simulation of a convective cloud in a 3-D model with explicit microphysics. Part I: Model description and sensitivity experiments, *J. Atmos. Sci.*, *48*, 1160–1189.
Koren, I., L. A. Remer, O. Altaratz, J. V. Martins, and A. Davidi (2010), Aerosol-induced changes of convective cloud anvils produce strong climate warming, *Atmos. Chem. Phys.*, *10*(10), 5001–5010.
Koren, I., et al. (2012), Aerosol-induced intensification of rain from the tropics to the mid-latitudes, *Nat. Geosci.*, *5*(2), 118–122.
Korolev, A., and I. Mazin (2003), Supersaturation of water vapor in clouds, *J. Atmos. Sci.*, *60*, 2957–2974.
Korolev, A., M. Pinsky, and A. P. Khain (2013b), A new mechanism of droplet size distribution broadening during diffusional growth, *J. Atmos. Sci.*, *70*, 2051–2071.
Korolev, A. V. (1994), A study of bimodal droplet size distributions in stratiform clouds, *Atmos. Res.*, *32*, 143–170.
Korolev, A. V. (1995), The influence of supersaturation fluctuations on droplet size spectra formation, *J. Atmos. Sci.*, *52*, 3620–3634.
Korolev, A. V., and G. A. Isaac (2003), Phase transformation of mixed-phase clouds, *Q. J. R. Meteorol. Soc.*, *129*, 19–38.
Korolev, A. V., G. A. Isaac, and J. Hallett (1999), Ice particle habits in Arctic clouds, *Geohys. Res. Lett.*, *26*, 1299–1302.
Korolev, A. V., E. F. Emery, J. W. Strapp, S. G. Cober, G. A. Isaac, M. Wasey, and D. Marcotte (2011), Small ice particles in tropospheric clouds: Fact or artifact? Airborne Icing Instrumentation Evaluation Experiment, *Bull. Am. Meteorol. Soc.*, *92*, 967–973, doi:10.1175/2010BAMS3141.1.
Korolev, A. V., E. F. Emery, J. W. Strapp, S. G. Cober, and G. A. Isaac (2013a), Quantification of the effects of shattering on airborne ice particle measurements, *J. Atmos. Oceanic Technol.*, *30*, 2527–2553.
Kovetz, A., and B. Olund (1969), The effect of coalescence and condensation on rain formation in a cloud of finite vertical extent, *J. Atmos. Sci.*, *26*, 1060–1065.
Krauss, T. W. (1999), Hail suppression, invited lecture at 7-th WMO scientific conference on weather modification, Chiang Mai, Thailand, 17–22 Feb.
Kumjian, M. R., and A. V. Ryzhkov (2012), The impact of size sorting on the polarimetric radar variables, *J. Atmos. Sci.*, *69*, 2042–2060, doi:10.1175/JAS-D-11-0125.1.
Kumjian, M. R., S. M. Ganson, and A. V. Ryzhkov (2012), Raindrop freezing in deep convective updrafts: A microphysical and polarimetric model, *J. Atmos. Sci.*, *69*, 3471–3490.
Kumjian, M. R., A. P. Khain, N. Benmoshe, E. Ilotoviz, A. V. Ryzhkov, and V. T. J. Phillips (2014), The anatomy and physics of ZDR columns: Investigating a polarimetric radar signature with a spectral bin microphysical model, *J. Appl. Meteorol. Climatol.*, *53*, 1820–1843.
Laird, N. F., H. T. Ochs III, R. M. Rauber, and L. J. Miller (2000), Initial precipitation formation in warm Florida cumulus, *J. Atmos. Sci.*, *57*, 3740–3751.
Lang, S., W.-K. Tao, R. Cifelli, W. Olson, J. Halverson, S. Rutledge, and J. Simpson (2007), Improving simulations of convective system from TRMM LBA: Easterly and westerly regimes, *J. Atmos. Sci.*, *64*, 1141–1164.
Lang, S., W.-K. Tao, J.-D. Chern, D. Wu, and X. Li (2014), Benefits of a 4th ice class in the simulated radar reflectivities of convective systems using a bulk microphysics scheme, *J. Atmos. Sci.*, *71*, 3583–3612, doi:10.1175/JAS-D-13-0330.1.
Lawson, R. P., B. Baker, B. Pilson, and Q. Mo (2006), In situ observations of the microphysical properties of wave, cirrus, and Anvil clouds. Part II: Cirrus clouds, *J. Atmos. Sci.*, *63*, 3186–3203.
Lebo Z. J., and J. H. Seinfeld (2011), Theoretical basis for convective invigoration due to increased aerosol concentration, *Atmos. Chem. Phys.*, *11*, 5407–5429, doi:10.5194/acp-11-5407-2011.
Lee, S. S., L. J. Donner, V. T. J. Phillips, and Y. Ming (2008), The dependence of aerosol effects on clouds and precipitation on cloud-system organization, shear and stability, *J. Geophys. Res.*, *113*, D16202, doi:10.1029/2007JD009224.
Lehmann, K., H. Siebert, and R. A. Shaw (2009), Homogeneous and inhomogeneous mixing in cumulus clouds: Dependence on local turbulence structure, *J. Atmos. Sci.*, *66*, 3641–3659.
Levin, Z., and W. R. Cotton (2009), *Aerosol Pollution Impact on Precipitation: A Scientific Review*, 386 pp., Springer.
Levin, Z., G. Feingold, S. Tzivion, and A. Waldvogel (1991), The Evolution of raindrop spectra: Comparison between modeled and observed spectra along a mountain slope in Switzerland, *J. Appl. Meteorol.*, *30*, 893–900.
Levin, Z., A. Teller, E. Ganor, B. Graham, M. O. Andreae, W. Maenhaut, A. H. Falkovich, and Y. Rudich (2003), The role of aerosol size and composition in nucleation scavenging within clouds, *J. Geophys. Res.*, *108*(D22), 4700, doi:10.1029/2003JD003647.
Li, X., W.-K. Tao, A. P. Khain, J. Simpson, and D. E. Johnson (2009a), Sensitivity of a cloud-resolving model to bulk and explicit bin microphysical schemes. Part I: Validation with a PRE-STORM case, *J. Atmos. Sci.*, *66*, 3–21, doi:10.1175/2008JAS2646.1.
Li, X., W.-K. Tao, A. P. Khain, J. Simpson, and D. E. Johnson (2009b), Sensitivity of a cloud-resolving model to bulk and explicit bin microphysical schemes. Part II: Cloud microphysics and storm dynamics interactions, *J. Atmos. Sci.*, *66*, 22–40.
Li, X., W.-K. Tao, T. Matsui, C. Liu, and H. Masunaga (2010), Improving a spectral bin microphysics scheme using TRMM satellite observations, *Q. J. R. Meteorol. Soc.*, *136*, 382–399, doi:10.1002/qj.569.
Lim, K.-S. S., and S.-Y. Hong (2010), Development of an effective double-moment cloud microphysics scheme with prognostic cloud condensation nuclei (CCN) for weather and climate models, *Mon. Weather Rev.*, *138*, 1587–1612, doi:10.1175/2009MWR2968.1.
Lin, Y., and B. A. Colle (2011), A new bulk microphysical scheme that includes riming intensity and temperature-dependent ice characteristics, *Mon. Weather Rev.*, *139*, 1013–1035, doi:10.1175/2010MWR3293.1.
Lin, Y.-L., R. D. Farley, and H. D. Orville (1983), Bulk parameterization of the snow field in a cloud model, *J. Clim. Appl. Meteorol.*, *22*, 1065–1092.
Liu, Y., P. H. Daum, R. McGraw, and R. Wood (2006), Parameterization of the autoconversion process. Part II: Generalization of Sundqvist-type parameterizations, *J. Atmos. Sci.*, *63*, 1103–1109.
Loftus, A. M., and W. R. Cotton (2014a), A triple-moment hail bulk microphysics scheme. Part II: Verification and comparison with two-moment bulk microphysics, *Atmos. Res.*, *150*, 97–128.
Loftus, A. M., and W. R. Cotton (2014b), Examination of CCN impacts on hail in a simulated supercell storm with triple-moment hail bulk microphysics, *Atmos. Res.*, *147-148*, 183–204.
Loftus, A. M., W. R. Cotton, and G. G. Carrio (2014), Examination of CCN impacts on hail with a triple-moment microphysics scheme. Part 1. Model description and initial evaluation, *Atmos. Res.*, *149*, 35–57.

Lohmann, U., and J. Feichter (1997), Impact of sulfate aerosols on albedo and lifetime of clouds: A sensitivity study with the ECHAM GCM, *J. Geophys. Res.*, *102*, 13,685–13,700, doi:10.1029/97JD00631.
Long, A. (1974), Solutions to the droplet collection equation for polynomial kernels, *J. Atmos. Sci.*, *31*, 1040–1052.
Low, T. B., and R. List (1982a), Collision coalescence and breakup of raindrops: Part I. Experimentally established coalescence efficiencies and fragments size distribution in breakup, *J. Atmos. Sci.*, *39*, 1591–1606.
Low, T. B., and R. List (1982b), Collision coalescence and breakup of raindrops: Part II. Parameterization of fragment size distributions in breakup, *J. Atmos. Sci.*, *39*, 1607–1618.
Luo, Y., K.-M. Xu, H. Morrison, and G. McFarquhar (2008), Arctic mixed-phase clouds simulated by a cloud-resolving model: Comparison with ARM observations and sensitivity to microphysics parameterizations, *J. Atmos. Sci.*, *65*, 1285–1303, doi:10.1175/2007JAS2467.1.
Lynn, B., and A. P. Khain (2007), Utilization of spectral bin microphysics and bulk parameterization schemes to simulate the cloud structure and precipitation in a mesoscale rain event, *J. Geophys. Res.*, *112*, D22205, doi:10.1029/2007JD008475.
Lynn, B., A. P. Khain, J. Dudhia, D. Rosenfeld, A. Pokrovsky, and A. Seifert (2005a), Spectral (bin) microphysics coupled with a mesoscale model (MM5). Part 1. Model description and first results, *Mon. Weather Rev.*, *133*, 44–58.
Lynn, B., A. P. Khain, J. Dudhia, D. Rosenfeld, A. Pokrovsky, and A. Seifert (2005b), Spectral (bin) microphysics coupled with a mesoscale model (MM5). Part 2: Simulation of a CaPe rain event with squall line, *Mon. Weather Rev.*, *133*, 59–71.
Lynn, B. H., A. P. Khain, J. W. Bao, S. A. Michelson, T. Yuan, G. Kelman, and N. Benmoshe (2014), The sensitivity of the WRF-simulated Hurricane Irene to physics configuration, Abstract at the 94-th AMS conference, Atlanta, February 2014.
Magaritz, L., M. Pinsky, A. Khain, and O. Krasnov (2009), Investigation of droplet size distributions and drizzle formation using a new trajectory ensemble model. Part 2: Lucky parcels in non-mixing limit, *J. Atmos. Sci.*, *66*, 781–805.
Magaritz, L., M. Pinsky, and A. P. Khain (2010), Effects of stratocumulus clouds on aerosols in the maritime boundary layer, *Atmos. Res.*, *97*, 498–512.
Magaritz-Ronen, L., M. Pinsky, and A. Khain (2014), Effects of turbulent mixing on the structure and macroscopic properties of stratocumulus clouds, *J. Atoms. Sci.*, *71*, 1843–1862.
Mansell, E. R., C. L. Ziegler, and E. C. Bruning (2010), Simulated electrification of a small thunderstorm with two-moment bulk microphysics, *J. Atmos. Sci.*, *67*, 171–194, doi:10.1175/2009JAS2965.1.
Marks, R. J., II (1991), *Introduction to Shannon Sampling and Interpolation Theory*, Springer, New York.
Matsui, T., X. Zeng, W.-K. Tao, H. Masunaga, W. Olson, and S. Lang (2009), Evaluation of long-term cloud-resolving model simulations using satellite radiance observations and multifrequency satellite simulators, *J. Atmos. Oceanic Technol.*, *26*, 1261–1274.
Mazin, I. P., A. Kh. Khrgian, and I. M. Imyanitov (1989), *Handbook of Clouds and Cloudy Atmosphere*, 647 p., Gidrometeoizdat.
McFarquhar, G. M., M. S. Timlin, R. M. Rauber, B. F. Jewett, J. A. Grim, and D. P. Jorgensen (2007), Vertical variability of cloud hydrometeors in the stratiform region of mesoscale convective systems and bow echoes, *Mon. Weather Rev.*, *135*, 3405–3428.
McFarquhar, G. M., et al. (2011), Indirect and Semi-Direct Aerosol Campaign (ISDAC): The impact of Arctic aerosols on clouds, *Bull. Am. Meteorol. Soc.*, *92*, 183–201, doi:10.1175/2010BAMS2935.1.
Meyers, M. P., P. J. DeMott, and W. R. Cotton (1992), New primary ice-nucleation parameterizations in an explicit cloud model, *J. Appl. Meteorol.*, *31*, 708–721.
Meyers, M. P., R. L. Walko, J. Y. Harrington, and W. R. Cotton (1997), New RAMS cloud microphysics parameterization. Part II: The two-moment scheme, *Atmos. Res.*, *45*, 3–39.
Milbrandt, J. A., and R. McTaggart-Cowan (2010), Sedimentation-induced errors in bulk microphysics schemes, *J. Atmos. Sci.*, *67*, 3931–3948.
Milbrandt, J. A., and M. K. Yau (2005a), A multimoment bulk microphysics parameterization. Part I: Analysis of the role of the spectral shape parameter, *J. Atmos. Sci.*, *62*, 3051–3064.
Milbrandt, J. A., and M. K. Yau (2005b), A multimoment bulk microphysics parameterization. Part II: A proposed three-moment closure and scheme description, *J. Atmos. Sci.*, *62*, 3065–3081.
Milbrandt, J. A., and M. K. Yau (2006), A multimoment bulk microphysics parameterization. Part III: Control simulation of a hailstorm, *J. Atmos. Sci.*, *63*, 3114–3136.
Mitchell, D. L., S. K. Chai, Y. Liu, A. J. Heymsfield, and Y. Dong (1996), Modeling cirrus clouds. Part I: Treatment of bimodal size spectra and case study analysis, *J. Atmos. Sci.*, *53*, 2952–2966.
Mitra, S. K., U. Barth, and H. R. Pruppacher (1990), A laboratory study of the efficiency with which aerosol particles are scavenged by the snow flakes, *Atmos. Environ.*, *24A*(5), 1247–1254.
Mitra, S. K., J. Brinkmann, and H. R. Pruppacher (1992), A wind tunnel study on the drop-to-particle conversion, *J. Aerosol Sci.*, *23*, 245–256.
Mizuno, H. (1990), Parameterization of the accretion process between different precipitation elements, *J. Meteorol. Soc. Jpn.*, *68*, 395–398.
Moncrieff, M. W. (2010), The multiscale organization of moist convection and the intersection of weather and climate, in *Climate Dynamics: Why Does Climate Vary?*, edited by D.-Z. Sun and F. Bryan, AGU, Washington, D. C., doi:10.1029/2008GM000838.
Morrison, H. (2012), On the numerical treatment of hydrometeor sedimentation in bulk and hybrid bulk–bin microphysics schemes, *Mon. Weather Rev.*, *140*, 1572–1588.
Morrison, H., and A. Gettelman (2008), A new two-moment bulk stratiform cloud microphysics scheme in the community atmosphere model, version 3 (CAM3). Part I: Description and numerical tests, *J. Clim.*, *21*, 3642–3658.
Morrison, H., and W. W. Grabowski (2007), Comparison of bulk and bin warm-rain microphysics models using a kinematic framework, *J. Atmos. Sci.*, *64*(8), 2839–2861.
Morrison, H., and W. W. Grabowski (2010), An improved representation of rimed snow and conversion to graupel in a multicomponent bin microphysics scheme, *J. Atmos. Sci.*, *67*, 1337–1360.
Morrison, H., and J. A. Milbrandt (2014), A new approach for parameterizing cloud microphysics based on the prediction of ice-phase particle properties, 14th Conference on Cloud Physics, Boston, Mass., p. 41, 7–11 July.
Morrison, H., J. A. Curry, and V. I. Khvorostyanov (2005a), A new double-moment microphysics parameterization for application in cloud and climate models. Part I: Description, *J. Atmos. Sci.*, *62*(6), 1665–1677.
Morrison, H., M. D. Shupe, J. O. Pinto, and J. A. Curry (2005b), Possible roles of ice nucleation mode and ice nuclei depletion in the extended lifetime of Arctic mixed-phase clouds, *Geophys. Res. Lett.*, *32*, L18801, doi:10.1029/2005GL023614.
Morrison, H., J. O. Pinto, J. A. Curry, and G. M. McFarquhar (2008), Sensitivity of modeled Arctic mixed-phase stratocumulus to cloud condensation and ice nuclei over regionally varying surface conditions, *J. Geophys. Res.*, *113*, D05203, doi:10.1029/2007JD008729.
Morrison, H., G. Thompson, and V. Tatarskii (2009a), Impact of cloud microphysics on the development of trailing stratiform precipitation in a simulated squall line: Comparison of one- and two-moment schemes, *Mon. Weather Rev.*, *137*, 991–1007.
Morrison, H., et al. (2009b), Intercomparison of model simulations of mixed-phase clouds observed during the ARM Mixed-Phase Arctic Cloud Experiment. II: Multi-layered cloud, *Q. J. R. Meteorol. Soc.*, *135*, 1003–1019, doi:10.1002/qj.415.

Morrison, H., et al. (2011), Intercomparison of cloud model simulations of Arctic mixed-phase boundary layer clouds observed during SHEBA, *J. Adv. Model. Earth Syst.*, *3*, M06003, doi:10.1029/2011MS000066.
Muhlbauer, A., T. Hashino, L. Xue, A. Teller, U. Lohmann, R. Rasmussen, I. Geresdi, and Z. Pan (2010), Intercomparison of aerosol-cloud-precipitation interactions in stratiform orographic mixed-phase clouds, *Atmos. Chem. Phys.*, *10*, 8173–8196.
Murakami, M. (1990), Numerical modeling of dynamical and microphysical evolution of an isolated convective cloud—The 19 July 1981 CCOPE cloud, *J. Meteorol. Soc. Jpn.*, *68*, 107–128.
Musil, D. J., A. J. Heymsfield, and P. L. Smith (1986), Microphysical characteristics of a well-developed weak echo region in a High Plains supercell thunderstorm, *J. Climate Appl. Meteorol.*, *25*(7), 1037–1051.
Niu, F., and Z. Li (2012), Systematic variations of cloud top temperature and precipitation rate with aerosols over the global tropics, *Atmos. Chem. Phys.*, *12*(18), 8491–8498.
Noppel, H., A. Pokrovsky, B. Lynn, A. P. Khain, and K. D. Beheng (2010a), A spatial shift of precipitation from the sea to the land caused by introducing submicron soluble aerosols: Numerical modeling, *J. Geophys. Res.*, *115*, D18212, doi:10.1029/2009JD012645.
Noppel, H., U. Blahak, A. Seifert, and K. D. Beheng (2010b), Simulations of a hailstorm and the impact of CCN using an advanced two-moment cloud microphysical scheme, *Atmos. Res.*, *96*, 286–301.
Onishi, R., and K. Takahashi (2011), A warm-bin–cold-bulk hybrid cloud microphysical model, *J. Atmos. Sci.*, *69*, 1474–1497.
Ovchinnikov, M., A. Korolev, and J. Fan (2011), Effects of ice number concentration on dynamics of a shallow mixed-phase stratiform cloud, *J. Geophys. Res.*, *116*, D00T06, doi:10.1029/2011JD015888.
Ovchinnikov, M., et al. (2013), Intercomparison of LES of Arctic mixed-phase clouds, Proc. of ASR meeting, March 2013.
Ovchinnikov, M., et al. (2014), Intercomparison of large-eddy simulations of Arctic mixed-phase clouds: Importance of ice size distribution assumptions, *J. Adv. Model. Earth Syst.*, *6*(1), 223–248.
Paluch, I. R. (1979), The entrainment mechanism in Colorado cumuli, *J. Atmos. Sci.*, *36*(12), 2467–2478.
Phillips, V. T. J., L. J. Donner, and S. T. Garner (2007a), Nucleation process in deep convection simulated by a cloud-system-resolving model with double-moment bulk microphysics, *J. Atmos. Sci.*, *64*, 738–761.
Phillips, V., A. P. Khain, and A. Pokrovsky (2007b), The influence of melting on the dynamics and precipitation production in maritime and continental storm-clouds, *J. Atmos. Sci.*, *64*(2), 338–359.
Phillips, V. T. J., P. J. DeMott, and C. Andronache (2008), An empirical parameterization of heterogeneous ice nucleation for multiple chemical species of aerosol, *J. Atmos. Sci.*, *65*, 2757–2783.
Phillips, V. T. J., C. Andronache, B. Christner, C. E. Morris, D. C. Sands, A. Bansemer, A. Lauer, C. McNaughton, and C. Seman (2009), Potential impacts from biological aerosols on ensembles of continental clouds simulated numerically, *Biogeosciences*, *6*, 1–28.
Phillips, V. T. J., P. J. DeMott, C. Andronache, K. A. Pratt, K. A. Prather, R. Subramanian, and C. Twohy (2013), Improvements to an empirical parameterization of heterogeneous ice nucleation and its comparison with observations, *J. Atmos. Sci.*, *70*, 378–409.
Phillips, V. T. J., A. Khain, N. Benmoshe, A. Ryzhkov, and E. Ilotovich (2014), Theory of time-dependent freezing. I: Description of scheme for wet growth of hail, *J. Atmos. Sci.*, *71*, 4527–4557.
Phillips, V. T. J., A. Khain, N. Benmoshe, A. Ryzhkov, and E. Ilotovich (2015), Theory of time-dependent freezing. II: Scheme for freezing raindrops and simulations by a cloud model with spectral bin microphysics, *J. Atmos. Sci.*, *72*, 262–286.
Pinsky, M., and A. P. Khain (2002), Effects of in-cloud nucleation and turbulence on droplet spectrum formation in cumulus clouds, *Q. J. R. Meteorol. Soc.*, *128*, 1–33.
Pinsky, M., A. P. Khain, and M. Shapiro (2001), Collision efficiency of drops in a wide range of Reynolds numbers: Effects of pressure on spectrum evolution, *J. Atmos. Sci.*, *58*, 742–764.
Pinsky, M., A. P. Khain, L. Magaritz, and A. Sterkin (2008a), Simulation of droplet size distributions and drizzle formation using a new trajectory ensemble model of cloud topped boundary layer. Part 1: Model description and first results in non-mixing limit, *J. Atmos. Sci.*, *65*, 2064–2086.
Pinsky, M., A. Khain, and H. Krugliak (2008b), Collisions of cloud droplets in a turbulent flow. Part 5: Application of detailed tables of turbulent collision rate enhancement to simulation of droplet spectra evolution, *J. Atmos. Sci.*, *63*, 357–374.
Pinsky, M., I. Mazin, A. Korolev, and A. Khain (2012), Analytical estimation of droplet concentration at cloud base, *J. Geophys. Res.*, *117*, D18211, doi:10.1029/2012JD017753.
Pinsky, M., I. P. Mazin, A. Korolev, and A. Khain (2013), Supersaturation and diffusional drop growth in liquid clouds, *J. Atmos. Sci.*, *70*, 2778–2793.
Pinsky, M. B., and A. P. Khain (2001), Fine structure of cloud drop concentration as seen from the Fast-FSSP measurements: Method of analysis and preliminary results, *J. Appl. Meteorol.*, *40*, 1515–1537.
Pinsky, M. B., and A. P. Khain (2003), Fine structure of cloud droplet concentration as seen from the Fast-FSSP measurements. Part 2: Results of in-situ observations, *J. Appl. Meteorol.*, *42*, 65–73.
Planche, C., J. H. Marsham, P. R. Field, K. S. Carslaw, A. A. Hill, G. W. Mann, and B. J. Shipway (2014), Damping of precipitation sensitivity to droplet number by ice processes, *Q. J. R. Meteorol. Soc.*, in press.
Plant, R. S. (2010), A review of the theoretical basis for bulk mass flux convective parameterization, *Atmos. Chem. Phys.*, *10*, 3529–3544, doi:10.5194/acp-10-3529-2010.
Prabha, T., A. P. Khain, B. N. Goswami, G. Pandithurai, R. S. Maheshkumar, and J. R. Kulkarni (2011), Microphysics of pre-monsoon and monsoon clouds as seen from in-situ measurements during CAIPEEX, *J. Atmos. Sci.*, *68*, 1882–1901.
Prabha, V. T., S. Patade, G. Pandithurai, A. Khain, D. Axisa, P. PradeepKumar, R. S. Maheshkumar, J. R. Kulkarni, and B. N. Goswami (2012), Spectral width of premonsoon and monsoon clouds over Indo-Gangetic valley during CAIPEEX, *J. Geophys. Res.*, *117*, D20205, doi:10.1029/2011JD016837.
Prenni, A. J., P. J. DeMott, S. M. Kreidenweis, J. Y. Harrington, A. Avramov, J. Verlinde, M. Tjernström, C. N. Long, and P. Q. Olsson (2007), Can ice-nucleating aerosols affect Arctic seasonal climate?, *Bull. Am. Meteorol. Soc.*, *88*, 541–550, doi:10.1175/BAMS-88-4-541.
Pruppacher, H. R., and J. D. Klett (1997), *Microphysics of Clouds and Precipitation*, 2nd ed., 963 pp., Springer, Dordrecht, Netherlands, doi:10.1007/978-0-306-48100-0.
Ramkrishna, D. (2000), *Population Balances: Theory and Applications to Particulated Systems in Engineering*, 355 pp., Academic Press, San Diego, Calif.
Rasmussen, R. M., I. Geresdi, G. Thompson, K. Manning, and E. Karplus (2002), Freezing drizzle formation in stably stratified layer clouds: The role of radiative cooling of cloud droplets, cloud condensation nuclei, and ice initiation, *J. Atmos. Sci.*, *59*, 837–860.
Reinike, J., and K. D. Beheng (1996), A note on the integral condensation rate, *Meteorol. Z., N.F.*, *5*, 283–292.
Reisin, T., Z. Levin, and S. Tzvion (1996a), Rain production in convective clouds as simulated in an axisymmetric model with detailed microphysics. Part I: Description of the model, *J. Atmos. Sci.*, *53*, 497–519.

Reisin, T., Z. Levin, and S. Tzivion (1996b), Rain production in convective clouds as simulated in as axisymmetric model with detailed microphysics. Part II: Effects of varying drops and ice initiation, *J. Atmos. Sci.*, *53*, 1815–1837.
Reisin, T., S. Tzivion, and Z. Levin (1996c), Seeding convective clouds with ice nuclei or hygroscopic particles: A numerical study using a model with detailed microphysics, *J. Appl. Meteorol.*, *35*, 1416–1434.
Reisner, R., R. M. Rasmussen, and R. T. Bruintjes (1998), Explicit forecasting of supercooled liquid water in winter storms using the MM5 mesoscale model, *Q. J. R. Meteorolog. Soc*, *124*, 1071–1107.
Respondek, P. S., A. I. Flossmann, R. R. Alheit, and H. R. Pruppache (1995), A theoretical study of the wet removal of atmospheric pollutants: Part V. The uptake, redistribution, and deposition of (NH4)2SO4 by a convective cloud containing ice, *J. Atmos. Sci.*, *52*, 2121–2132.
Riechelmann, T., Y. Noh, and S. Raasch (2012), A new method for large-eddy simulations of clouds with Lagrangian droplets including the effects of turbulent collision, *New J. Phys.*, *14*, 065008, doi:10.1088/1367-2630/14/6/065008.
Rissler, J., A. Vestin, E. Swietlicki, G. Fisch, J. Zhou, P. Artaxo, and M. O. Andreae (2006), Size distribution and hygroscopic properties of aerosol particles from dry-season biomass burning in Amazonia, *Atmos. Chem. Phys.*, *6*, 471–491, doi:10.5194/acp-6-471-2006.
Roberts, P., and J. Hallett (1967), A laboratory study of the ice nucleating properties of some mineral particulates, *Q. J. R. Meteorol. Soc.*, *94*, 25–34.
Rosenfeld, D., and G. Gutman (1994), Retrieving microphysical properties near the tops of potential rain clouds by multispectral analysis of AVHRR data, *Atmos. Res.*, *34*, 259–283.
Rosenfeld, D., and W. L. Woodley (2000), Deep convective clouds with sustained highly supercooled liquid water until −37.5°C, *Nature*, *405*, 440–442.
Rosenfeld, D., U. Lohmann, G. B. Raga, C. D. O'Dowd, M. Kulmala, S. Fuzzi, A. Reissell, and M. O. Andreae (2008), Flood or drought: How do aerosols affect precipitation?, *Science*, *321*, 1309–1313.
Rosenfeld, D., W. L. Woodley, A. Khain, W. R. Cotton, G. Carrió, I. Ginis, and J. H. Golden (2012), Aerosol effects on microstructure and intensity of tropical cyclones, *Bull. Am. Meteorol. Soc.*, *2012*, 987–1001.
Rotunno, R., J. B. Klemp, and M. L. Weisman (1988), A theory for strong, long-lived squall lines, *J. Atmos. Sci.*, *45*, 463–485.
Rutledge, S. A., and P. V. Hobbs (1984), The mesoscale and microscale structure and organization of clouds and precipitation in midlatitude cyclones. XII: A diagnostic modeling study of precipitation development in narrow cold-frontal rainbands, *J. Atmos. Sci.*, *41*, 2949–2972.
Rutledge, S. A., R. A. Houze Jr., M. I. Biggerstaff, and T. Matejka (1988), The Oklahoma– Kansas mesoscale convective system of 10–11 June 1985: Precipitation structure and single-Doppler radar analysis, *Mon. Weather Rev.*, *116*, 1409–1430.
Saito, K., J. Ishida, K. Aranami, T. Hara, T. Segawa, M. Narita, and Y. Honda (2007), Nonhydrostatic atmospheric models and operational development at JMA, *J. Meteorol. Soc. Jpn.*, *85B*, 271–304.
Saleeby, S. M., and W. R. Cotton (2004), A large-droplet mode and prognostic number concentration of cloud droplets in the Colorado State University Regional Atmospheric Modeling System (RAMS). Part I: Module descriptions and supercell test simulations, *J. Appl. Meteorol. Climatol.*, *43*, 182–195.
Saleeby, S. M., and W. R. Cotton (2008), A binned approach to cloud-droplet riming implemented in a bulk microphysics model, *J. Appl. Meteorol. Climatol.*, *47*, 694–703.
Saleeby, S. M., and S. C. van den Heever (2013), Developments in the CSU-RAMS aerosol model: Emissions, nucleation, regeneration, deposition, and radiation, *J. Appl. Meteorol. Climatol.*, *52*, 2601–2622.
Sant, V., U. Lohmann, and A. Seifert (2013), Performance of a triclass parameterization for the collision–coalescence process in shallow clouds, *J. Atmos. Sci.*, *70*, 1744–1767, doi:10.1175/JAS-D-12-0154.1.
Sastry, S. (2005), Water: Ins and outs of ice nucleation, *Nature*, *438*, 746–747.
Sato, K., and H. Okamoto (2006), Characterization of Ze and LDR of nonspherical and inhomogeneous ice particles for 95-GHz cloud radar: Its implication to microphysical retrievals, *J. Geophys. Res.*, *111*, D22213, doi:10.1029/2005JD006959.
Schultz, P. (1995), An explicit cloud physics parameterization for operational numerical weather prediction, *Mon. Weather Rev.*, *123*, 3331–3343.
Sednev I., and S. Menon (2012), Analyzing numerics of bulk microphysics schemes in community models: Warm rain processes, *Geosci. Model Dev.*, *5*, 975–987, doi:10.5194/gmd-5-975-2012.
Segal, Y., and A. P. Khain (2006), Dependence of droplet concentration on aerosol conditions in different cloud types: Application to droplet concentration parameterization of aerosol conditions, *J. Geophys. Res.*, *111*, D15204, doi:10.1029/2005JD006561.
Segal, Y., A. P. Khain, and M. Pinsky (2003), Thermodynamic factors influencing the bimodal spectra formation in cumulus clouds, *Atmos. Res.*, *66*, 43–64.
Segal, Y., A. P. Khain, M. Pinsky, and A. Sterkin (2004), Effects of atmospheric aerosol on precipitation in cumulus clouds as seen from 2000-bin cloud parcel microphysical model: Sensitivity study with cloud seeding applications, *Q. J. R. Meteorol. Soc.*, *130*, 561–582.
Seifert, A., and K. D. Beheng (2001), A double-moment parameterization for simulating autoconversion, accretion and self collection, *Atmos. Res.*, *59–60*, 265–281.
Seifert, A., and K. D. Beheng (2006a), A two-moment cloud microphysics parameterization for mixed-phase clouds. Part 1: Model description, *Meteorol. Atmos. Phys.*, *92*, 45–66.
Seifert, A., and K. D. Beheng (2006b), A two-moment cloud microphysics parameterization for mixed-phase clouds. Part 2: Maritime vs. continental deep convective storms, *Meteorol. Atmos. Phys.*, *92*, 67–82.
Seifert, A., A. Khain, A. Pokrovsky, and K. D. Beheng (2006), A comparison of spectral bin and two-moment bulk mixed-phase cloud microphysics, *Atmos. Res.*, *80*(1), 46–66.
Seifert, A., L. Nuijens, and B. Stevens (2010), Turbulence effects on warm-rain autoconversion in precipitating shallow convection, *Q. J. R. Meteorol. Soc.*, *136*, 1753–1762.
Seifert, A., C. Koehler, and K. D. Beheng (2011), Aerosol-cloud-precipitation effects over Germany as simulated by a convective-scale numerical weather prediction model, *Atmos. Chem. Phys. Discuss.*, *11*, 20,203–20,243, doi:10.5194/acpd-11-20203-2011.
Seigel, R. B., and S. C. van den Heever (2012), Mineral dust pathways into supercell storm, *J. Atmos. Sci.*, *69*, 1453–1473.
Sekhon, R. S., and R. C. Srivastava (1970), Snow size spectra and radar reflectivity, *J. Atmos. Sci.*, *27*, 299–307.
Shaw, R. A., A. J. Durant, and Y. Mi (2005), Heterogeneous surface crystallization observed in undercooled water, *J. Phys. Chem. B*, *109*, 9865–9868.
Shima, S., K. Kusano, A. Kawano, T. Sugiyama, and S. Kawahara (2009), The super-droplet method for the numerical simulation of clouds and precipitation: A particle-based and probabilistic microphysics model coupled with a non-hydrostatic model, *Q. J. R. Meteorol. Soc.*, *135*, 1307–1320.
Shipway, B. J., and A. A. Hill (2012), Diagnosis of systematic differences between multiple parameterizations of warm rain microphysics using a kinematic framework, *Q. J. R. Meteorol. Soc.*, *138*, 2196–2211.
Shpund, J., M. Pinsky, and A. Khain (2011), Evolution of sea spray in the marine boundary layer as seen from simulations using spectral bin microphysics-2D Lagrangian Model—Part 1: Effect of large eddies, *J. Atmos. Sci.*, *68*, 2366–2383.

Shupe, M. D., and J. M. Intrieri (2004), Cloud radiative forcing of the Arctic surface: The influence of cloud properties, surface albedo, and solar zenith angle, *J. Clim.*, *17*, 616–628.
Siebert, H., K. Lehmann, and M. Wendisch (2006), Observations of small-scale turbulence and energy dissipation rates in the cloudy boundary layer, *J. Atmos. Sci.*, *63*, 1451–1466.
Siewert, C., R. Kunnen, M. Meinke, and W. Schroder (2014), Orientation statistics and settling velocity of ellipsoids in decaying turbulence, *Atmos. Res.*, *142*, 45–56.
Skamarock, W. C., J. B. Klemp, J. Dudhia, D. O. Gill, D. M. Barker, M. G. Duda, Xiang-Yu Huang, W. Wang, and J. G. Powers (2008), A Description of the Advanced Research WRF Version 3, *NCAR/TN-475+STR NCAR Tech. Note*, pp. 113, Boulder, Colo.
Stephens, G. L., et al. (2002), The CloudSat mission and the A-Train, *Bull. Am. Meteorol. Soc.*, *83*, 1771–1790.
Stevens, B., G. Feingold, R. L. Walko, and W. R. Cotton (1996), On elements of the microphysical structure of numerically simulated non-precipitating stratocumulus, *J. Atmos. Sci.*, *53*, 980–1006.
Stevens, B., et al. (2005), Evaluation of large-eddy simulations via observations of nocturnal marine stratocumulus, *Mon. Weather Rev.*, *133*, 1443–1455.
Stith, J. L., J. E. Dye, A. Bansemer, A. J. Heymsfield, C. A. Grainger, W. A. Petersen, and R. Cifelli (2002), Microphysical observations of tropical clouds, *J. Appl. Meteorol.*, *41*(2), 97–117.
Storer, R. L., and S. C. van den Heever (2013), Microphysical processes evident in aerosol forcing of tropical deep convective clouds, *J. Atmos. Sci.*, *70*, 430–446.
Straka, J. M. (2009), *Cloud and Precipitation Microphysics*, 392 pp., Cambridge Univ. Press, Cambridge, U. K.
Sulia, K. J., and J. Y. Harrington (2011), Ice aspect ratio influences on mixed-phase clouds: Impacts on phase partitioning in parcel models, *J. Geophys. Res.*, *116*, D21309, doi:10.1029/2011JD016298.
Suzuki, K., T. Nakajima, T. Y. Nakajima, and A. P. Khain (2010), A study of microphysical mechanisms for correlation patterns between droplet radius and optical thickness of warm clouds with a spectral bin microphysics cloud model, *J. Atmos. Sci.*, *67*, 1126–1141.
Suzuki, K., G. L. Stephens, S. C. van den Heever, and T. Y. Nakajima (2011), Diagnosis of the warm rain process in cloud-resolving models using joint CloudSat and MODIS observations, *J. Atmos. Sci.*, *68*, 2655–2670.
Swann, H. (1998), Sensitivity to the representation of precipitating ice in CRM simulations of deep convection, *Atmos. Res.*, *48*, 415–435.
Szumowski, M. J., W. W. Grabowski, and H. T. Ochs III (1998), Simple two-dimensional kinematic framework designed to test warm rain microphysics models, *Atmos. Res.*, *45*, 299–326.
Takahashi, T. (1976), Hail in an axisymmetric cloud model, *J. Atmos. Sci.*, *33*, 1579–1601.
Tampieri, F., and C. Tomasi (1978), Size distribution models of fog and cloud droplets in terms of the modified gamma function, *Tellus*, *28*, 333–347.
Tao, W.-K., and M. W. Moncrieff (2009), Multiscale cloud system modeling, *Rev. Geophys.*, *47*, RG4002, doi:10.1029/2008RG000276.
Tao, W.-K., J. Simpson, and M. McCumber (1989), An ice-water saturation adjustment, *Mon. Weather Rev.*, *117*, 231–235.
Tao, W.-K., J. Simpson, C.-H. Sui, B. Ferrier, S. Lang, J. Scala, M.-D. Chou, and K. Pickering (1993), Heating, moisture, and water budgets of tropical and midlatitude squall lines. Comparisons and sensitivity to longwave radiation, *J. Atmos. Sci.*, *50*, 673–690.
Tao, W.-K., et al. (2003), Microphysics, radiation and surface processes in the Goddard Cumulus Ensemble (GCE) model, *Meteor. Atmos. Phys.*, *82*, 97–137.
Tao, W.-K., X. Li, A. Khain, T. Matsui, S. Lang, and J. Simpson (2007), The role of atmospheric aerosol concentration on deep convective precipitation: Cloud-resolving model simulations, *J. Geophys. Res.*, *112*, D24S18, doi:10.1029/2007JD008728.
Tao, W.-K., et al. (2009a), Multi-scale modeling system: Development, applications and critical issues, *Bull. Am. Meteorol. Soc.*, *90*, 515–534.
Tao, W.-K., et al. (2009b), The Goddard multi-scale modeling system with unified physics, *Ann. Geophys.*, *27*, 3055–3064.
Tao, W.-K., J. J. Shi, S. S. Chen, S. Lang, P.-L. Lin, S.-Y. Hong, C. Peters-Lidard, and A. Hou (2011), The impact of microphysical schemes on hurricane intensity and track, Asia-Pacific, *J. Atmos. Sci.*, *47*(1), 1–16.
Tao, W.-K., J.-P. Chen, Z. Li, C. Wang, and C. Zhang (2012), Impact of aerosols on convective clouds and precipitation, *Rev. Geophys.*, *50*, RG2001, doi:10.1029/2011RG000369.
Teller, A., and Z. Levin (2008), Factorial method as a tool for estimating the relative contribution to precipitation of cloud microphysical processes and environmental conditions: Method and application, *J. Geophys. Res.*, *113*, D02202, doi:10.1029/2007JD008960.
Teller, A., L. Xue, and Z. Levin (2012), The effects of mineral dust particles, aerosol regeneration and ice nucleation parameterizations on clouds and precipitation, *Atmos. Chem. Phys.*, *12*, 9303–9320.
Thompson, G., and T. Eidhammer (2014), A study of aerosol impacts on clouds and precipitation development in a large winter cyclone, *J. Atmos. Sci.*, (in press).
Thompson, G., R. M. Rasmussen, and K. Manning (2004), Explicit forecasts of winter precipitation using an improved bulk microphysics scheme. Part I: Description and sensitivity analysis, *Mon. Weather Rev.*, *132*, 519–542.
Thompson, G., P. R. Field, W. D. Hall, and R. Rasmussen (2006), A new bulk microphysical parameterization for WRF (& MM5), paper presented at WRF Conference, Natl. Cent. for Atmos. Res., Boulder, Colo., June.
Thompson, G., P. R. Field, R. M. Rasmussen, and W. D. Hall (2008), Explicit forecasts of winter precipitation using an improved bulk microphysics scheme. Part II: Implementation of a new snow parameterization, *Mon. Weather Rev.*, *136*, 5095–5115, doi:10.1175/2008MWR2387.1.
Tian, L., G. M. Heymsfield, L. Li, A. J. Heymsfield, A. Bansemer, C. H. Twohy, and R. C. Srivastava (2010), A study of cirrus ice particle size distribution using TC4 observations, *J. Atmos. Sci.*, *67*, 195–216.
Tripoli, G. J., and W. R. Cotton (1980), A numerical investigation of several factors contributing to the observed variable intensity of deep convection over south Florida, *J. Appl. Meteorol.*, *19*, 1037–1063.
Tsai, T.-C., J.-P. Chen, and W.-K. Tao (2012), Evaluating aerosol impact on precipitation with CLR double-moment microphysical scheme in WRF model, ICCP, 2012.
Tzivion, S., G. Feingold, and Z. Levin (1987), An efficient numerical solution to the stochastic collection equation, *J. Atmos. Sci.*, *44*, 3139–3149.
Tzivion, S., G. Feingold, and Z. Levin (1989), The evolution of raindrop spectra II: Collisional collection/breakup and evaporation in a rain shaft, *J. Atmos. Sci.*, *46*, 3312–3327.
Tzivion, S., T. G. Reisin, and Z. Levin (2001), A new formulation of the spectral multi-moment method for calculating the kinetic collection equation: More accuracy with fewer bins, *J. Comput. Phys.*, *171*, 418–422.
van den Heever, S. C., and W. R. Cotton (2004), The impact of hail size on simulated supercell storms, *J. Atmos. Sci.*, *61*(2004), 1596–1609.
van den Heever, S. C., and W. R. Cotton (2007), Urban aerosol impacts on downwind convective storms, *J. Appl. Meteorol. Climatol.*, *46*, 828–850.
van den Heever, S. C., G. G. Carrió, W. R. Cotton, P. J. Demott, and A. J. Prenni (2006), Impacts of nucleating aerosol on Florida storms. Part I: Mesoscale simulations, *J. Atmos. Sci.*, *63*(7), 1752–1775.

van den Heever, S. C., G. L. Stephens, and N. B. Wood (2011), Aerosol indirect effects on tropical convection characteristics under conditions of radiative-convective equilibrium, *J. Atmos. Sci.*, *68*, 699–718.
Verlinde, J., P. J. Flatau, and W. R. Cotton (1990), Analytical solutions to the collection growth equation: Comparison with approximate methods and application to cloud micro-physics parameterization schemes, *J. Atmos. Sci.*, *47*, 2871–2880.
Verlinde, J., et al. (2007), The Mixed-Phase Arctic Cloud Experiment, *Bull. Am. Meteorol. Soc.*, *88*, 205–221, doi:10.1175/BAMS-88-2-205.
Vohl, O., S. K. Mitra, S. C. Wurzler, and H. R. Pruppacher (1999), A wind tunnel study on the effects of turbulence on the growth of cloud drops by collision and coalescence, *J. Atmos. Sci.*, *56*, 4088–4099, doi:10.1175/1520-0469(1999)056<4088:AWTSOT>2.0.CO;2.
Voloshuk, V. M., and Y. S. Sedunov (1975), *Coagulation Processes in Dispersive Systems*, 320 pp., Gidrometizdat, Sant Petersburg.
Wacker, U., and C. Lupkes (2009), On the selection of prognostic moments in parametrization schemes for drop sedimentation, *Tellus*, *61A*, 498–511.
Walko, R. L., W. R. Cotton, M. P. Meyers, and J. Y. Harrington (1995), New RAMS cloud microphysics parameterization Part I: The single-moment scheme, *Atmos. Res.*, *38*, 2942.
Wang, L.-P., O. Ayala, and W. W. Grabowski (2005), On improved formulations of the superposition method, *J. Atmos. Sci.*, *62*, 1255–1266.
Wang, L.-P., Y. Xue, and W. W. Grabowski (2007), A bin integral method for solving the kinetic collection equation, *J. Comput. Phys.*, *226*, 159–88.
Wang, Y., J. Fan, R. Zhang, L. R. Leung, and C. Franklin (2013), Improving bulk microphysics parameterizations in simulations of aerosol effects, *J. Geophys. Res. Atmos.*, *118*, 5361–5379, doi:10.1002/jgrd.50432.
Warner, J. (1969), The microstructure of cumulus cloud. Part 1: General features of the droplet spectrum, *J. Atmos. Sci.*, *26*, 1049–1059.
Westbrook, C. D., R. J. Hogan, and A. J. Illingworth (2008), The capacitance of pristine ice crystals and aggregate snowflakes, *J. Atmos. Sci.*, *65*(1), 206–219.
Wisner, C., H. D. Orville, and C. Myers (1972), A numerical model of a hail-bearing cloud, *J. Atmos. Sci.*, *29*, 1160–1181.
Wood, R. (2005), Drizzle in stratiform boundary layer clouds. Part III: Microphysical aspects, *J. Atmos. Sci.*, *62*, 3034–3050.
Wood, R., T. L. Kubar, and D. L. Hartmann (2009), Understanding the importance of microphysics and macrophysics for warm rain in marine low clouds. Part II: Heuristic models of rain formation, *J. Atmos. Sci.*, *66*, 2973–2990.
Wurzler, S. C., A. I. Flossmann, H. R. Pruppacher, and S. E. Schwartz (1995), The scavenging of nitrate by clouds and precipitation, Part 1, *J. Atmos. Chem.*, *20*, 259–280.
Xue, L., A. Teller, R. Rasmussen, I. Geresdi, and Z. Pan (2010), Effects of aerosol solubility and regeneration on warm-phase orographic clouds and precipitation simulated by a detailed bin microphysical scheme, *J. Atmos. Sci.*, *67*, 3336–3354.
Xue, L., A. Teller, R. Rasmussen, I. Geresdi, Z. Pan, and X. Liu (2012), Effects of aerosol solubility and regeneration on mixed-phase orographic clouds and precipitation, *J. Atmos. Sci.*, *69*, 1994–2010.
Yang, F., M. Ovchinnikov, and R. A. Shaw (2013), Minimalist model of ice microphysics in mixed-phase stratiform clouds, *Geophys. Res. Lett.*, *40*, 3756–3760, doi:10.1002/grl.50700.
Yangang, L., Y. Laiguang, Y. Weinong, and L. Feng (1995), On the size distribution of cloud droplets, *Atmos. Res.*, *35*, 201–216.
Yano, J.-I. (1998), Planetary-scale coherent structures of tropical moist convection, *Aust. J. Phys.*, *51*, 865–874.
Yano, J.-I., and H. Baizig (2012), Single SCA-plume dynamics, *Dyn. Atmos. Ocean.*, *58*, 62–94.
Yano, J.-I., and D. Bouniol (2010), A minimum bulk microphysics, *Atmos. Chem. Phys. Discuss.*, *10*, 30,305–30,345, doi:10.5194/acpd-10-30305-2010.
Yano, J.-I., and R. S. Plant (2012), Convective quasi-equilibrium, *Rev. Geophys.*, *50*, RG4004, doi:10.1029/2011RG000378.
Yano, J.-I., J.-L. Redelsperger, F. Guichard, and P. Bechtold (2005), Mode decomposition as a methodology for developing convective-scale representations in global models, *Q. J. R. Meteorol. Soc.*, *131*, 2313–2336.
Yano, J.-I., P. Benard, F. Couvreux, and A. Lahellec (2010), NAM-SCA: A nonhydrostatic anelastic model with segmentally-constant approximations, *Mon. Weather Rev.*, *138*, 1957–1974.
Yano, J.-I., S. Kumar, and G. L. Roff (2012a), Towards compressed super-parameterization: Test of NAM-SCA under single-column GCM configurations, *Atmos. Phys. Chem. Discuss.*, *12*, 28,237–28,303.
Yano, J.-I., C. Liu, and M. W. Moncrieff (2012b), Atmospheric convective organization: Homeostasis or self-organized criticality?, *J. Atmos. Sci.*, *69*, 3449–3462.
Yano, J. I., M. Bister, Z. Fuchs, L. Gerard, V. Phillips, S. Barkidija, and J. M. Piriou (2013), Phenomenology of convection-parameterization closure, *Atmos. Phys. Chem.*, *13*, 4111–4131.
Yin, Y., Z. Levin, T. Reisin, and S. Tzivion (2000), Seeding convective clouds with hygroscopic flares: Numerical simulations using a cloud model with detailed microphysics, *J. Appl. Meteorol.*, *39*, 1460–1472.
Yin, Y., Q. Chen, L. Jin, B. Chen, S. Zhu, and X. Zhang (2012), The effects of deep convection on the concentration and size distribution of aerosol particles within the upper troposphere: A case study, *J. Geophys. Res.*, *117*, D22202, doi:10.1029/2012JD017827.
Young, K. C. (1975), The evolution of drop spectra due to condensation, coalescence and breakup, *J. Atmos. Sci.*, *32*, 965–973.
Yuter, S. E., D. Kingsmill, L. B. Nance, and M. Löffler-Mang (2006), Observations of precipitation size and fall speed characteristics within coexisting rain and wet snow, *J. Appl. Meteorol. Climatol.*, *45*, 1450–1464.
Zeng, X., W.-K. Tao, T. Matsui, S. Xie, S. Lang, M. Zhang, D. Starr, and X. Li (2011), Estimating the ice crystal enhancement factor in the tropics, *J. Atmos. Sci.*, *68*, 1424–1434.
Zhang, D.-L., K. Gao, and D. B. Parsons (1989), Numerical simulation of an intense squall line during 10–11 June 1985 PRE-STORM, Part 1: Model verification, *Mon. Weather Rev.*, *117*, 960–994.
Zhang, G. (2014), Microphysics parameterization for convection in GCM and its effects on cloud simulation in the NCAR CAM5 (invited lecture at the COST final Workshop), Toulouse, March.
Zhang, H., G. M. McFarquhar, S. M. Saleeby, and W. R. Cotton (2007), Impacts of Saharan dust as CCN on the evolution of an idealized tropical cyclone, *Geophys. Res. Lett.*, *34*, L14812, doi:10.2029/2007GL029876.
Zhang, H., G. M. McFarquhar, W. R. Cotton, and Y. Deng (2009), Direct and indirect impacts of Saharan dust acting as cloud condensation nuclei on tropical cyclone eyewall development, *Geophys. Res. Lett.*, *36*, L06802, doi:10.1029/2009GL037276.
Zuidema, P., et al. (2005), An Arctic springtime mixed-phase cloudy boundary layer observed during SHEBA, *J. Atmos. Sci.*, *62*, 160–176, doi:10.1175/JAS-3368.1.